Quantum thermochemical engines

Ugo Marzolino[1,2,3,*]

[1]*University of Trieste, Trieste I-34151, Italy*
[2]*National Institute of Nuclear Physics, Trieste Unit, Trieste I-34151, Italy*
[3]*Scuola Normale Superiore, Pisa I-56126, Italy*

Conversion of chemical energy into mechanical work is the fundamental mechanism of several natural phenomena at the nanoscale, like molecular machines and Brownian motors. Quantum mechanical effects are relevant for optimizing these processes and to implement them at the atomic scale. This paper focuses on engines that transform chemical work into mechanical work through energy and particle exchanges with thermal sources at different chemical potentials. Irreversibility is introduced by modeling the engine transformations with finite-time dynamics generated by a time-dependent quantum master equation. Quantum degenerate gases provide maximum efficiency for reversible engines, whereas the classical limit implies small efficiency. For irreversible engines, both the output power and the efficiency at maximum power are much larger in the quantum regime than in the classical limit. The analysis of ideal homogeneous gases grasps the impact of quantum statistics on the above performances, which are expected to persist in the presence of interactions and more general trapping. The performance dependence on different types of Bose-Einstein condensates (BECs) is also studied. The BECs under consideration are standard BECs with a finite fraction of particles in the ground state, and generalized BECs where eigenstates with parallel momenta, or those with coplanar momenta, are macroscopically occupied according to the confinement anisotropy. Quantum gases are therefore a resource for enhanced performances of converting chemical into mechanical work.

I. INTRODUCTION

Energy conversion is at the basis of fundamental natural phenomena and ubiquitous or breakthrough technologies [1,2]. A paradigmatic model is represented by heat engines that convert heat into work with the limitations implied by the second law of thermodynamics [3,4]. Similarly, chemical engines transform several kinds of chemical energy into other forms of energy. For instance, mechanical work, e.g., volume expansion or directed drifts and rotations, is generated from chemical potential gradients [5–11], from the splitting of chemical bonds (molecular motors) [12,13] as in adenosine triphosphate (ATP) hydrolysis, from thermal diffusion modeled by the Langevin and Fokker-Planck equations (Brownian motors) [10,14,15], and from surface energy in interface phenomena like "tears of wine," beating oil lenses, and self-oscillating pendant droplets [16]. Recent technologically oriented applications are syngas production [17], capacitive deionization for desalinization of brackish water [18,19], CO_2 capture by carbonation-decarbonation cycles [20], solar-driven CO_2 reduction

[21], chemical looping for hydrogen production [22,23] and for energy and carbon storage [24,25], low-grade heat harvesting [26–28], and pyrolytic reactions to increase the efficiency of turbine engines [29].

Heat engines have been investigated also in the quantum domain both at thermal equilibrium [30–38] and out of equilibrium [39–49]. Quantum effects become relevant already in systems at the nanoscale and in modern nanotechnologies that exhibit intermediate behavior between the classical and quantum regimes [14,50,51]. Considerable advances have been made to observe the intermediate regime by tuning system parameters [52–56]. Chemical engines are indeed realized at these size scales, where quantum effects improve the performance of existing synthetic molecular motors [57–60]. Nanomotors based on quantum dots have been conceived for charge pumping [8,61,62], and for converting electric work into mechanical work with high efficiency [63–65]. Quantum statistics is also relevant for metabolic activity and related diseases [66–70] and in solar energy conversion [71,72]. Therefore, investigating the impact of fundamental quantum features on small-sized engines enables us to understand the deep quantum regime of these machines and the transition to the classical regime.

————————
*ugo.marzolino@ts.infn.it

A. Overview of the paper

Taking inspiration from thermodynamic cycles modeling heat engines, this paper focuses on quantum engines that convert the chemical work of a working substance into mechanical work, by means of energy and particle exchanges with thermochemical sources that control external driving (e.g., temperature, chemical potential, volume, or particle number). These machines, henceforth called thermochemical engines, are analogous to heat engines, where heat, temperature, and entropy are replaced, respectively, by chemical work, chemical potential, and particle number. Nevertheless, the second law of thermodynamics does not prevent the transformation of all the supplied chemical work into mechanical work without waste. Irreversibility due to finite-time dynamics is introduced through quantum master equations that generalize the Langevin and Fokker-Planck equations of Brownian motors.

The results presented in this paper show that quantum degenerate gases as working substances provide maximum efficiency, i.e., without energy waste, while small efficiency and mechanical work output are obtained in the classical regime. Quantum degenerate gases also imply large output power for finite-time irreversible cycles that perturb quasistatic processes. Particular attention is devoted to the roles of standard and generalized Bose-Einstein condensates (BECs). Standard BECs occur when a macroscopic particle number occupies the ground state [73,74], and have been experimentally realized with ultracold atoms [75–77] or molecules [78,79], photons [80], and quasiparticles (polaritons [80–82], magnons [83,84], and phonons [85,86]) even at room temperature. Generalized BECs consist in large occupation of effective low-dimensional gases in the presence of highly anisotropic confinement volumes [87–97]. Generalized BECs describe liquid helium in thin films [98–102], the magnetic flux of superconducting rings [103], and gravito-optical traps [104,105], and have stimulated experimental advances with ultracold atoms [106–109].

The above experimental realizations, together with recent progress in quantum simulators [110,111], represent a plethora of platforms to implement thermochemical engines that are optimized in the deep quantum regime. Of particular interest at the nanoscale are BEC implementations with plasmon polaritons in a lattice of metal nanoparticles, which show ultrafast condensation at the subpicosecond scale [112,113], and with magnon BECs in ferromagnetic nanostructures [114,115]. Implementations with atomic gases exchanging particles and with highly anisotropic confinement allow for new atomtronic components [116] based on high-performance energy conversion.

The quantitative aspects of this paper are shown for ideal homogeneous gases, but similar behaviors remain valid for more general models. Indeed, they rely on physical conditions, on the chemical potentials, and on mathematical properties of the average particle number that persist in the presence of different trapping potentials, density of states, and interactions, as discussed later.

The rest of the paper is organized as follows. Section II describes the general scheme of thermochemical engines. Sections II A and II B are dedicated to equilibrium machines, called isothermal chemical Carnot cycle and isothermal chemical Otto cycle following the aforementioned analogy between thermochemical and heat engines. The effect of irreversibility as a perturbation of quasistatic processes on the efficiency and on the output power is discussed in Sec. III. Conclusions are drawn in Sec. IV, and technical details are provided in six appendices.

II. THERMOCHEMICAL ENGINES

The state of the working substance in thermochemical engines at thermodynamic equilibrium is determined by the conjugated couples (P, V), (T, S), and $(\mu, \mathcal{N})$, where P is the pressure, V the volume, T the absolute temperature, S the entropy, μ the chemical potential, and $\mathcal{N}$ the average particle number. At thermal equilibrium the substance is described by the grand canonical statistical ensemble, with density matrix $\varrho = e^{-\beta(H-\mu N)}/Z$, Hamiltonian operator H, particle number operator $N = \sum_k a_k^\dagger a_k$ (with k labeling an orthogonal set of system modes), $\beta = 1/(k_B T)$ the inverse temperature, and $Z = \mathrm{Tr}\, e^{-\beta(H-\mu N)}$ the partition function.

The grand canonical ensemble provides a more transparent treatment of the effects of quantum statistics, and accounts for statistical fluctuating energy and particle number. Allowing also for statistical fluctuations of the volume, the relevant ensemble is the so-called μPT ensemble [117–119], studied for small systems and nanothermodynamics [120–126], which predicts equations of state equivalent to the grand canonical ones. Therefore the optimal performances of quantum thermochemical engines, proved in the following for the grand canonical ensemble, can be straightforwardly generalized to the μPT ensemble.

Thermodynamic transformations are parameterized by the free parameters of the grand canonical ensemble, i.e., V, β, and μ. The other thermal quantities are determined by the partition function:

$$\beta PV = \ln Z, \tag{1}$$

$$\mathcal{N} = \mathrm{Tr}(\varrho N) = \frac{1}{\beta}\frac{\partial \ln Z}{\partial \mu}, \tag{2}$$

$$U = \mathrm{Tr}(\varrho H) = -\frac{\partial \ln Z}{\partial \beta} + \mu \mathcal{N}, \tag{3}$$

$$S = -k_B \mathrm{Tr}(\varrho \ln \varrho) = (U + PV - \mu \mathcal{N})/T. \tag{4}$$

Quasistatic transformations, where the system is always at thermal equilibrium, are described by a curve in the parameter space. Examples considered here are transformations fixing two of the aforementioned free parameters [127].

The variation of the internal energy during a thermodynamic process is $\Delta U = Q - W^M - W^C$, where $Q = \int T \, dS$ is the heat, $W^M = \int P \, dV$ is the mechanical work due to volume variations, and $W^C = -\int \mu \, d\mathcal{N}$ is the chemical work due to particle exchanges. Fluxes of these energy contributions are generated when the working substance is put in contact with thermochemical sources. Consider thermodynamic cycles consisting of several strokes, where ΔU_j, Q_j, W_j^M, and W_j^C are the energy exchanges during the jth stroke, and P_j, V_j, μ_j, $\mathcal{N}_j$, and $\rho_j = \mathcal{N}_j/V_j$ are the thermal quantities at the beginning of the jth stroke. The product of a cycle, also called *load*, is the total mechanical work, which is positive if it is done by the working substance on the surroundings. The energy supplied to the working substance is the absorbed chemical work, i.e., the positive contribution to the internal energy due to particle exchanges, $W_{in}^C = -\sum_j W_j^C \Theta(-W_j^C)$, where $\Theta(\cdot)$ is the Heaviside function. The energy released to the sources, $W_{out}^C = \sum_j W_j^C \Theta(W_j^C)$, contributes negatively to the internal energy. The energy W_{out}^C is released to sources different from those that supply chemical work: the released chemical work can be delivered back to the substance only with a further energetic cost, so that W_{out}^C is the waste generated for bringing the substance to the initial condition after a cycle. Consistently, and in analogy with heat engines, the *thermochemical efficiency* is the ratio between the load and the supplied energy [16]:

$$\eta = \frac{W^M}{W_{in}^C} = 1 - \frac{W_{out}^C + \Delta U - Q}{W_{in}^C}, \qquad (5)$$

where ΔU and Q are the internal energy and the heat variations, respectively, during a cycle.

When reversible cycles are considered, the figures of merit are the load per volume, W^M/V_{max}, and the efficiency (5) with the condition $\Delta U = 0$. These figures of merit will be used to compare the performances of quantum and classical engines. Moreover, assuming that the temperature is kept constant along the cycle, infinitesimal heat variations are exact differentials and so $Q = T \int_{cycle} dS = 0$. Therefore, the efficiency for reversible isothermal cycles becomes

$$\eta_{rev} = 1 - \frac{W_{out}^C}{W_{in}^C}, \qquad (6)$$

and the load per volume is

$$\frac{W^M}{V_{max}} = -\frac{W^C}{V_{max}} = \frac{W_{in}^C - W_{out}^C}{V_{max}}. \qquad (7)$$

The maximum efficiency $\eta_{rev} \to 1$ is then achieved if the chemical potential is non-negative when the particles are injected into the working substance and is negative when the substance particles decrease. These conditions imply

that $W_{out}^C = 0$, recalling that $W^C = -\int \mu \, d\mathcal{N}$ for each transformation.

Ideal and interacting fermionic gases can exhibit both negative (at low density or high temperature) and positive (at high density or low temperature) chemical potentials [128,129], so that the thermochemical sources can fix their signs in order to obtain $\eta_{rev} = 1$. Ideal bosonic gases face a similar situation with positive chemical potentials replaced by vanishing chemical potentials in BEC phases, since the non-negativity of energy eigenstate occupancies implies the non-positivity of the chemical potential. Bosonic gases with interactions also achieve maximum efficiency. Indeed, repulsing particles approaching the BEC transition show positive chemical potentials, proportional to the interaction strength and to the density, under several approximations, like the Bogoliubov, Hartree-Fock, and Thomas-Fermi approximations [73,74,130], and effective mean-field [131,132] and hard-core models [133], and with scattering length much larger than the interparticle distance (unitary gases) [134]. Quantum van der Waals interactions with a hard-core potential [135,136] increase the chemical potential for repulsive interactions or for small attractive interactions (see Appendix C). Therefore, the efficiency is maximized ($\eta_{rev} = 1$) for both fermions and bosons in the deep quantum regime.

Classical gases, especially with repulsive interactions, can also exhibit both negative and positive chemical potentials [137]. Nevertheless, the effects of quantum statistics can be neglected when (see Appendix A)

$$\mathcal{N} \ll V \left(\frac{2mK}{\hbar^2 \mathcal{N}} \right)^{3/2}, \qquad (8)$$

where $\hbar$ is the Planck constant, m is the particle mass, K is the average kinetic energy of the substance, and $K/\mathcal{N}$ is an intensive quantity, e.g., $K/\mathcal{N} = 3k_B T/2$ for classical gases. The condition (8) bounds the mechanical work of reversible isothermal engines: $W^M = -W^C = \int_{cycle} \mu \, d\mathcal{N} \ll \mathcal{O}(V_{max})$, where V_{max} is the maximum volume attained during the cycle (see Appendix A). Since quantum gases are not constrained by Eq. (8), quantum engines provide a load per volume (7) much larger than classical engines at comparable masses and energy densities. Another consequence of the constraint (8) is that the chemical potential of the classical van der Waals gas is always negative, thus preventing maximum efficiency, as detailed in Appendix A, contrary to what happens with the quantum van der Waals gas (see Appendix C).

The rest of the paper is dedicated to concrete cycles where the efficiency η_{rev} is maximized with quantum degenerate gases, while small efficiency and load are obtained in the classical regime. Ideal homogeneous gases are discussed, and similar behaviors extend to interacting models that do not limit the efficiency range (as those discussed above), and in the presence of general trapping

potentials and densities of states [138–142] that do not alter the qualitative behaviors of homogeneous gases (e.g., the monotonicity and the (un)boundedness of the average particle number discussed in Appendix B).

A. Isothermal chemical Carnot cycle

From the analogy with heat engines with the roles of heat and temperature replaced by chemical work and chemical potential, the isothermal chemical Carnot cycle is defined by the following strokes:

(1) particle release at constant temperature T and constant chemical potential $\mu_1 = \mu_2$,

(2) compression at constant temperature T and constant particle number $\mathcal{N}_2 = \mathcal{N}_3$,

(3) particle injection at constant temperature T and constant chemical potential $\mu_3 = \mu_4$, and

(4) expansion at constant temperature T and constant particle number $\mathcal{N}_4 = \mathcal{N}_1$.

This cycle has the advantage of fixing the chemical potentials when chemical work is done, as depicted in Fig. 1, so that the condition for achieving $\eta_{\text{rev}} = 1$ is directly controlled.

The supplied chemical work W_{in}^{C}, the released chemical work $W_{\text{out}}^{\text{C}}$, and the efficiency η_{rev} are, respectively,

$$W_{\text{in}}^{\text{C}} = \begin{cases} -W_1^{\text{C}} = \mu_1(\mathcal{N}_2 - \mathcal{N}_1) & \text{if } \mu_{1,3} < 0, \\ -W_3^{\text{C}} = \mu_3(\mathcal{N}_4 - \mathcal{N}_3) & \text{if } \mu_{1,3} > 0, \\ -W_1^{\text{C}} - W_3^{\text{C}} = W^{\text{M}} & \text{if } \mu_1 < 0 \text{ and } \mu_3 \geqslant 0, \end{cases}$$
(9)

$$W_{\text{out}}^{\text{C}} = \begin{cases} W_3^{\text{C}} = \mu_3(\mathcal{N}_3 - \mathcal{N}_4) & \text{if } \mu_{1,3} < 0, \\ W_1^{\text{C}} = \mu_1(\mathcal{N}_1 - \mathcal{N}_2) & \text{if } \mu_{1,3} > 0, \\ 0 & \text{if } \mu_1 < 0 \text{ and } \mu_3 \geqslant 0, \end{cases}$$
(10)

$$\eta_{\text{rev}} = \begin{cases} 1 - \mu_3/\mu_1 & \text{if } \mu_{1,3} < 0, \\ 1 - \mu_1/\mu_3 & \text{if } \mu_{1,3} > 0, \\ 1 & \text{if } \mu_1 < 0 \text{ and } \mu_3 \geqslant 0. \end{cases}$$
(11)

The load per volume,

$$\frac{W^{\text{M}}}{V_1} = (\mu_3 - \mu_1)\left(1 - \frac{\mathcal{N}_3}{\mathcal{N}_1}\right)\rho_1,$$
(12)

increases with the initial density ρ_1 and with the difference of chemical potentials fixed by the sources, $\mu_3 - \mu_1$.

We focus now on the isothermal chemical Carnot cycle working with ideal homogeneous gases whose thermal quantities are reported in Appendix B. The classical limit holds for small fugacities $z = e^{\beta\mu} = \lambda_T^3\rho \ll 1$, thus at negative chemical potentials and low densities. This condition implies small efficiency and load per volume. On the other hand, fermionic gases do not have restrictions on the chemical potentials and densities, so that $\eta_{\text{rev}} = 1$ and arbitrary load per volume are achieved by fixing $\mu_1 < 0$ and $\mu_3 \geqslant 0$. For bosonic particles, the chemical potentials are non-positive and approach zero at the formation of BECs. Therefore, maximum efficiency $\eta_{\text{rev}} = 1$, without restrictions on the load per volume, is attained if $\mu_3 \to 0$, namely when the working substance is a BEC during the third stroke.

Figure 2 shows the pressure-volume diagrams for fermions (a) and bosons (b), rescaled using factors kept constant during the cycle in order to plot dimensionless variables. The line integral, namely the area, of the closed line in the pressure-volume diagram is the extensive load and increases when μ_3 increases, in accordance with Eq. (12).

The analysis so far has revealed that the performances of the isothermal chemical Carnot cycle are optimized when the substance is in the deep quantum regime during the particle injection (third stroke), while the classical regime greatly underperforms.
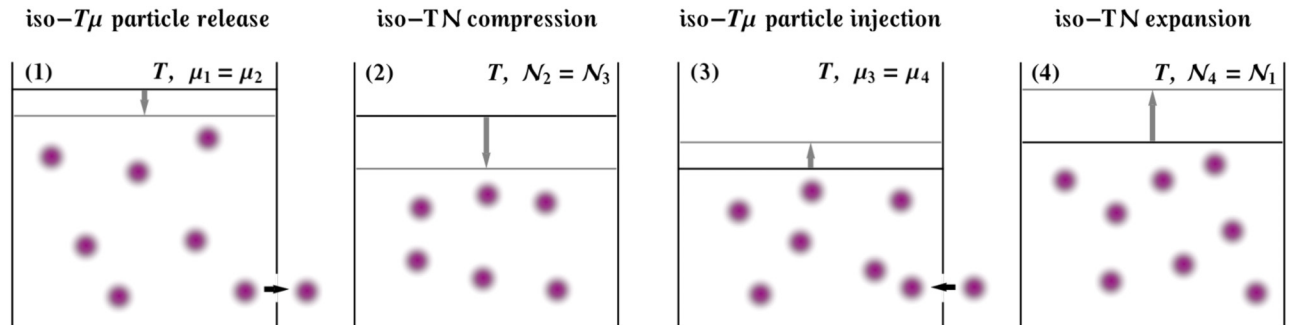

FIG. 1. Pictorial representation of the isothermal chemical Carnot cycle as described in the text: (1) particle release at constant temperature T and chemical potential $\mu_1 = \mu_2$; (2) compression at constant temperature T and particle number $\mathcal{N}_2 = \mathcal{N}_3$; (3) particle injection at constant temperature T and chemical potential $\mu_3 = \mu_4$; and (4) expansion at constant temperature T and particle number $\mathcal{N}_4 = \mathcal{N}_1$.

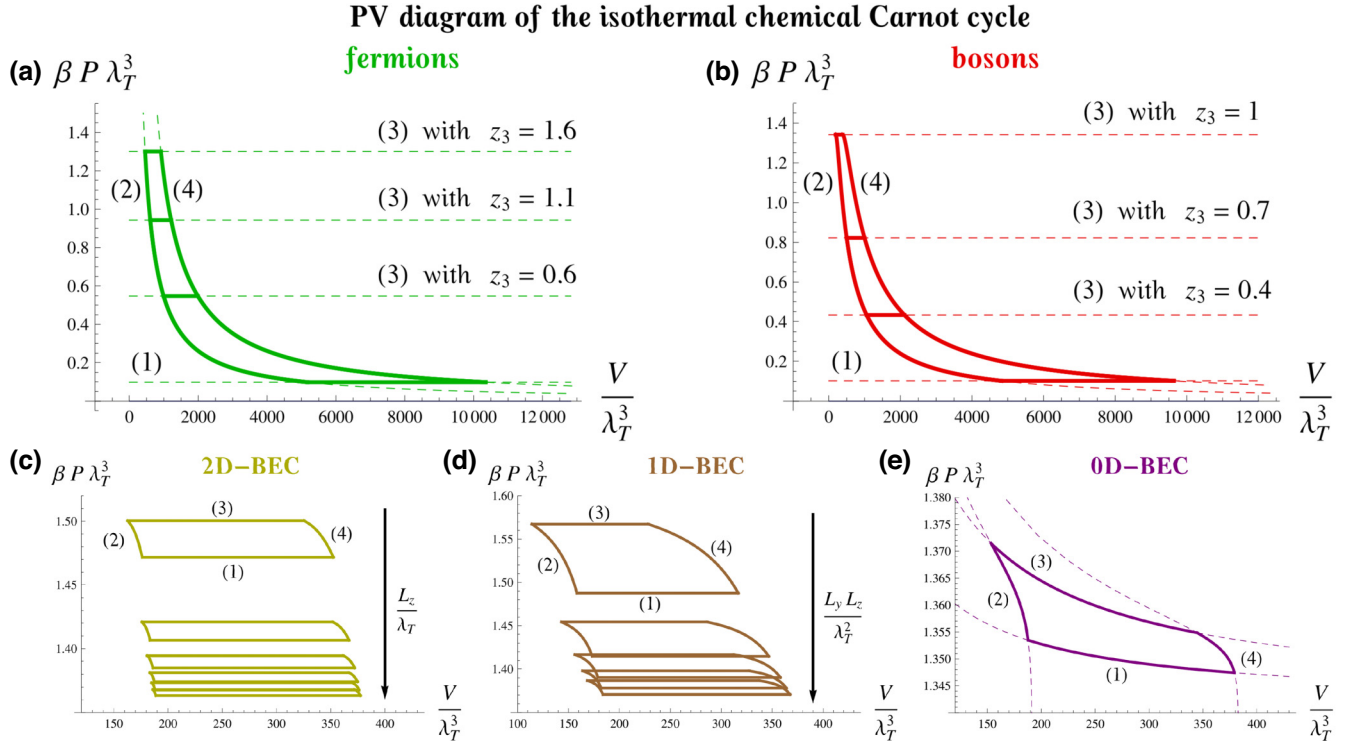**PV diagram of the isothermal chemical Carnot cycle**

FIG. 2. Rescaled pressure-volume diagrams of the isothermal chemical Carnot cycle: the numbers in parentheses indicate the strokes of the cycle corresponding to the closest curve. (a) Fermionic gas with $\mathcal{N}_1 = 1000$, $\mathcal{N}_3 = 500$, $z_1 = e^{\beta\mu_1} = 0.1$, and $z_3 = e^{\beta\mu_3} = 0.6$, 1.1, and 1.6. (b) Bosonic gas with $\mathcal{N}_1 = 1000$, $\mathcal{N}_3 = 500$, $z_1 = e^{\beta\mu_1} = 0.1$, and $z_3 = e^{\beta\mu_3} = 0.4$, 0.7, and 1. (c)–(e) Bosonic gases always in the same BEC phase during the cycle with $\mathcal{N}_1 = 1000$, $\mathcal{N}_3 = 500$, $z_1 = e^{\beta\mu_1} = 0.9$, and $z_3 = e^{\beta\mu_3} = 0.99$: (c) two-dimensional BEC with increasing $L_z/\lambda_T = 10$, 20, 30, 40, 50, and 60 in the direction of the arrow; (d) one-dimensional BEC with increasing $L_yL_z/\lambda_T^2 = 10$, 20, 30, 40, and 50 in the direction of the arrow; and (e) standard ground-state BEC here called zero-dimensional BEC.

When the substance is a BEC also during the first stroke, i.e., $\mu_1 \to 0$, the efficiency depends on the geometry of the confinement volume $V = L_xL_yL_z$. This geometric effect on thermodynamic quantities of BECs is detailed in Appendix B. Briefly, if the confinement sizes L_x, L_y, L_z are much larger in a number d of directions than the others, the whole set of excited states with moments in the less confined d directions is macroscopically occupied below a critical temperature. In this case, the BEC is described by a d-dimensional bosonic gas and is called dD-BEC in the rest of this paper. The terminology dD-BEC therefore refers to the spatial dimensionality of the modes forming the BEC, and is useful to make some equations and notation of this paper more compact. Consistently, a 0D-BEC is the standard BEC consisting only in the ground state, and occurs in isotropic volumes as there are no ($d = 0$) directions much larger than the others. Consider now three different settings corresponding to standard ground-state BECs (0D-BECs), one-dimensional BECs (1D-BECs), and two-dimensional BECs (2D-BECs), provided $L_x \gtrsim L_y \gtrsim L_z$.

If $L_x \sim L_y \sim L_z$ during the cycle, the BECs consist in the macroscopic occupation of the ground state (0D-BEC).

The chemical potential scales as $\mu \simeq -(\beta f \mathcal{N})^{-1}$, where $f = 1 - \rho_c/\rho = 1 - (T/T_c)^{3/2}$ is the condensate fraction, ρ_c is the critical density (i.e., the smallest density in the BEC phase), and T_c is the condensation temperature [see Eq. (B7)]. The efficiency becomes, using also $\mu_1 = \mu_2$ and $\mathcal{N}_2 = \mathcal{N}_3$,

$$\eta_{\text{rev}} = 1 - \frac{\mathcal{N}_2 - \rho_c V_2}{\mathcal{N}_2 - \rho_c V_3}. \tag{13}$$

If $L_x \gtrsim \alpha' L_y L_z$, for a constant α', the BECs are effective one-dimensional gases consisting of states with momenta parallel to L_x (1D-BEC). The chemical potentials are $-\beta\mu \simeq \pi (f \lambda_T \mathcal{N}/L_x)^{-2}$, and the efficiency reads

$$\eta_{\text{rev}} = 1 - \frac{(\mathcal{N}_2 - \rho_c V_2)^2 L_{x,3}^2}{(\mathcal{N}_2 - \rho_c V_3)^2 L_{x,2}^2}. \tag{14}$$

If $L_y \gtrsim e^{\alpha L_z} \text{poly}(L_z)$, where α is a constant and $\text{poly}(L_z)$ stands for a polynomial in L_z, the BECs are effective two-dimensional gases made of states with momenta in the x-y plane (2D-BEC). The chemical potentials are $-\beta\mu \simeq$

$e^{-f\lambda_T^2 \mathcal{N}/(L_x L_y)}$ and the efficiency

$$\eta_{\text{rev}} = 1 - e^{(\rho_c - \rho_3)L_{z,3}\lambda_T^2 - (\rho_c - \rho_2)L_{z,2}\lambda_T^2} \qquad (15)$$

approaches 1 in the thermodynamic limit, e.g., if $L_{z,3} = L_{z,2}$ or $L_{x,3}L_{y,3} = L_{x,2}L_{y,2}$ recalling $V_3 < V_2$.

If the substance is in a dD-BEC during the first stroke and in a d'D-BEC in the third stroke, with $d' < d$, $L_x \gg \alpha' L_y L_z$ for the 1D-BEC, and $L_y \gg e^{\alpha L_z}\text{poly}(L_z)$ for the 2D-BEC, then $\eta_{\text{rev}} \to 1$ in the thermodynamic limit.

The rescaled pressure-volume diagrams are plotted in Fig. 2 for substances always in a 2D-BEC (c), in a 1D-BEC (d), and in a 0D-BEC (e). The load, i.e., the area enclosed within the closed curve, is subextensive but the efficiency can achieve large values as shown above.

B. Isothermal chemical Otto cycle

Following the aforementioned analogy between heat and thermochemical engines, the isothermal chemical Otto cycle consists in the following strokes:

(1) particle release at constant temperature T and constant volume $V_1 = V_2$,

(2) compression at constant temperature T and constant particle number $\mathcal{N}_2 = \mathcal{N}_3$,

(3) particle injection at constant temperature T and constant volume $V_3 = V_4$, and

(4) expansion at constant temperature T and constant particle number $\mathcal{N}_4 = \mathcal{N}_1$.

This cycle has the advantage of fixing extensive quantities, V_j and $\mathcal{N}_j$ (see Fig. 3), that are easily controllable in some implementations.

Thermal quantities for ideal homogeneous gases are detailed in Appendix B. Using them in the general form of chemical work exchanged during the isothermal-isochoric strokes, shown in Appendix D, one obtains

$$W_1^C = \pm \frac{V_1}{\beta \lambda_T^3}\left(\text{Li}_{5/2}\text{Li}_{3/2}^{-1}(\pm\lambda_T^3\rho_2) - \text{Li}_{5/2}\text{Li}_{3/2}^{-1}(\pm\lambda_T^3\rho_1) - \lambda_T^3\rho_2\ln\left(\pm\text{Li}_{3/2}^{-1}(\pm\lambda_T^3\rho_2)\right) + \lambda_T^3\rho_1\ln\left(\pm\text{Li}_{3/2}^{-1}(\pm\lambda_T^3\rho_1)\right)\right),$$

$$(16)$$

$$W_3^C = \pm \frac{V_3}{\beta \lambda_T^3}\left(\text{Li}_{5/2}\text{Li}_{3/2}^{-1}(\pm\lambda_T^3\rho_4) - \text{Li}_{5/2}\text{Li}_{3/2}^{-1}(\pm\lambda_T^3\rho_3) - \lambda_T^3\rho_4\ln\left(\pm\text{Li}_{3/2}^{-1}(\pm\lambda_T^3\rho_4)\right) + \lambda_T^3\rho_3\ln\left(\pm\text{Li}_{3/2}^{-1}(\pm\lambda_T^3\rho_3)\right)\right),$$

$$(17)$$

where the upper (lower) signs refer to the bosonic gas without BEC (fermionic gas), $\text{Li}_s(z)$ is the polylogarithm function [143], and $\text{Li}_s^{-1}(z)$ its inverse ($\text{Li}_s\text{Li}_s^{-1}(z) = z$). The chemical work in Eqs. (16) and (17), and thus the efficiency (6) and the load per volume (7), depend only on $\lambda_T^3\rho_3$, $\lambda_T^3\rho_4$, and $v = V_3/V_1 = \rho_1/\rho_4 = \rho_2/\rho_3 < 1$.

The load is the area within the closed line in the pressure-volume diagram plotted in Fig. 4 for fermions (a) and bosons (b). As happens for the chemical Carnot cycle, the load is extensive and increases when the deep quantum regime is approached during the third stroke. The actual maximum is achieved at small ρ_3 and large ρ_4, which
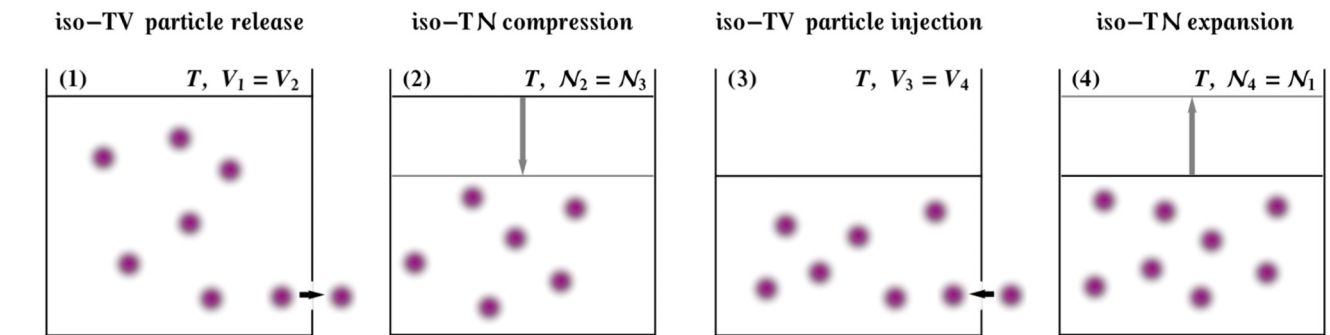

FIG. 3. Pictorial representation of the isothermal chemical Otto cycle as described in the text: (1) particle release at constant temperature T and volume $V_1 = V_2$; (2) compression at constant temperature T and particle number $\mathcal{N}_2 = \mathcal{N}_3$; (3) particle injection at constant temperature T and volume $V_3 = V_4$; and (4) expansion at constant temperature T and particle number $\mathcal{N}_4 = \mathcal{N}_1$.
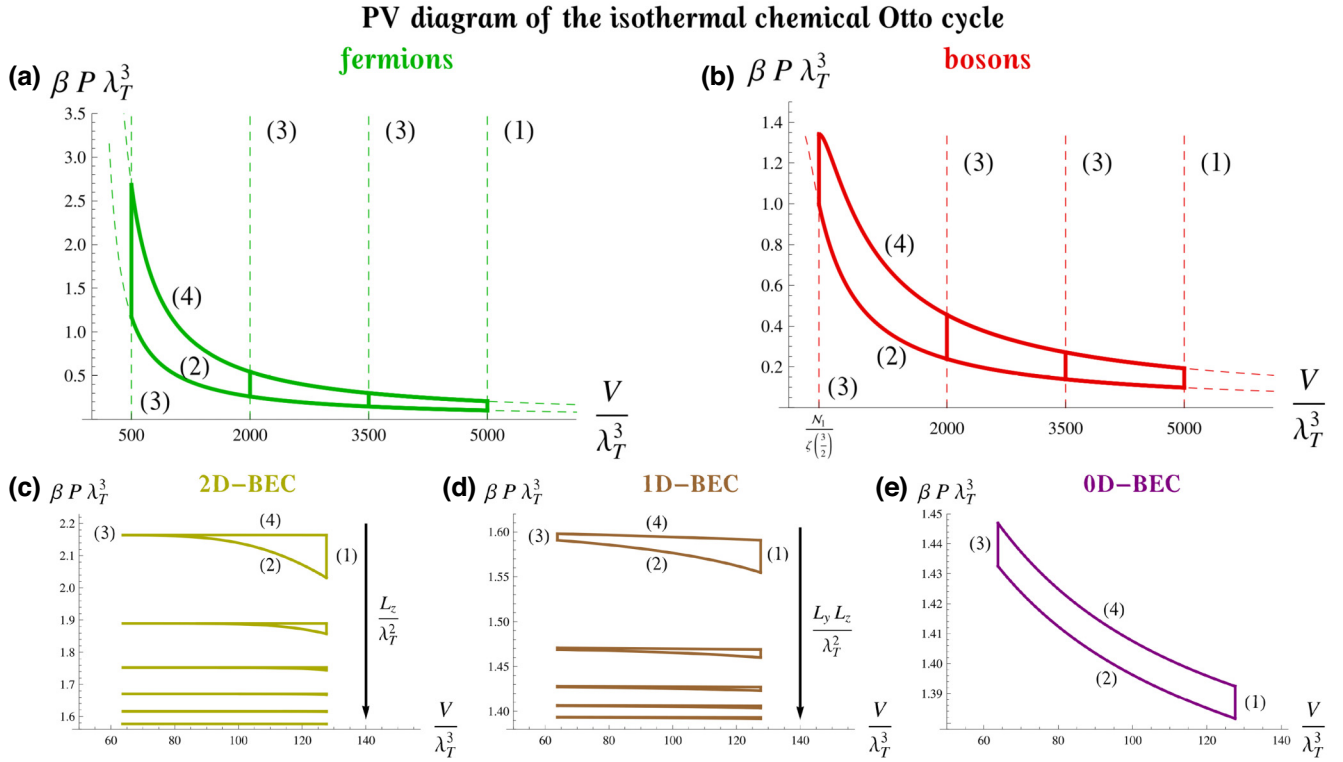
FIG. 4.   Rescaled pressure-volume diagrams of the isothermal chemical Otto cycle: the numbers in parentheses indicate the strokes of the cycle corresponding to the closest curve. (a) Fermionic gas with $\mathcal{N}_1 = 1000$, $\mathcal{N}_3 = 500$, $V_1/\lambda_T^3 = 5000$, and $V_3/\lambda_T^3 = 500$, 2000, and 3500. (b) Bosonic gas with $\mathcal{N}_1 = 1000$, $\mathcal{N}_3 = 500$, $V_1/\lambda_T^3 = 5000$, and $V_3/\lambda_T^3 = \mathcal{N}_1/\zeta(3/2)$, 2000, and 3500. The value $V_3/\lambda_T^3 = \mathcal{N}_1/\zeta(3/2)$ is attained when bosonic substances are in a BEC phase at the end of the third stroke. (c)–(e) Bosonic gases always in the same BEC phase during the cycle with $\mathcal{N}_1 = 1000$ and $\mathcal{N}_3 = 1.5V_1\rho_c = 3V_3\rho_c = 500$: (c) 2D-BEC with increasing $L_z/\lambda_T = 2, 3, 4, 5, 6,$ and 7 in the direction of the arrow; (d) 1D-BEC with increasing $L_yL_z/\lambda_T^2 = 10, 20, 30, 40,$ and 50 in the direction of the arrow; and (e) standard ground-state BEC here called 0D-BEC.

corresponds to the third stroke curve in Fig. 4 (the leftmost continuous vertical line) ranging from small to high pressures. The efficiency η_{rev} is plotted in Fig. 5 with $v = 1/3$ for fermions (green) and bosons (red, yellow, brown, and purple). The plots for different values of v are qualitatively similar.

The classical limit, $z_j = e^{\beta\mu_j} = \lambda_T^3\rho_j \propto \epsilon \ll 1$, implies vanishingly small efficiency $\eta_{\mathrm{rev}} \propto -1/\ln\epsilon$. In the quantum regime, the efficiency η_{rev} assumes all values in the interval $[0, 1]$ at different densities. For the fermionic gas, η_{rev} has a plateau at 1 when the signs of chemical potentials allow for $W_{1,3}^{\mathrm{C}} < 0$.

The chemical potential of the bosonic gas is always nonpositive, then $W_1^{\mathrm{C}} = -W_{\mathrm{in}}^{\mathrm{C}}$, $W_3^{\mathrm{C}} = W_{\mathrm{out}}^{\mathrm{C}}$ (with and without BECs). If the system is a BEC during the third stroke ($\lambda_T^3\rho_{3,4} \geqslant \lambda_T^3\rho_c = \zeta(3/2)$) but not during the first stroke ($\lambda_T^3\rho_{1,2} = v\lambda_T^3\rho_{4,3} < \lambda_T^3\rho_c = \zeta(3/2)$), then $W_{\mathrm{out}}^{\mathrm{C}} \neq 0$ and $W_{\mathrm{out}}^{\mathrm{C}} \simeq 0$ because μ_3 and μ_4 approach zero and $P_3 \simeq P_4$ (see Appendix B). Therefore, the efficiency is maximized, $\eta_{\mathrm{rev}} \simeq 1$. Within this parameter region, the maximum load per volume is attained when $\rho_3 = \rho_c$.

If the system is a BEC also during the first stroke ($\lambda_T^3\rho_{1,2} = v\lambda_T^3\rho_{4,3} \geqslant \lambda_T^3\rho_c = \zeta(3/2)$), one derives

$W_{1,3}^{\mathrm{C}} \simeq 0$ from the thermodynamic quantities of different BEC phases reported in Appendix B. The load is subextensive as shown in the pressure-volume diagram (see Fig. 4) for substances always in a 2D-BEC (c), in a 1D-BEC (d), and in a 0D-BEC (e). Nevertheless, the efficiency plotted in Fig. 5 for different types of BECs can achieve large values.

For the ground-state BEC (0D-BEC), namely $L_x \sim L_y \sim L_z$, the chemical work is

$$W_{1,\mathrm{0D\text{-}BEC}}^{\mathrm{C}} = \frac{1}{\beta} \ln \frac{v\rho_3 - \rho_c}{v\rho_4 - \rho_c}, \tag{18}$$

$$W_{3,\mathrm{0D\text{-}BEC}}^{\mathrm{C}} = \frac{1}{\beta} \ln \frac{\rho_4 - \rho_c}{\rho_3 - \rho_c}, \tag{19}$$

and the efficiency η_{rev} is plotted in purple in Fig. 5(a) and as the purple full curve in Fig. 5(b). Note that, if $\rho_j \gg \rho_c$ for all $j = 1, 2, 3, 4$, then $\eta_{\mathrm{rev}} \to 0$.

For the one-dimensional BEC (1D-BEC), namely $L_x \gtrsim \alpha'L_yL_z$,

$$W_{1,\mathrm{1D\text{-}BEC}}^{\mathrm{C}} = \frac{\pi L_{x,1}^2}{\beta\lambda_T^2 V_1} \frac{\rho_2 - \rho_1}{(\rho_2 - \rho_c)(\rho_1 - \rho_c)}, \tag{20}$$
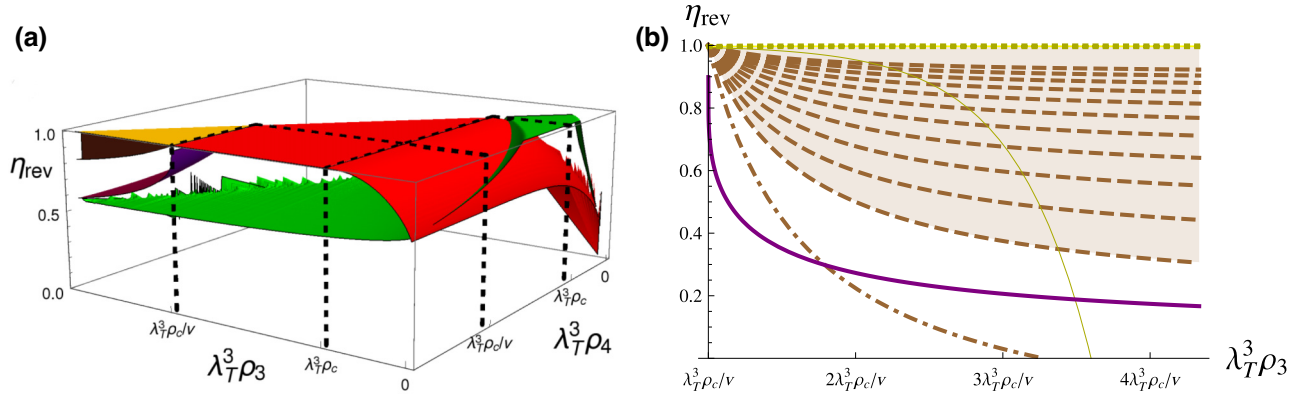
(a)

(b)

FIG. 5.   Efficiency η_{rev} of the isothermal chemical Otto cycle with $v = 1/3$ and for ideal homogeneous gases. (a) Fermions (green); bosons without BECs ($\rho_j < \rho_c$) and with a BEC during the third stroke ($\rho_{1,2} < \rho_c \leqslant \rho_{3,4}$) (red); and bosons in dD-BEC during the whole cycle ($\rho_j \geqslant \rho_c$) with (i) $d = 2$, $L_{z,3}/\lambda_T \geqslant 1$, $L_{x,3}L_{y,3}/(L_{x,1}L_{y,1}) = v^{r'}$, and $r' \geqslant 0$ (yellow), (ii) $d = 1$, $L_{x,3}/L_{x,1} = v^r$, and $r \geqslant 0$ (brown), and (iii) $d = 0$, i.e., standard ground-state BECs (purple). (b) Section of the left panel for $\rho_4 = (1 + 4/v)\rho_c$ and with a dD-BEC during the whole cycle. The brown dashed curves are the efficiencies for $d = 1$ and r ranging from 0 (lowermost curve) to 1 (uppermost curve) with a step of 0.1; the brown shading above the top brown curve corresponds to values $r > 1$. The yellow dotted curves are the efficiencies for $d = 2$ with $r' = 0$ and $r' = 1$: the two curves overlap almost perfectly as they are exponentially close to 1. For completeness, also the efficiency for the 2D-BEC with $L_{z,3}/\lambda_T^2 = 1$ and $r' = -0.2$ (thin yellow full curve) and that for the 1D-BEC with $r = -0.2$ (brown dash-dotted curve) are also plotted.

$$W^{\text{C}}_{3,\text{1D-BEC}} = \frac{\pi L_{x,3}^2}{\beta \lambda_T^2 V_3} \frac{\rho_4 - \rho_3}{(\rho_3 - \rho_c)(\rho_4 - \rho_c)}. \quad (21)$$

The corresponding efficiency η_{rev} depends on the ratio between the 3D volumes $V_3/V_1 = v$ and on the ratio between the 1D volumes $L_{x,3}/L_{x,1} = v^r$. The brown region in Fig. 5(a) and the brown dashed lines and brown shading in Fig. 5(b) represent η_{rev} for $r \geqslant 0$: within this interval, the efficiency increases with r, approaching 1 very fast for $r > 1$. When $r < 0$ [brown dash-dotted curve in Fig. 5(b)], η_{rev} decreases to zero and then assumes negative values, implying negative total mechanical work. These behaviors are more explicit in the asymptotic regime $\rho_j \gg \rho_c$ for all $j = 1, 2, 3, 4$, where $\eta_{\text{rev}} \to 1 - v^{2r}$.

For the two-dimensional BEC (2D-BEC), namely $L_y \gtrsim e^{\alpha L_z} \text{poly}(L_z)$, the chemical work is

$$W^{\text{C}}_{1,\text{2D-BEC}} = \frac{V_1 e^{\rho_c \lambda_T^2 L_{z,1}}}{\beta \lambda_T^2 L_{z,1}} \left(e^{-\rho_1 \lambda_T^2 L_{z,1}} - e^{-\rho_2 \lambda_T^2 L_{z,1}} \right), \quad (22)$$

$$W^{\text{C}}_{3,\text{2D-BEC}} = \frac{V_3 e^{\rho_c \lambda_T^2 L_{z,3}}}{\beta \lambda_T^2 L_{z,3}} \left(e^{-\rho_3 \lambda_T^2 L_{z,3}} - e^{-\rho_4 \lambda_T^2 L_{z,3}} \right). \quad (23)$$

The efficiency as a function of $\lambda_T^3 \rho_{3,4}$, plotted in yellow in Fig. 5, depends on the ratio between the 3D volumes $V_3/V_1 = v$, on the ratio between the 2D volumes $L_{x,3}L_{y,3}/(L_{x,1}L_{y,1}) = v^{r'}$ (such that $L_{z,3}/L_{z,1} = v^{1-r'}$), and on the parameter $L_{z,3}/\lambda_T$. The η_{rev} value is exponentially close to 1 for the physically relevant condition $L_{z,3}/\lambda_T \geqslant 1$ and for $r' \geqslant 0$ [yellow region in Fig. 5(a) and yellow dotted

curves in Fig. 5(b)], while it decreases to zero and becomes negative for $r' < 0$ [thin yellow curve in Fig. 5(b)]. If $\rho_j \gg \rho_c$ for all $j = 1, 2, 3, 4$, then $\eta_{\text{rev}} \simeq 1 - v^{r'} e^{(v^{r'} - 1)\rho_3 \lambda_T^2 L_{z,3}}$ if $r' \neq 0$ and $\eta_{\text{rev}} \simeq 1 - e^{(1 - 1/v)\rho_c \lambda_T^2 L_{z,3}}$ if $r' = 0$.

Also in the isothermal chemical Otto cycle, $\eta_{\text{rev}} \to 1$ if the substance is in a dD-BEC during the first stroke and in a d'D-BEC in the third stroke with $d' < d$, provided $L_x \gg \alpha' L_y L_z$ for the 1D-BEC, and $L_y \gg e^{\alpha L_z} \text{poly}(L_z)$ for the 2D-BEC.

In conclusion, if the substance is a BEC only during the third stroke, the load $W^{\text{M}} = -W^{\text{C}}$ is extensive and the efficiency is maximum $\eta_{\text{rev}} \simeq 1$, while the classical limit entails poor performances. If the system remains in a BEC phase also during the first stroke, the load is subextensive, but the engine works at maximum efficiency for generalized BECs.

III. IRREVERSIBLE CYCLES

Quasistatic transformations require infinite time and vanishing output power. Therefore, realistic engines consist in irreversible transformations implemented in finite time, τ_j for the jth transformation ($j = 1, 2, 3, 4$), which provide finite output power $\pi = W^{\text{M}}/\sum_j \tau_j$. Work and heat definitions for systems exchanging energy and particles due to irreversible transformations are detailed in Appendix D. This section is devoted to show that working substances in the quantum regime provide higher power and higher efficiency at maximum power than in the classical limit.

Irreversible transformations are described by the dynamics of open systems in contact with a grand canonical bath. During the substance-bath interaction, the chemical potential $\mu(t)$ and the system volume $V(t)$ (and $L_x(t)$, $L_y(t)$, and $L_z(t)$) slowly change in time. For isothermal cycles, such as those considered in Sec. II, the bath temperature β is constant. The time evolution is the solution of a time-dependent master equation with instantaneous relaxation times, $\theta(t)$, that are the relaxation times as if the explicit dependence on t (through $\mu(t)$ and $V(t)$) were frozen. We define also the maximum relaxation time $\bar{\theta} = \max_t \theta(t)$. Following Ref. [144], irreversible effects are treated perturbatively when the dynamics is slow compared to the instantaneous relaxation, namely $\tau_j \gg \bar{\theta}$. Within this regime, the limit of equilibrium quasistatic transformations is recovered for infinite times $\tau_j/\bar{\theta} \to \infty$ when grand canonical states with the same temperature and chemical potential of the bath are unique steady states at each time. This condition is met in master equations derived within the standard weak-coupling regime (i.e., Born, Markov, and secular approximations) [145], as in the concrete model discussed in the following.

The energy exchanges during irreversible transformations in the above perturbative regime are

$$W_j^{\mathrm{M/C}} = W_{j,\mathrm{rev}}^{\mathrm{M/C}} + \frac{\bar{\theta}}{\tau_j} W_{j,\mathrm{irr}}^{\mathrm{M/C}}, \qquad (24)$$

$$Q_j = Q_{j,\mathrm{rev}} + \frac{\bar{\theta}}{\tau_j} Q_{j,\mathrm{irr}}, \qquad (25)$$

$$\Delta U_j = \Delta U_{j,\mathrm{rev}} + \frac{\bar{\theta}}{\tau_j} \Delta U_{j,\mathrm{irr}}, \qquad (26)$$

where the subscript "rev" denotes energy exchanges of reversible transformations. The dependence on the initial state is an exponential decay in $\tau_j/\bar{\theta}$ and therefore contributes to much higher orders than those in Eqs. (24), (25), and (26). In other words, the final state of each irreversible process at the first order in $\bar{\theta}/\tau_j$ depends only on the initial state of the corresponding quasistatic transformation. Consequently, the internal energy variation may not vanish after the first irreversible cycle, but the initial and the final states of all the subsequent cycles coincide without further internal energy variations. Therefore, the internal energy variation ΔU after many cycles is negligible with respect to the total mechanical work.

The output power can be rewritten as

$$\pi = \frac{1}{\sum_j \tau_j} \left(W_{\mathrm{rev}}^{\mathrm{M}} + \sum_j \frac{Q_{j,\mathrm{irr}} - W_{j,\mathrm{irr}}^{\mathrm{C}}}{\tau_j} \right), \qquad (27)$$

where $W_{\mathrm{rev}}^{\mathrm{M}}$ is the total mechanical work of the reversible cycle. Power π is maximized at times

$$\tau_j^* = \frac{2\bar{\theta}\sqrt{W_{j,\mathrm{irr}}^{\mathrm{C}} - Q_{j,\mathrm{irr}}}}{W_{\mathrm{rev}}^{\mathrm{M}}} \sum_k \sqrt{W_{k,\mathrm{irr}}^{\mathrm{C}} - Q_{k,\mathrm{irr}}}, \qquad (28)$$

where the physically relevant condition $W_{j,\mathrm{irr}}^{\mathrm{C}} - Q_{j,\mathrm{irr}} \geqslant 0$ has been considered. This condition implies that the irreversibility contributions decrease the internal energy and that the optimal times τ_j^* are finite.

The thermochemical engine then operates with the optimal times τ_j^* (28) for each stroke. These optimal times should also be compatible with the validity regime of the long-time perturbative approach, namely $\tau_j^* \gg \bar{\theta}$. In the following, we compare the size scalings of optimal times and power of bosonic quantum gases with those in the classical limit. In some cases, the times τ_j^* have the same scaling of the relaxation time $\bar{\theta}$, violating the requirement $\tau_j^* \gg \bar{\theta}$. In these cases, therefore, let us consider the maximum power within the region $\tau_j^* \gg \bar{\theta}$, that is, at times as close as possible to $\bar{\theta}$, as the power decreases with increasing time. The optimal times at stake are then $\tau_j^* = \bar{\theta}/s$ with arbitrary size-independent $s \ll 1$, which preserves the optimal size scaling while remaining within the validity region of the approximation.

As a concrete model, consider that the substance is an ideal bosonic homogeneous gas and the bath is made of harmonic oscillators, with Hamiltonian $H_B = \hbar \int d\omega\, \omega b_\omega^\dagger b_\omega$, and canonical commutation relations $[b_\omega, b_{\omega'}^\dagger] = \delta(\omega - \omega')$. The substance-bath interaction Hamiltonian is of the form $H_I = \lambda \sum_{\boldsymbol{p}} \int d\omega\, h(\hbar\omega_x + \hbar\omega_y + \hbar\omega_z) T_{\boldsymbol{\omega},\boldsymbol{p}} (a_{\boldsymbol{p}}^\dagger b_{\boldsymbol{\omega}} + b_{\boldsymbol{\omega}}^\dagger a_{\boldsymbol{p}})$, where the coefficients $T_{\boldsymbol{\omega},\boldsymbol{p}}$ belong to a large set discussed in Appendix E. The master equation of the substance dynamics in the weak-coupling regime and its long-time dynamics are also reported in Appendix E. In particular, instantaneous relaxation times scale as $\bar{\theta} = \mathcal{O}(L_z/V)$, where L_x, L_y, L_z, and V denote typical values during the cycle here and in the following size scalings.

The first-order corrections of work (24) and heat (25) are explicitly written in Eqs. (E32), (E33), and (E34), whose size scalings are estimated in Sec. E 5 in Appendix E. These estimations are used to derive the size scalings of the optimal times τ_j^*, of the maximum power denoted by π_*, and of the efficiency at maximum power η_* (see Appendix F).

In the following subsections, the performances π_* and η_* of irreversible chemical Carnot and Otto cycles in quantum regimes are shown to outperform those in the classical limit. The size scalings of the optimal power normalized to its classical limit, $\pi_*/\pi_{\mathrm{class}}$, are summarized in Fig. 6 for Carnot (a) and Otto (b) cycles. Cycles without BECs and with a 0D-BEC in the third stroke have the same scaling of
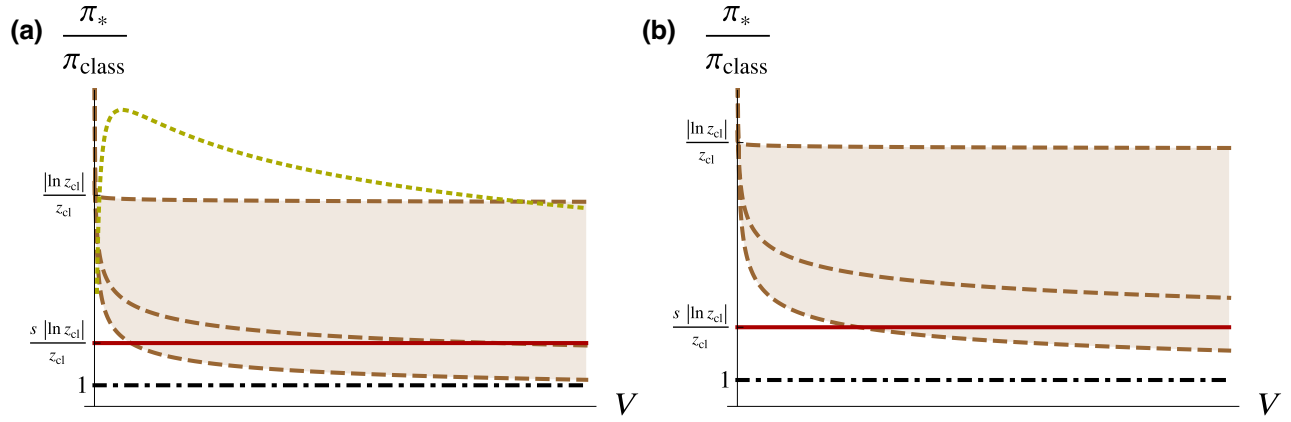
FIG. 6. Size scaling of the maximum power normalized to its classical limit. (a) Irreversible isothermal chemical Carnot cycle with 2D-BEC (yellow dotted), with 1D-BEC (brown dashed) with $L_x = \mathcal{O}(L_y L_z)^\chi$ and $\chi = 1.01, 1.5,$ and 2 from the uppermost to the lowermost curve, with 0D-BEC or without BECs (red full line). (b) Irreversible isothermal chemical Otto cycle with 1D-BEC (brown dashed) with $L_x = \mathcal{O}(L_y L_z)^\chi$ and $\chi = 2.01, 2.5,$ and 3 from the uppermost to the lowermost curve, with other BECs or without BECs (red full line). The black dash-dotted line is the classical limit, z_{cl} is the fugacity in the classical limit, and $s > z_{cl}/|\ln z_{cl}|$ has been considered.

the power (red solid line). The Otto cycle with a 2D-BEC in the third stroke also shows the same scaling, while the Carnot cycle with the same BEC results in a much larger output power (yellow dotted curve). The power scaling with a 1D-BEC in the third stroke depends on the strength of the anisotropy: setting $L_x = \mathcal{O}(L_y L_z)^\chi$, the power can be much larger than the power without BECs when $\chi > 1$ for the Carnot cycle and when $\chi > 2$ for the Otto cycle (brown dashed curves). Moreover, the values of π_*/π_{class} in the quantum regime are always very large since the parameter z_{cl} in the y axis of Fig. 6 is the fugacity in the classical limit, and $z_{cl} \ll 1$ as discussed below.

A. Irreversible cycles without BECs and in the classical limit

In the absence of BEC phases during the cycle, the computations in Sec. E 5 in Appendix E and in Appendix F prove that the maximum power scales as $\pi_* = \mathcal{O}(sV^2/L_z)$ and the efficiency as $\eta_* = \eta_{rev} + \mathcal{O}(sV^0)$. The factor $s \ll 1$ has been introduced in order to remain in the perturbative regime, when the optimal times in Eq. (28) scale as the relaxation times $\bar{\theta} = \mathcal{O}(L_z/V)$, as discussed above.

In the classical limit, the condition (8), which reads $\mathcal{N} \simeq z_{cl}V/\lambda_T^3$ with small fugacity $z_{cl} = e^{\beta \mu_{cl}} \ll 1$ for ideal gases (see Appendices A and B), affects the above scalings. In particular, the optimal time from Eq. (28) is $\tau_{class} = \mathcal{O}((L_z/V)|\ln z_{cl}|)$, the maximum power is $\pi_{class} = \mathcal{O}(z_{cl}V^2/(|\ln z_{cl}|L_z))$, and the efficiency at maximum power reads $\eta_{class} = \mathcal{O}(z_{cl})$.

In the cycles discussed in Sec. II, η_{rev} is finite and approaches 1 close to BEC transitions, and thus the quantum regime even without BECs exhibits much higher

efficiency than the classical limit and larger power if $s > z_{cl}/|\ln z_{cl}|$.

B. Irreversible cycles with BECs

When the working substance of the engine undergoes a BEC transition, one has to carefully consider the confinement anisotropy that leads to standard or generalized BECs, in order to rephrase the size scalings in terms of the volume. In the following, three different anisotropic boxes are considered, each one favoring a different BEC phase. The sizes $L_z = \mathcal{O}(\ln V)$ and $L_x \simeq L_y = \mathcal{O}(\sqrt{V/\ln V})$ favors the formation of a 2D-BEC. The emergence of a 1D-BEC is studied when $L_x = \mathcal{O}(L_y L_z)^\chi$ with $\chi \geqslant 1$, such that $L_x = \mathcal{O}(V^{\chi/(\chi+1)})$ and $L_y \sim L_z = \mathcal{O}(V^{1/(2\chi+2)})$. Lastly, assume the scaling $L_x \sim L_y \sim L_z = \mathcal{O}(\sqrt[3]{V})$ when the substance is a 0D-BEC.

The size scaling of the work and heat corrections in Eqs. (24) and (25) depend on the function $h(\varepsilon)$, and are explicitly computed in Sec. E 5 in Appendix E assuming $h(\varepsilon_p) \neq 0$ and that $h(0)$ is finite. The condition $h(\varepsilon_p) \neq 0$ guarantees that the grand canonical ensemble is the unique steady state at every time, otherwise also the instantaneous Hamiltonian eigenstates with energy ε_p such that $h(\varepsilon_p) = 0$ are steady states. This large class of functions contains the constant function, the exponential decay, and the Lorentzian.

The performances of the isothermal chemical Carnot and Otto cycles are reported explicitly in the following, when the substance is a BEC only during the third stroke. These configurations show efficiency and output power overcoming the classical ones. The cases of the working substance always being in a BEC are discussed in Appendix F.

1. Irreversible chemical Carnot cycle with a BEC during the third stroke

The size scalings of irreversible energy corrections imply the following efficiency at maximum power for the isothermal chemical Carnot cycle with a BEC only during particle injection (see Appendix F):

$$\eta_* = \begin{cases} \dfrac{\eta_{\rm rev}}{2} + \mathcal{O}\left(\dfrac{(\ln V)^5}{V}\right)^{\frac{1}{4}} & \text{2D-BEC,} \\[3ex] \dfrac{\eta_{\rm rev}}{2} + \mathcal{O}\left(\dfrac{1}{V^{\frac{\chi-1}{2\chi+2}}}\right) & \text{1D-BEC, } \chi > 1, \\[3ex] \eta_{\rm rev} + \mathcal{O}(sV^0) & \text{other BECs.} \end{cases} \tag{29}$$

Recall that $\eta_{\rm rev} = 1 - \mu_3/\mu_1 \simeq 1$ for large size, as discussed in Sec. II A, and finite size corrections (through those of μ_3 in the BEC phases) are smaller that those due to irreversibility in Eq. (29). Therefore, the efficiencies (29) are much larger than in the classical limit $\eta_{\rm class} = \mathcal{O}(z_{\rm cl}) \ll 1$, where $z_{\rm cl}$ is the classical fugacity.

The ratio between the maximum power in BEC phases and the maximum power in the classical limit with the same $L_{x,y,z}$ is

$$\frac{\pi_*}{\pi_{\rm class}} = \begin{cases} \mathcal{O}\left(\dfrac{|\ln z_{\rm cl}|}{z_{\rm cl}}\dfrac{(\ln V)^{\frac{5}{2}}}{\sqrt{V}}\right) & \text{2D-BEC,} \\[3ex] \mathcal{O}\left(\dfrac{|\ln z_{\rm cl}|}{z_{\rm cl}V^{\frac{2\chi-2}{2\chi+2}}}\right) & \text{1D-BEC, } \chi > 1, \\[3ex] \mathcal{O}\left(\dfrac{s|\ln z_{\rm cl}|}{z_{\rm cl}}\right) & \text{other BECs.} \end{cases} \tag{30}$$

The output power is larger than the classical limit if $V/(\ln V)^5 < |\ln z_{\rm cl}|^2/z_{\rm cl}^2$ for 2D-BECs, if $V < (|\ln z_{\rm cl}|/z_{\rm cl})^{(2\chi+2)/(2\chi-2)}$ for 1D-BECs with $\chi > 1$, and when $s > z_{\rm cl}/|\ln z_{\rm cl}|$ for 0D-BECs and 1D-BECs with $\chi = 1$.

2. Irreversible chemical Otto cycle with a BEC during the third stroke

The size scalings for the irreversible isothermal chemical Otto cycle, with BECs only when chemical work is released, provide the following efficiency at maximum power (see Appendix F):

$$\eta_* = \begin{cases} \dfrac{\eta_{\rm rev}}{2} + \mathcal{O}\left(\dfrac{1}{V^{\frac{\chi-2}{2\chi+2}}}\right) & \text{1D-BEC, } \chi > 2, \\[3ex] \eta_{\rm rev} + \mathcal{O}(sV^0) & \text{other BECs.} \end{cases} \tag{31}$$

From Fig. 5, $\eta_{\rm rev} \simeq 1$, so that the efficiencies (31) are much larger than in the classical limit $\eta_{\rm class} = \mathcal{O}(z_{\rm cl}) \ll 1$, where $z_{\rm cl}$ is the classical fugacity.

The maximum power in BEC phases normalized to that in the classical limit with the same $L_{x,y,z}$ is

$$\frac{\pi_*}{\pi_{\rm class}} = \begin{cases} \mathcal{O}\left(\dfrac{|\ln z_{\rm cl}|}{z_{\rm cl}\,V^{\frac{\chi-2}{\chi+1}}}\right) & \text{1D-BEC, } \chi > 2, \\[3ex] \mathcal{O}\left(\dfrac{s|\ln z_{\rm cl}|}{z_{\rm cl}}\right) & \text{other BECs.} \end{cases} \tag{32}$$

Therefore, the output power is larger than the classical limit if $V < (|\ln z_{\rm cl}|/z_{\rm cl})^{(\chi+1)/(\chi-2)}$ for 1D-BECs with $\chi > 2$, and when $s > z_{\rm cl}/|\ln z_{\rm cl}|$ for other BECs.

IV. CONCLUSIONS AND DISCUSSION

This paper explores the performances of quantum thermochemical engines, which convert chemical work into mechanical work by putting a working substance in contact with thermochemical sources. The sources control different thermodynamic quantities of the substance, allowing for several thermodynamic strokes. For the sake of concreteness, the isothermal chemical Carnot and Otto cycles are discussed in detail.

When the working substance is a quantum (either fermionic or bosonic) degenerate gas, the above cycles achieve the full range of efficiency $\eta \in [0, 1]$ and approach the maximum efficiency for a wide region of system parameters. On the other hand, the classical limit implies low efficiency and small output mechanical work. In other words, the chemical potential values that minimize the wasted chemical work leave the validity domain of the classical limit. Therefore, the quantum behavior of identical particles enhances thermochemical engine performances, as already proven for heat engines [146–152], batteries [153], metrology [154–159], and information protocols [160–162].

This paper presents a detailed analysis for ideal homogeneous gases in the grand canonical ensemble. Special attention has been devoted to the role of BEC phases where the ground state alone, or eigenstates with parallel momenta, or those with coplanar momenta, are macroscopically occupied according to the confinement anisotropy. The presence of BEC phases only during the particle injection entails maximum efficiency and extensive output mechanical work for reversible bosonic cycles. If the substance is in BEC phases during the entire cycle, the efficiency is maximum for a larger parameter region but with subextensive output mechanical work.

These results can be generalized in several directions. Firstly, although the grand canonical ensemble provides the simplest description of quantum gases, equivalent equations of state and chemical potential ranges are found in the so-called μPT ensemble [117–119], which allows also for volume statistical fluctuations and have been studied for small systems and nanothermodynamics [120–126].

Therefore, the aforementioned quantum enhanced performances of thermochemical engines are observed also in the μPT ensemble.

A second generalization is the presence of general trapping potentials and densities of states [138–142]. In these cases the range of chemical potentials is not changed and the equations of state show the same qualitative behavior of the ideal homogeneous gas, e.g., with upper-bounded bosonic particle number in the continuum approximation and the emergence of BEC phases above critical densities and at vanishing chemical potentials. Also these generalizations allow for enhanced performances for converting chemical into mechanical work in quantum regimes.

Interacting systems can be taken into account for a further generalization; nevertheless, they are often analytically intractable. The computation of thermodynamic quantities in general requires numerical approaches [163], also within some approximation schemes that involve self-consistent relations. Alternatively, one can resort to exactly solvable models that reduce the computational cost to that of more tractable problems [164–166], but often still rely on numerics for explicit computations. Fortunately, the inclusion of interactions under several approximations does not limit the accessible range of chemical potentials [73,74,128,129]. In particular, the general conditions to achieve maximum efficiency $\eta_{\text{rev}} \to 1$ are allowed: enhanced performances of thermochemical engines are again observed in the quantum regime. The emergence of standard BECs and the analytical estimation of some thermodynamic quantities at low temperature have been intensively studied for interacting gases under the Bogoliubov, Hartree-Fock and Thomas-Fermi approximations. Standard as well as generalized BECs are proven also in effective mean-field models [131] and van der Waals interactions (see Appendix C) above a critical density. The features of quantum gases, which can be employed as a resource for thermochemical engines, then persist in several physical models.

The quasistaticity of reversible cycles implies vanishing output power, and points to the need to consider irreversible cycles. Irreversible cycles have been modeled through interactions with a grand canonical bath and slowly varying control parameters for process durations much larger than instantaneous relaxation times. The classical limit still provides small efficiency and output mechanical work, while quantum gases, especially with BECs during particle injection, entail much larger efficiencies and much larger output power at comparable volumes.

The main challenge for experimental realizations of thermochemical engines described here is the control of substance parameters. The confinement volume can be controlled by superimposing optical and magnetic potentials also achieving highly anisotropic confinements and generalized BECs [167–169]. Other experimentally

feasible strategies for controlling external parameters, such as those determining the confinement volume, have been developed and realized within the framework of optimal control theory [170–173]. Atoms can be pumped in external potentials, e.g., by overlapping optical dipole traps and magneto-optical traps [174,175]. Particle injection and release in quasiparticle systems can be achieved by the same techniques employed for preparing grand canonical occupation numbers. For instance, magnons can be excited and annihilated through microwave magnetic fields [83,84], rapid cooling of phonons interacting with magnons [176], nuclear magnetic resonance [177], spin-polarized current induced by temperature gradients [178], or by the spin Hall effect [179,180]. A proposal for the control of the chemical potential is based on the application of time-periodic external potentials [181].

In conclusion, the aforementioned results indicate a quantum advantage for the efficiency and the power of machines that convert chemical work into mechanical work. Exploiting existing realizations of quantum degenerate gases [73,74,128,129] and recent developments in quantum simulators [110,111], the thermochemical engines discussed in this paper could open the way for the development of new quantum enhanced engines and motors. Moreover, quantum advantages occur also without the need for a BEC but away from the classical limit, and could shed light on phenomena at the border between the quantum and the classical domains.

APPENDIX A: CLASSICAL LIMIT OF QUANTUM STATISTICAL MECHANICS

Quantum systems behave as classical models when fundamental aspects of quantum mechanics have negligible effects. In statistical mechanics, this condition is realized when elementary cells in the single-particle phase space, with volume $\hbar^3$, can be approximated with points [182], for instance, when the number of particles is much smaller than the number of elementary cells. Therefore, at most one particle lies in an elementary cell and quantum statistics due to indistinguishability reduces to Boltzmann statistics.

The number of elementary cells is the extension of the thermal state in the single-particle phase space, e.g., estimated by the variances of canonical variables, divided by $\hbar^3$. The above condition then reads

$$\mathcal{N} \ll \frac{\Delta x \Delta y \Delta z \Delta p_x \Delta p_y \Delta p_z}{\hbar^3}, \tag{A1}$$

where (x, y, z) and (p_x, p_y, p_z) are the position and momentum operators of just one particle, $\Delta x = \sqrt{\langle x^2 \rangle - \langle x \rangle^2}$, $\Delta p_x = \sqrt{\langle p_x^2 \rangle - \langle p_x \rangle^2}$, and similarly for the other variances with grand canonical averages $\langle \cdot \rangle$. The symmetry under particle permutation in systems of identical particles implies that every particle provides the same variances in Eq. (A1).

The product $V_* = \Delta x \Delta y \Delta z$ is proportional to the volume occupied by the system: e.g., it can be easily computed that $V_* \propto L_x L_y L_z$ for a homogeneous gas, and $V_* \propto (m^3 \beta^3 \omega_x^2 \omega_y^2 \omega_z^2)^{-1/2}$ for an ideal gas in a harmonic potential where the large-volume limit is $\omega_{x,y,z} \to 0$ and the density is proportional to $\mathcal{N} \omega_x \omega_y \omega_z$ [183]. Moreover, V_* increases when repulsive interactions dominate, and decreases for strong attractive interactions. If the Hamiltonian is invariant under time reversal ($\boldsymbol{p} \leftrightarrow -\boldsymbol{p}$), for instance, for momentum-independent interactions and external potentials, then $\langle p_{x,y,z} \rangle = 0$, and one estimates $\Delta^2 p_{x,y,z} = \langle p_{x,y,z}^2 \rangle \leqslant \langle p_x^2 \rangle + \langle p_y^2 \rangle + \langle p_z^2 \rangle \simeq 2mK/\mathcal{N}$, where K is the average kinetic energy of the system. Therefore, the condition (A1) becomes

$$\mathcal{N} \ll V_* \left(\frac{2mK}{\hbar^2 \mathcal{N}} \right)^{3/2} \propto V \left(\frac{2mK}{\hbar^2 \mathcal{N}} \right)^{3/2}, \quad \text{(A2)}$$

or, after simple manipulations,

$$\mathcal{N} \ll V \left(\frac{2mK}{\hbar^2 V} \right)^{3/5}, \quad \text{(A3)}$$

where $K/\mathcal{N}$ and K/V are intensive quantities.

The expectations $\langle p_{x,y,z}^2 \rangle$ can be written in a mathematically elegant form, known as the quantum counterpart of the equipartition theorem [184,185], which reduces to the classical formula $\langle p_{x,y,z}^2 \rangle = mk_B T$ for high temperature or for an ideal homogeneous gas. Since Eq. (A1) is the condition for quantum gases behaving classically, it is meaningful to plug the classical formula $\langle p_{x,y,z}^2 \rangle = mk_B T$ there, thus obtaining $\mathcal{N} \ll V/\lambda_T^3$ up to a multiplicative constant, where $\lambda_T = \sqrt{2\pi \hbar^2 \beta/m}$ is the thermal wavelength. This form is equivalent to small fugacities $z = e^{\beta \mu} \ll 1$ for ideal gases (see Appendix B).

The constraint implied by the classical limit impinges on the work production of thermochemical cycles. Indeed, the chemical work during each stroke is estimated using the integral mean-value theorem: denoting the integral along the jth stroke by $\int_j$, and recalling that $\mathcal{N}_j$ is the particle number at the beginning of the jth stroke (with $\mathcal{N}_{J+1} = \mathcal{N}_1$ for a cycle consisting of J strokes), one obtains

$$|W_j^C| = \left| \int_j \mu \, d\mathcal{N} \right| = \left| \bar{\mu}_j \left(\mathcal{N}_{J+1} - \mathcal{N}_j \right) \right|$$

$$\ll |\bar{\mu}_j| \, \mathcal{O}\big(\max\{V_j, V_{j+1}\} \big), \quad \text{(A4)}$$

where $\bar{\mu}_j$ is an average chemical potential during the jth stroke. For reversible isothermal thermochemical cycles, the load, namely the mechanical work, is then $W^M = -W^C \ll \mathcal{O}(V_{max})$, where V_{max} is the maximum volume attained during the cycle.

APPENDIX B: IDEAL HOMOGENEOUS GAS

An ideal homogeneous gas consists in non-interacting particles confined in a cube of size $L_{x,y,z}$ [186]. The gas Hamiltonian is $H = \sum_{\boldsymbol{p}} \varepsilon_p a_{\boldsymbol{p}}^\dagger a_{\boldsymbol{p}}$ with $\varepsilon_p = (p_x^2 + p_y^2 + p_z^2)/(2m) = p^2/(2m)$, and the momenta $\boldsymbol{p} = (p_x, p_y, p_z) = 2\pi \hbar (n_x/L_x, n_y/L_y, n_z/L_z)$ label its eigenmodes ($n_{x,y,z} \in \mathbb{Z}$ and $[a_{\boldsymbol{p}}, a_{\boldsymbol{p}'}^\dagger] = \delta_{\boldsymbol{p}, \boldsymbol{p}'}$). Thermodynamic quantities satisfy the following relations:

$$U = \pm \frac{3V}{2\beta \lambda_T^3} \mathrm{Li}_{5/2}(\pm e^{\beta \mu}) = \frac{3}{2} PV, \quad \text{(B1)}$$

$$\mathcal{N} = \pm \frac{V}{\lambda_T^3} \mathrm{Li}_{3/2}(\pm e^{\beta \mu}). \quad \text{(B2)}$$

Here the upper signs hold for bosonic particles and the lower signs for fermions, $\lambda_T = \sqrt{2\pi \hbar^2 \beta/m}$ is the thermal wavelength, m is the particle mass,

$$\mathrm{Li}_s(z) = \sum_{k=1}^{\infty} \frac{z^k}{k^s} = \frac{1}{\Gamma(s)} \int_0^\infty dt \frac{t^{s-1}}{z^{-1} e^t - 1} \quad \text{(B3)}$$

is the polylogarithm function [143], and $\Gamma(s)$ is the Gamma function. The following series representations [143] will be used for estimating thermal quantities at small chemical potentials:

$$\mathrm{Li}_s(e^{\beta \mu}) = \Gamma(1-s)(-\beta \mu)^{s-1} + \sum_{k=0}^{\infty} \frac{\zeta(s-k)}{k!} (\beta \mu)^k \quad \text{(B4)}$$

if $s \notin \mathbb{N}^+$, and

$$\mathrm{Li}_s(e^{\beta \mu}) = \frac{(\beta \mu)^{s-1}}{(s-1)!} \big(H_{s-1} - \ln(-\beta \mu) \big)$$

$$+ \sum_{\substack{k=0 \\ k \neq s-1}}^{\infty} \frac{\zeta(s-k)}{k!} (\beta \mu)^k \quad \text{(B5)}$$

if $s \in \mathbb{N}^+$, where $H_s = \sum_{n=1}^s 1/n$ is the harmonic number.

The condition for the energy eigenstate occupancies of bosonic gases, $(e^{\beta(\varepsilon_p - \mu)} - 1)^{-1} \geqslant 0$, constrains the chemical potential to non-positive values, approaching zero at the formation of a Bose-Einstein condensate. The chemical potential of the fermionic gas has no restrictions. The classical limit is achieved for small fugacities $z = e^{\beta \mu} \ll$

1, thus at negative chemical potentials, which implies $\mathrm{Li}_s(z) \simeq z$ and the known equation of state $PV = \mathcal{N}k_BT$ from Eqs. (B1) and (B2).

The density $\rho = \mathcal{N}/V$ of the bosonic gas, from Eq. (B2), has an upper bound when $z = 1$ or $\mu = 0$:

$$\rho = \frac{\mathcal{N}}{V} \leqslant \frac{1}{\lambda_T^3}\, \zeta(3/2) \equiv \rho_c, \tag{B6}$$

also called critical density, where $\zeta(s)$ is the Riemann zeta function. For densities larger than ρ_c, $\mathcal{N} > \rho_c V$, or equivalently when the temperature is lowered below the critical one, i.e.,

$$T_c = \frac{2\pi\hbar^2}{mk_B}\left(\frac{\rho}{\zeta(3/2)}\right)^{2/3}, \tag{B7}$$

the chemical potential approaches zero, and the fraction of particles

$$f = \frac{\mathcal{N} - \rho_c V}{\mathcal{N}} = 1 - \left(\frac{T}{T_c}\right)^{3/2} \tag{B8}$$

accumulates in a Bose-Einstein condensate (BEC).

The nature of the BEC depends on the relative scaling of the box sizes. The BEC consists in a macroscopic number of particles in the ground state for isotropic confinement volume [73,74], but is modeled by a two- or one-dimensional gas in highly anisotropic external potentials [87–97]. Assuming $L_x \geqslant L_y \geqslant L_z$, there are three different scenarios.

(i) If $L_y \gtrsim e^{\alpha L_z}\mathrm{poly}(L_z)$, where α is a constant and $\mathrm{poly}(L_z)$ stands for a polynomial in L_z, the BEC consists in the macroscopic occupation of the effective two-dimensional gas made of states with momenta perpendicular to L_z (2D-BEC). For this reason, $\mathcal{O}(\lambda_T^2/L_y^2) \leqslant -\beta\mu \ll \lambda_T^2/L_z^2$. Moreover, the condensate occupation is

$$f\mathcal{N} = \frac{L_x L_y}{\lambda_T^2}\,\mathrm{Li}_1(e^{\beta\mu}) = -\frac{L_x L_y}{\lambda_T^2}\ln(1 - e^{\beta\mu})$$

$$\underset{\mu\simeq 0}{\simeq} -\frac{L_x L_y}{\lambda_T^2}\ln(-\beta\mu), \tag{B9}$$

such that the chemical potential is $-\beta\mu \simeq e^{-f\rho L_z\lambda_T^2}$. Using this scaling of μ, the total pressure of the noncondensed part of the gas and of the 2D-BEC is

$$P = \frac{\mathrm{Li}_{5/2}(e^{\beta\mu})}{\beta\lambda_T^3} + \frac{\mathrm{Li}_2(e^{\beta\mu})}{\beta\lambda_T^2 L_z}$$

$$\underset{\mu\simeq 0}{\simeq} \frac{\zeta(5/2)}{\beta\lambda_T^3} + \frac{\zeta(2)}{\beta\lambda_T^2 L_z} - \frac{\mu\ln(-\beta\mu)}{\lambda_T^2 L_z} + \frac{\mu}{\lambda_T^2 L_z}. \tag{B10}$$

(ii) If $L_x \gtrsim \alpha' L_y L_z$, for a constant α', the BEC is formed by an effective one-dimensional gas consisting of states with

momenta parallel to L_x (1D-BEC). Therefore, $\mathcal{O}(\lambda_T^2/L_x^2) \leqslant -\beta\mu \ll \lambda_T^2/L_y^2$. The condensate occupation is

$$f\mathcal{N} = \frac{L_x}{\lambda_T^2}\,\mathrm{Li}_{1/2}(e^{\beta\mu}) \underset{\mu\simeq 0}{\simeq} \frac{L_x}{\lambda_T^2}\sqrt{\frac{\pi}{-\beta\mu}}, \tag{B11}$$

and consequently the chemical potential is $-\beta\mu \simeq \pi(f\rho L_y L_z\lambda_T)^{-2}$. The correction to the pressure due to the 1D-BEC at the lowest orders is

$$P = \frac{\mathrm{Li}_{5/2}(e^{\beta\mu})}{\beta\lambda_T^3} + \frac{\mathrm{Li}_{3/2}(e^{\beta\mu})}{\beta\lambda_T L_y L_z}$$

$$\underset{\mu\simeq 0}{\simeq} \frac{\zeta(5/2)}{\beta\lambda_T^3} + \frac{\zeta(3/2)}{\beta\lambda_T L_y L_z} + \sqrt{-\frac{\mu}{\beta}}\,\frac{\Gamma(-1/2)}{\lambda_T L_y L_z}. \tag{B12}$$

(iii) If $L_x \sim L_y \sim L_z$, a standard BEC with the ground state macroscopically occupied is created (0D-BEC), with condensate number

$$f\mathcal{N} = \frac{1}{e^{-\beta\mu} - 1} \underset{\mu\simeq 0}{\simeq} -\frac{1}{\beta\mu}, \tag{B13}$$

and chemical potential $-\beta\mu = (f\rho V)^{-1}$. The pressure of the noncondensed gas and the 0D-BEC is

$$P = \frac{\mathrm{Li}_{5/2}(e^{\beta\mu})}{\beta\lambda_T^3} + \frac{\mathrm{Li}_1(e^{\beta\mu})}{\beta L_x L_y L_z} \underset{\mu\simeq 0}{\simeq} \frac{\zeta(5/2)}{\beta\lambda_T^3} - \frac{\ln(-\beta\mu)}{\beta V}. \tag{B14}$$

If the volume sizes fulfill more that one among the above scalings, subsequent BEC transitions happen from a dD-BEC to a d'D-BEC with $d' < d$ when the temperature decreases or the density increases.

Quantum gases in more general trapping potentials and densities of states exhibit average particle numbers similar to Eq. (B2), with the polylogarithm function $\mathrm{Li}_{3/2}(\pm e^{\beta\mu})$ replaced by $\mathrm{Li}_s(\pm e^{\beta\mu})$ and a model-dependent parameter s [138–140]. The average particle number is expressed in terms of these functions also in several weak, mean-field, and hard-core interactions [130–133,135] (see, for instance, Appendix C). This mathematical analogy allows us to extend some qualitative features of homogeneous gases to more general systems. In particular, BECs above a critical density occur when the polylogarithm functions in the expressions of $\mathcal{N}$ are bounded from above, i.e., $s > 1$ [see Eq. (B4)]. BECs above a critical density also occur with different mathematical forms of $\mathcal{N}$ [141,142].

APPENDIX C: VAN DER WAALS GASES

The classical van der Waals model describes hard-core particles interacting through the Lennard-Jones potential within a mean-field approximation [187,188]. The

equation of state is

$$(P + a\rho^2)(1 - b\rho) = \rho k_B T, \qquad \text{(C1)}$$

where $b > 0$ is the volume excluded for each particle by other hard-core particles, and a, i.e., the average interaction per unit density, is proportional to b and to a characteristic energy scale, ϕ, of the potential. The chemical potential is

$$\mu = k_B T \ln(\lambda_T^3 \rho) - k_B T \ln(1 - b\rho) + \frac{k_B T b\rho}{1 - b\rho} - 2a\rho. \qquad \text{(C2)}$$

The first contribution in Eq. (C2) is the chemical potential of the ideal gas, $k_B T \ln(\rho \lambda_T^3)$, which is negative with large magnitude from the classical limit $\rho = \mathcal{N}/V \ll 1/\lambda_T^3$ derived in Appendix A. Moreover, $b\rho \leqslant 1$ from the definition of b, and the maximum density $\rho = 1/b$ is approached at vanishing temperature, i.e., $1 - b\rho \propto k_B T$ from Eq. (C1). Consequently, the second and third terms in Eq. (C2) are positive and bounded. Indeed, at $b\rho \approx 1$, the particles have very little space in which to move, thus small average kinetic energy and low temperature. Nevertheless, the classical limit is achieved at high temperature, otherwise, for example, there would be substantial deviations from the equipartition theorem [184,185]. The last term in Eq. (C2) is negative (positive) for attractive (repulsive) interactions $a > 0$ ($a < 0$), and its magnitude is fixed by the microscopic details, $2|a|\rho \propto |\phi|b\rho \leqslant |\phi|$, and does not dominate $k_B T \ln(\rho \lambda_T^3)$ in the classical limit $\lambda_T^3 \rho \ll 1$. In conclusion, the chemical potential of the van der Waals gas is negative.

A quantum extension of the van der Waals model [135, 136] is described by the equation of state

$$P(T, \mu) = P_{\text{id}}(T, \mu') - a\rho^2, \qquad \text{(C3)}$$

where the subscript "id" denotes the functional forms of ideal (either bosonic or fermionic) gases, and

$$\mu'(\rho, T) = \mu_{\text{id}}\left(\frac{\rho}{1 - b\rho}, T\right). \qquad \text{(C4)}$$

Moreover, μ_{id} and ρ_{id} fulfill

$$\mu' = \mu - bP_{\text{id}}(T, \mu') + 2a\rho, \qquad \text{(C5)}$$

$$\rho(T, \mu) = \frac{\rho_{\text{id}}(T, \mu')}{1 + b\rho_{\text{id}}(T, \mu')}. \qquad \text{(C6)}$$

With μ' being the chemical potential of an ideal gas, it ranges over $(-\infty, 0]$. Therefore, the chemical potential μ can be positive for repulsive interactions ($a < 0$) or for small attractive interactions ($a > 0$) if $bP_{\text{id}}(T, \mu') > 2a\rho \propto \phi b\rho$.

Note from Eq. (C6) that $\rho(T, \mu)$ has a finite maximum when also $\rho_{\text{id}}(T, \mu')$ is maximum. Consequently, the mechanism of BEC formation is inherited from that of the ideal bosonic gas, shown in Appendix B, when $\mu' \to 0$. The critical density of the bosonic van der Waals gas is obtained by replacing ρ_{id} with its maximum in Eq. (C6),

$$\rho_c = \frac{\zeta(3/2)}{\lambda_T^2 + b\,\zeta(3/2)}, \qquad \text{(C7)}$$

which is smaller than the critical density of the ideal gas.

APPENDIX D: THERMODYNAMIC TRANSFORMATIONS

In this appendix, general formulas for energy exchanges are derived. We start with a general thermodynamic transformation in the Schrödinger picture, where the density matrix evolves quasistatically and is described by a grand canonical ensemble, $\varrho = e^{-\beta(H - \mu N)}/Z$, at every time. Plugging the grand canonical state into $S = -k_B \text{Tr}(\varrho \ln \varrho)$, one obtains the following form for the heat:

$$Q = \int T\, dS = \int \text{Tr}\big((H - \mu N)\, d\varrho\big). \qquad \text{(D1)}$$

In isothermal transformations, such as those considered here, the heat exchange is

$$\begin{aligned} Q &= T(S_{\text{f}} - S_{\text{i}}) \\ &= U_{\text{f}} - U_{\text{i}} + P_{\text{f}}V_{\text{f}} - P_{\text{i}}V_{\text{i}} - \mu_{\text{f}}\mathcal{N}_{\text{f}} + \mu_{\text{i}}\mathcal{N}_{\text{i}}, \end{aligned} \qquad \text{(D2)}$$

where the subscripts "i" and "f" indicate, respectively, the initial and final quantities of the transformation. The Hamiltonian H and the number operator N depend on the volume, through their eigenvectors and the eigenvalues of H, but do not depend on the temperature and on the chemical potential, which are thermodynamic forces. Consequently, the chemical work is

$$\begin{aligned} W^{\text{C}} &= -\int \mu\, d\mathcal{N} = -\int \mu\, \text{Tr}(N\, d\varrho + \varrho\, dN) \\ &= -\int \mu\left(\text{Tr}(N\, d\varrho) + \text{Tr}\left(\varrho\, \frac{\partial N}{\partial V}\right) dV\right). \end{aligned} \qquad \text{(D3)}$$

Using $U = \text{Tr}(H\varrho)$, the first law of thermodynamics $\Delta U = Q - W^{\text{M}} - W^{\text{C}}$, and expressions (D1) and (D3), one derives the following expression for the mechanical work:

$$\begin{aligned} W^{\text{M}} &= -\int \text{Tr}(\varrho(dH - \mu\, dN)) \\ &= -\int \text{Tr}\left(\varrho\left(\frac{\partial H}{\partial V} - \mu\, \frac{\partial N}{\partial V}\right)\right) dV. \end{aligned} \qquad \text{(D4)}$$

We now apply the above equations to work exchanges for the reversible transformations exploited in the cycles under consideration.

(a) Transformation at constant temperature T and constant chemical potential $\mu = \mu_i = \mu_f$:

$$W_{\text{iso-}T\mu}^{\text{C}} = -\mu(\mathcal{N}_f - \mathcal{N}_i), \tag{D5}$$

$$W_{\text{iso-}T\mu}^{\text{M}} = P_f V_f - P_i V_i. \tag{D6}$$

(b) Transformation at constant temperature T and constant particle number $\mathcal{N} = \mathcal{N}_i = \mathcal{N}_f$:

$$W_{\text{iso-}T\mathcal{N}}^{\text{C}} = 0, \tag{D7}$$

$$W_{\text{iso-}T\mathcal{N}}^{\text{M}} = P_f V_f - P_i V_i - (\mu_f - \mu_i)\mathcal{N}. \tag{D8}$$

(c) Transformation at constant temperature T and constant volume $V = V_i = V_f$:

$$W_{\text{iso-}TV}^{\text{C}} = (P_f - P_i)V - \mu_f \mathcal{N}_f + \mu_i \mathcal{N}_i, \tag{D9}$$

$$W_{\text{iso-}TV}^{\text{M}} = 0. \tag{D10}$$

Equations (D3) and (D4) and the identification of heat with the right-hand side of Eq. (D1) are extended to nonequilibrium transformations. These energy exchanges generalize the usual definitions of quantum thermodynamics [189] to the presence of particle fluxes, and are analogous to those discussed in Ref. [190]. There, however, the number operator N does not depend on the external driving, whereas the engines considered in this paper require one to account for the changes of N with volume.

APPENDIX E: IRREVERSIBLE TRANSFORMATIONS

In this appendix, irreversible transformations are modeled by finite-time dynamics of the engine substance interacting with a grand canonical thermal bath. In the limit of infinite time, these transformations reduce to reversible, quasistatic transformations. The total Hamiltonian is $H + H_B + H_I$, where $H = \sum_p \varepsilon_p a_p^\dagger a_p$ is the substance Hamiltonian for an ideal homogeneous gas with $\varepsilon_p = (p_x^2 + p_y^2 + p_z^2)/(2m) = p^2/(2m)$, momenta $\boldsymbol{p} = (p_x, p_y, p_z) = 2\pi\hbar(n_x/L_x, n_y/L_y, n_z/L_z)$ with $n_{x,y,z} \in \mathbb{Z}$, and canonical commutation relations $[a_p, a_{p'}^\dagger] = \delta_{p,p'}$.

The bath is made of harmonic oscillators with Hamiltonian $H_B = \sum_{\boldsymbol{m} \in \mathbb{N}^3} \hbar \boldsymbol{m} \cdot \boldsymbol{\Omega} \, b_{\boldsymbol{m}}^\dagger b_{\boldsymbol{m}}$, with $\boldsymbol{m} = (m_x, m_y, m_z)$, $\boldsymbol{\Omega} = (\Omega_x, \Omega_y, \Omega_z)$, and discrete modes ($[b_{\boldsymbol{m}}, b_{\boldsymbol{m}'}^\dagger] = \delta_{\boldsymbol{m},\boldsymbol{m}'}$).

In the continuum limit $\Omega_{x,y,z} \to 0$ with the new variables $\omega_{x,y,z} = m_{x,y,z}\Omega_{x,y,z}$ and $\boldsymbol{\omega} = (\omega_x, \omega_y, \omega_z)$, one defines the continuous bosonic modes $b_{\boldsymbol{\omega}} = b_{\boldsymbol{m}}/\sqrt{\Omega_x \Omega_y \Omega_z}$ ($[b_{\boldsymbol{\omega}}, b_{\boldsymbol{\omega}'}^\dagger] \to \delta(\boldsymbol{\omega} - \boldsymbol{\omega}')$), and the bath Hamiltonian becomes $H_B \to \hbar \int d\boldsymbol{\omega} \, (\omega_x + \omega_y + \omega_z) \, b_{\boldsymbol{\omega}}^\dagger b_{\boldsymbol{\omega}}$.

The substance-bath interaction is bilinear in the system and bath bosonic operators: $H_I = \lambda \sum_p \int d\boldsymbol{\omega} \, h(\hbar\omega_x + \hbar\omega_y + \hbar\omega_z) T_{\boldsymbol{\omega},\boldsymbol{p}}(a_p^\dagger b_{\boldsymbol{\omega}} + b_{\boldsymbol{\omega}}^\dagger a_p)$. The following computations for general irreversible dynamics can be very convoluted. Let us therefore describe a class of system-bath interactions, through mathematical properties of the coefficients $T_{\boldsymbol{\omega},\boldsymbol{p}}$, that greatly simplify the computations. Consider any injective function $\boldsymbol{w} : \boldsymbol{p} \to \boldsymbol{w}(\boldsymbol{p}) = (w_x(\boldsymbol{p}), w_y(\boldsymbol{p}), w_z(\boldsymbol{p}))$ such that $w_x(\boldsymbol{p}) + w_y(\boldsymbol{p}) + w_z(\boldsymbol{p}) = \varepsilon_p/\hbar$. Consider also $\boldsymbol{\omega}'$ and $\boldsymbol{\omega}''$ in the image of $\boldsymbol{w}$, i.e., if there exist vectors $\boldsymbol{p}'$ and $\boldsymbol{p}''$ with $\boldsymbol{\omega}' = \boldsymbol{w}(\boldsymbol{p}')$ and $\boldsymbol{\omega}'' = \boldsymbol{w}(\boldsymbol{p}'')$, then assume that the interaction coefficients satisfy the following conditions:

$$\sum_{\substack{\boldsymbol{p} \\ \varepsilon_p = \varepsilon}} T_{\boldsymbol{w}(\boldsymbol{p}'),\boldsymbol{p}} \, \overline{T_{\boldsymbol{w}(\boldsymbol{p}''),\boldsymbol{p}}} = 0 \quad \text{if } \boldsymbol{p}' \neq \boldsymbol{p}'', \tag{E1}$$

$$M_{\boldsymbol{p}'} = \sum_{\substack{\boldsymbol{p} \\ \varepsilon_p = \varepsilon}} |T_{\boldsymbol{w}(\boldsymbol{p}'),\boldsymbol{p}}|^2 \sim \sum_{\substack{\boldsymbol{p} \\ \varepsilon_p = \varepsilon}} 1 \equiv \mathcal{M}_\varepsilon, \tag{E2}$$

where the bar stands for complex conjugation. Moreover, $T_{\boldsymbol{\omega},\boldsymbol{p}}$ are arbitrary if $\omega_x + \omega_y + \omega_z \neq \varepsilon_p/\hbar$. When $\omega_x + \omega_y + \omega_z = \varepsilon_p/\hbar$ but $\boldsymbol{\omega}$ is not in the image of $\boldsymbol{w}$, then $T_{\boldsymbol{\omega},\boldsymbol{p}} = 0$: this set of $\boldsymbol{\omega}$ values has vanishing measure when the moments $\boldsymbol{p}$ vary continuously (i.e., for infinitely large size $L_{x,y,z}$), because the function $\boldsymbol{w}$ becomes surjective in $\mathbb{R}^3$. A specific example from the above defined class of coefficients $T_{\boldsymbol{\omega},\boldsymbol{p}}$ has been considered in the different context of permutationally invariant generalizations of Jacobi coordinates in many-body problems [191].

1. Master equation

Consider the bath in the grand canonical state and so large that it is not substantially perturbed by the interaction with the substance. The master equation of the substance dynamics is then derived by tracing out the bath degrees of freedom and applying the standard weak-coupling regime (Born, Markov, and secular approximations [192,193]):

$$\frac{d\varrho}{dt} = \mathbb{L}[\varrho] = -\frac{i}{\hbar}[H + \lambda^2 H_{LS}, \varrho] + \sum_{\substack{\boldsymbol{p},\boldsymbol{p}',\boldsymbol{p}'' \\ \varepsilon_p = \varepsilon_{p'} = \varepsilon_{p''}}} \frac{\lambda^2}{\hbar^2} \gamma_p \big(n(\varepsilon_p) + 1\big) T_{\boldsymbol{w}(\boldsymbol{p}''),\boldsymbol{p}} \, T_{\boldsymbol{w}(\boldsymbol{p}''),\boldsymbol{p}'}^\dagger \left(a_p \varrho \, a_{p'}^\dagger - \tfrac{1}{2}\big\{a_{p'}^\dagger a_p, \varrho\big\}\right)$$

$$+ \sum_{\substack{\boldsymbol{p},\boldsymbol{p}',\boldsymbol{p}'' \\ \varepsilon_p = \varepsilon_{p'} = \varepsilon_{p''}}} \frac{\lambda^2}{\hbar^2} \gamma_p \, n(\varepsilon_p) T_{\boldsymbol{w}(\boldsymbol{p}''),\boldsymbol{p}}^\dagger \, T_{\boldsymbol{w}(\boldsymbol{p}''),\boldsymbol{p}'} \left(a_p^\dagger \varrho \, a_{p'} - \tfrac{1}{2}\big\{a_{p'} a_p^\dagger, \varrho\big\}\right), \tag{E3}$$

where $\gamma_p = 2\pi h^2(\varepsilon_p)$, the occupation number of the bath mode with energy ε is $n(\varepsilon) = (e^{\beta(\varepsilon-\mu)} - 1)^{-1}$, and

$$H_{LS} = \sum_{\substack{\boldsymbol{p},\boldsymbol{p}',\boldsymbol{p}'' \\ \varepsilon_p=\varepsilon_{p'}=\varepsilon_{p''}}} \Delta_p \, T_{w(\boldsymbol{p}''),\boldsymbol{p}} \, T^\dagger_{w(\boldsymbol{p}''),\boldsymbol{p}'} \, a^\dagger_{\boldsymbol{p}} a_{\boldsymbol{p}'} \qquad \text{(E4)}$$

is the Lamb shift Hamiltonian induced by the interaction with the bath, with

$$\Delta_p = \int d\omega \, \frac{h^2(\hbar\omega)}{\varepsilon_p - \hbar\omega} \qquad \text{(E5)}$$

(where $\int$ stands for the Cauchy principal value).

In order to decouple the dynamical degrees of freedom, it is convenient to rewrite Eq. (E3) in terms of the rotated modes defined by the bosonic operators

$$A_{\boldsymbol{p}} = \frac{1}{\sqrt{M_{\boldsymbol{p}}}} \sum_{\substack{\boldsymbol{p}' \\ \varepsilon_{p'}=\varepsilon_p}} T_{w(\boldsymbol{p}),\boldsymbol{p}'} \, a_{\boldsymbol{p}'} \qquad \text{(E6)}$$

with $M_{\boldsymbol{p}} = \mathcal{O}(\mathcal{M}_{\varepsilon_p})$ from Eq. (E2), and $[A_{\boldsymbol{p}}, A^\dagger_{\boldsymbol{p}'}] = \delta_{\boldsymbol{p},\boldsymbol{p}'}$. One then computes

$$\frac{d\varrho}{dt} = \mathbb{L}[\varrho] = -\frac{i}{\hbar}[H + \lambda^2 H_{LS}, \varrho] + \frac{\lambda^2}{\hbar^2} \sum_{\boldsymbol{p}} \gamma_p \, M_{\boldsymbol{p}}$$

$$\times \left[(n(\varepsilon_p) + 1)\left(A_{\boldsymbol{p}} \varrho \, A^\dagger_{\boldsymbol{p}} - \tfrac{1}{2}\{A^\dagger_{\boldsymbol{p}} A_{\boldsymbol{p}}, \varrho\} \right) \right.$$

$$\left. + n(\varepsilon_p)\left(A^\dagger_{\boldsymbol{p}} \varrho \, A_{\boldsymbol{p}} - \tfrac{1}{2}\{A_{\boldsymbol{p}} A^\dagger_{\boldsymbol{p}}, \varrho\} \right) \right], \quad \text{(E7)}$$

$$H_{LS} = \sum_{\boldsymbol{p}} \Delta_p \, M_{\boldsymbol{p}} \, A^\dagger_{\boldsymbol{p}} A_{\boldsymbol{p}}, \qquad \text{(E8)}$$

$$H = \sum_{\boldsymbol{p}} \varepsilon_p \, A^\dagger_{\boldsymbol{p}} A_{\boldsymbol{p}}, \qquad \text{(E9)}$$

which describe the dissipative dynamics of independent bosonic modes whose steady state is the grand canonical state [145].

In thermochemical engines, the system volume $V(t)$ (and $L_x(t)$, $L_y(t)$, and $L_z(t)$), the chemical potential $\mu(t)$, and the inverse temperature $\beta(t)$ of the bath change in time, so that the master equation generator $\mathbb{L}$ is time-dependent (similar to those derived in Refs. [194–198]) and the steady state at time t is the time-dependent grand canonical state

$$\varrho_{\text{rev}}(t) = \frac{e^{-\beta(t)\left(H(t)-\mu(t)N(t)\right)}}{\text{Tr}\left(e^{-\beta(t)\left(H(t)-\mu(t)N(t)\right)}\right)}. \qquad \text{(E10)}$$

Recall that the Hamiltonian H and the number operator N depend on the volume, through their eigenvectors and the eigenvalues of H, and therefore vary in time. Slow

dynamics described by the master equation (E3) approximates equilibrium quasistatic transformations if $\varrho_{\text{rev}}(t)$ is the unique instantaneous steady state. Note, however, that, if $\gamma_{\tilde{p}} = 0$ for some value $\tilde{p}$, also the instantaneous eigenstates of the Hamiltonian H where all particles occupy modes with momenta $\boldsymbol{p}$ and $p^2 = \tilde{p}^2$ are instantaneous steady states. We therefore assume $\gamma_p \neq 0$ for all finite p, in order to ensure that $\varrho_{\text{rev}}(t)$ is the unique instantaneous steady state at time t.

Before deriving the dynamics at long times, the next subsection introduces some approximations for large volumes that will be used later, e.g., for approximating the volume derivatives of H and N.

2. Continuum approximation

The limit of large size allows for approximating the discrete momenta $\boldsymbol{p} = 2\pi\hbar \, (n_x/L_x, n_y/L_y, n_z/L_z)$ with continuous variable $\boldsymbol{p} = (p_x, p_y, p_z) \in \mathbb{R}^3$. One then estimates the unconstrained sum of $\boldsymbol{p}$ with arbitrary operators f :

$$\sum_{\boldsymbol{p}} f(\boldsymbol{p}) \simeq \frac{V}{(2\pi\hbar)^3} \int d\boldsymbol{p} \, f(\boldsymbol{p}). \qquad \text{(E11)}$$

Applications are as follows:

$$H \simeq \frac{V}{(2\pi\hbar)^3} \int_{\mathbb{R}^3} d\boldsymbol{p} \, \varepsilon_p a^\dagger_{\boldsymbol{p}} a_{\boldsymbol{p}}, \qquad \text{(E12)}$$

$$N \simeq \frac{V}{(2\pi\hbar)^3} \int_{\mathbb{R}^3} d\boldsymbol{p} \, a^\dagger_{\boldsymbol{p}} a_{\boldsymbol{p}}. \qquad \text{(E13)}$$

Within the continuum approximation, momenta are continuous variables that range over a volume-independent domain, i.e., $\mathbb{R}^3$, so that the energy ε_p as well as the creation and annihilation operators, $a^\dagger_{\boldsymbol{p}}$ and $a_{\boldsymbol{p}}$, no longer depend on the volume. Therefore, this approximation provides a simple estimation of the following volume derivatives:

$$\frac{\partial H}{\partial V} \simeq \frac{H}{V}, \qquad \text{(E14)}$$

$$\frac{\partial N}{\partial V} \simeq \frac{N}{V}. \qquad \text{(E15)}$$

The sum of $\boldsymbol{p}'$ constrained to $2m\varepsilon_{p'} = (2\pi\hbar)^2(n_x'^2/L_x^2 + n_y'^2/L_y^2 + n_z'^2/L_z^2) = p^2 = 2m\varepsilon_p$, as in the master equation (E3), is approximated with the surface integral over the ellipsoid with semiaxes $(2\pi\hbar)^2/(pL_x)^2$, $(2\pi\hbar)^2/(pL_y)^2$, and $(2\pi\hbar)^2/(pL_z)^2$, when the energy ε_p is larger than $\lambda_T^2/(\beta L_z^2)$. This energy value is the energy contribution due to the smallest nonzero component of the momentum along the z axis. Below this energy, particles have vanishing momenta along the z axis, and the sum of $\boldsymbol{p}'$ is constrained to $(2\pi\hbar)^2(n_x'^2/L_x^2 + n_y'^2/L_y^2) = p^2$, and approximated with the surface integral over the ellipse with semiaxes $(2\pi\hbar)^2/(pL_x)^2$ and $(2\pi\hbar)^2/(pL_y)^2$ when $\varepsilon_p \geqslant \lambda_T^2/(\beta L_y^2)$. If $\varepsilon_p < \lambda_T^2/(\beta L_y^2)$, also momenta along the y axis vanish,

and the sum of $\boldsymbol{p}'$ is constrained to $(2\pi\hbar n'_x/L_x)^2 = p^2$, when $\varepsilon_p \geqslant \lambda_T^2/(\beta L_x^2)$. All particles with energy smaller than $\lambda_T^2/(\beta L_x^2)$ have vanishing momenta such that $\varepsilon_p = \varepsilon_{p'} = 0$. Therefore, one obtains

$$
\sum_{\substack{\boldsymbol{p}' \\ \varepsilon_p = \varepsilon_{p'}}} f(\boldsymbol{p},\boldsymbol{p}') = \sum_{n'_x,n'_y,n'_z} f(\boldsymbol{p},\boldsymbol{p}')\,\delta_{(2\pi\hbar)^2\left(\frac{n'^2_x}{L^2_x}+\frac{n'^2_y}{L^2_y}+\frac{n'^2_z}{L^2_z}\right),p^2} = f(\boldsymbol{0},\boldsymbol{0}) + \sum_{n'_x\neq 0} f(\boldsymbol{p},\boldsymbol{p}')\,\delta_{\left(\frac{2\pi\hbar n'_x}{L_x}\right)^2,p^2}
$$

$$
+ \sum_{n'_x,n'_y\neq 0} f(\boldsymbol{p},\boldsymbol{p}')\,\delta_{(2\pi\hbar)^2\left(\frac{n'^2_x}{L^2_x}+\frac{n'^2_y}{L^2_y}\right),p^2} + \sum_{n'_x,n'_y,n'_z\neq 0} f(\boldsymbol{p},\boldsymbol{p}')\,\delta_{(2\pi\hbar)^2\left(\frac{n'^2_x}{L^2_x}+\frac{n'^2_y}{L^2_y}+\frac{n'^2_z}{L^2_z}\right),p^2}
$$

$$
\simeq \begin{cases} \dfrac{L_xL_yp^2}{(2\pi\hbar)^2}\displaystyle\int_0^\pi \sin\vartheta\,d\vartheta\int_0^{2\pi} d\varphi\, f(\boldsymbol{p},\boldsymbol{p}')\sqrt{\cos^2\vartheta + \dfrac{L_z^2}{L_x^2}\sin^2\vartheta\cos^2\varphi + \dfrac{L_z^2}{L_y^2}\sin^2\vartheta\sin^2\varphi} & \text{if } \varepsilon_p \geqslant \dfrac{\lambda_T^2}{\beta L_z^2}, \\[3mm] \dfrac{L_xp}{2\pi\hbar}\displaystyle\int_0^{2\pi} d\varphi\, f(\boldsymbol{p},\boldsymbol{p}')\sqrt{\sin^2\varphi + \dfrac{L_y^2}{L_x^2}\cos^2\varphi} & \text{if } \dfrac{\lambda_T^2}{\beta L_y^2} \leqslant \varepsilon_p < \dfrac{\lambda_T^2}{\beta L_z^2}, \\[3mm] f(\boldsymbol{p},\boldsymbol{p}) + f(\boldsymbol{p},-\boldsymbol{p}) & \text{if } \dfrac{\lambda_T^2}{\beta L_x^2} \leqslant \varepsilon_p < \dfrac{\lambda_T^2}{\beta L_y^2}, \\[3mm] f(\boldsymbol{0},\boldsymbol{0}) & \text{if } \varepsilon_p = 0. \end{cases}
$$

$$(\text{E16})$$

Here $\boldsymbol{p}'$ is identified in spherical coordinates by the polar and the azimuthal angles with respect to the equatorial x-y plane, ϑ and φ respectively, and the modulus $p' = p$. Recall that $L_x \geqslant L_y \geqslant L_z$, such that the square roots in Eq. (E16) are bounded. The careful treatment of the energy scales $\lambda_T^2/(\beta L_{x,y,z}^2)$ allows us to identify the relevant contributions to heat and work corrections in irreversible transformations with dD-BECs.

Equation (E16) is also used to approximate $\mathcal{M}_{\varepsilon_p}$ and thus to estimate the size scaling of $M_{\mathbf{p}}$ in Eq. (E2). Indeed, using $f(\boldsymbol{p},\boldsymbol{p}') = 1$ in Eq. (E16), one obtains

$$
\mathcal{M}_{\varepsilon_p} \simeq \begin{cases} \dfrac{L_xL_y p^2}{(2\pi\hbar)^2}\,C & \text{if } \varepsilon_p \geqslant \dfrac{\lambda_T^2}{\beta L_z^2}, \\[3mm] \dfrac{L_x p}{2\pi\hbar}\,G & \text{if } \dfrac{\lambda_T^2}{\beta L_y^2} \leqslant \varepsilon_p < \dfrac{\lambda_T^2}{\beta L_z^2}, \\[3mm] 2 & \text{if } \dfrac{\lambda_T^2}{\beta L_x^2} \leqslant \varepsilon_p < \dfrac{\lambda_T^2}{\beta L_y^2}, \\[3mm] 1 & \text{if } \varepsilon_p = 0, \end{cases} \qquad (\text{E17})
$$

with

$$
C = \int_0^\pi \sin\vartheta\,d\vartheta\int_0^{2\pi} d\varphi
$$
$$
\times \sqrt{\cos^2\vartheta + \frac{L_z^2}{L_x^2}\sin^2\vartheta\cos^2\varphi + \frac{L_z^2}{L_y^2}\sin^2\vartheta\sin^2\varphi},
$$
$$(\text{E18})$$

$$
G = \int_0^{2\pi} d\varphi\,\sqrt{\sin^2\varphi + \frac{L_y^2}{L_x^2}\cos^2\varphi}. \qquad (\text{E19})
$$

3. Instantaneous relaxation times

The instantaneous relaxation time is the time the dynamics takes to approach the steady state as if the master equation (E3) had time-independent coefficients evaluated at t. From the structure of single-mode master equations that are quadratic in the bosonic operators [199,200], as in Eq. (E7), the relaxation time of each mode $(A_{\boldsymbol{p}}, A_{\boldsymbol{p}}^\dagger)$ is $\theta_{\boldsymbol{p}}(t) = \hbar^2/(\lambda^2\gamma_p M_{\boldsymbol{p}})$, where $\gamma_p = 2\pi h^2(\varepsilon_p)$ and $M_{\boldsymbol{p}}$ is given in Eq. (E2). Recall that $M_{\boldsymbol{p}} \sim \mathcal{M}_{\varepsilon_p}$ from Eq. (E2), and the size scaling of $M_{\boldsymbol{p}}$ is given by Eq. (E17). Therefore, the instantaneous relaxation times for $\varepsilon_p \geqslant \lambda_T^2/\beta L_z^2$ are estimated at large size by

$$
\theta_{\boldsymbol{p}} \sim \frac{4\pi^2\hbar^4}{\lambda^2\gamma_p p^2 L_xL_y}\left(\int_0^\pi \sin\vartheta\,d\vartheta\int_0^{2\pi} d\varphi \right.
$$
$$
\times \left(\cos^2\vartheta + \frac{L_z^2}{L_x^2}\sin^2\vartheta\cos^2\varphi \right.
$$
$$
\left.\left. + \frac{L_z^2}{L_y^2}\sin^2\vartheta\sin^2\varphi\right)^{1/2}\right)^{-1}. \qquad (\text{E20})
$$

For later convenience, we also define the maximum relaxation time $\bar{\theta} = \max_{\boldsymbol{p},t}\theta_{\boldsymbol{p}}(t)$ which scales as $\mathcal{O}(L_z/V)$.

The number of bosonic modes with energy $\varepsilon_p < \lambda_T^2/\beta L_z^2$ is vanishingly small for large size and they provide negligible contributions to the substance state and to instantaneous relaxation times (E20) without BECs. These contributions are negligible also in 2D-BEC or 1D-BEC phases where the condensates consist of all momenta lying respectively in the x-y plane or along the x direction. The 0D-BEC consists only of the ground state which contributes to thermodynamic quantities with vanishing energy $\varepsilon_0 = 0$, and with particle number relaxing to $\langle a_0^\dagger a_0 \rangle = f\mathcal{N} = \mathcal{N} - V\rho_c$ when the number of noncondensed particles approaches the critical value $V\rho_c$. As Eq. (E20) gives the relevant instantaneous relaxation times for almost all excited states (except the aforementioned vanishingly small number of modes), it does also for 0D-BECs.

4. Time evolution

For infinitely slow dynamics compared to the instantaneous relaxation rates, relaxation to $\rho_{\rm rev}(t)$ at each t happens in negligible time, recovering an equilibrium quasistatic transformation. Given a large but finite total time of the dynamics τ, the time evolution is a perturbation of the quasistatic transformation [144]. Consider then the following perturbative expansion:

$$\varrho(t) = \varrho_{\rm rev}(t) + \frac{\bar\theta}{\tau}\varrho_{\rm irr}(t) + \mathcal{O}\left(\frac{\bar\theta}{\tau}\right)^2. \qquad (E21)$$

Defining $t' = t/\tau \in [0,1]$, the master equation reads $d\varrho/dt' = \tau\,\mathbb{L}[\varrho]$. Plugging the expansion (E21) into this master equation provides a self-consistency condition:

$$\frac{d\varrho_{\rm rev}}{dt'} = \bar\theta\,\mathbb{L}[\varrho_{\rm irr}]. \qquad (E22)$$

The left-hand side of the self-consistency condition (E22) is

$$\begin{aligned}
\frac{d\varrho_{\rm rev}}{dt'} &= \frac{\partial\mu}{\partial t'}\,\beta\big(N - {\rm Tr}(N\varrho_{\rm rev})\big)\varrho_{\rm rev} \\
&\quad - \frac{\partial V}{\partial t'}\,\beta\bigg(\frac{\partial(H-\mu N)}{\partial V} \\
&\quad - {\rm Tr}\bigg(\varrho_{\rm rev}\frac{\partial(H-\mu N)}{\partial V}\bigg)\bigg)\varrho_{\rm rev} \\
&\quad - \frac{\partial\beta}{\partial t'}\big(H - \mu N - {\rm Tr}((H-\mu N)\varrho_{\rm rev})\big)\varrho_{\rm rev}.
\end{aligned} \qquad (E23)$$

The contribution proportional to $\partial_{t'}\beta$ vanishes in isothermal transformations, as those considered in this paper. The volume derivatives within the continuum approximation are expressed in Eqs. (E14) and (E15).

The self-consistency condition (E22) will be exploited to derive the first-order correction to the quasistatic evolution, namely $\varrho_{\rm irr}$. First, write the general form of $\varrho_{\rm irr}$, by noting that the master equation (E3) [or equivalently Eq. (E7)] is quadratic in the field operators $\{a_p, a_p^\dagger\}_p$, as well as in $\{A_p, A_p^\dagger\}_p$, and therefore preserves the Gaussianity of ϱ. Consequently, the exact state can be written as

$$\varrho(t) = \frac{\exp[-\beta H(t) + \beta\mu(t)N(t) + (\beta\bar\theta/\tau)X(t)]}{{\rm Tr}\,\exp[-\beta H(t) + \beta\mu(t)N(t) + (\beta\bar\theta/\tau)X(t)]}, \qquad (E24)$$

with a quadratic Hermitian operator $X = \sum_{p,p'}\chi_{p,p'}A_p^\dagger A_{p'}$. Expanding in powers of $\bar\theta/\tau$ [201],

$$\begin{aligned}
& e^{-\beta\left(H-\mu N - \frac{\bar\theta}{\tau}X\right)} \\
&= e^{-\beta(H-\mu N)} + \frac{\bar\theta}{\tau}\int_0^\beta ds\, e^{-s(H-\mu N)}Xe^{-(\beta-s)(H-\mu N)} \\
&\quad + \mathcal{O}\left(\frac{\bar\theta}{\tau}\right)^2,
\end{aligned} \qquad (E25)$$

$$\begin{aligned}
& {\rm Tr}\left(e^{-\beta\left(H-\mu N - \frac{\bar\theta}{\tau}X\right)}\right) \\
&= {\rm Tr}\big(e^{-\beta(H-\mu N)}\big) + \frac{\beta\bar\theta}{\tau}{\rm Tr}\big(Xe^{-\beta(H-\mu N)}\big) \\
&\quad + \mathcal{O}\left(\frac{\bar\theta}{\tau}\right)^2,
\end{aligned} \qquad (E26)$$

and using canonical commutation relations of bosonic operators, $[A_p, A_{p'}^\dagger] = \delta_{p,p'}$, one obtains for $\varrho_{\rm irr}$

$$\begin{aligned}
\varrho_{\rm irr} &\simeq \tau(\varrho - \varrho_{\rm rev}) \\
&\simeq -\beta\,{\rm Tr}(X\varrho_{\rm rev})\varrho_{\rm rev} \\
&\quad + \frac{1}{Z_{\rm rev}}\int_0^\beta ds\, e^{-s(H-\mu N)}Xe^{-(\beta-s)(H-\mu N)} \\
&= \sum_{p,p'}\frac{e^{\beta(\varepsilon_{p'}-\varepsilon_p)}-1}{\varepsilon_{p'}-\varepsilon_p}\chi_{p,p'}A_p^\dagger A_{p'}\varrho_{\rm rev} \\
&\quad - \beta\,{\rm Tr}(X\varrho_{\rm rev})\varrho_{\rm rev}.
\end{aligned} \qquad (E27)$$

Using the expression (E27) and after algebraic manipulations of bosonic operators, one finds

$$\begin{aligned}
\mathbb{L}[\varrho_{\rm irr}] &= -\frac{i}{\hbar}\sum_{p,k}\frac{e^{\beta(\varepsilon_k-\varepsilon_p)}-1}{\varepsilon_k-\varepsilon_p}\chi_{p,k}(\varepsilon_p \\
&\quad + \lambda^2 M_p\Delta_p)A_p^\dagger A_k\varrho_{\rm rev}
\end{aligned}$$

$$+ \frac{i}{\hbar} \sum_{\boldsymbol{p},\boldsymbol{k}} \frac{e^{\beta(\varepsilon_p - \varepsilon_k)} - 1}{\varepsilon_p - \varepsilon_k} \chi_{\boldsymbol{k},\boldsymbol{p}}(\varepsilon_p$$

$$+ \lambda^2 M_{\boldsymbol{p}} \Delta_p) A_{\boldsymbol{k}}^\dagger A_{\boldsymbol{p}} \varrho_{\text{rev}}$$

$$+ \frac{\lambda^2 \beta}{\hbar^2} \sum_{\boldsymbol{p}} \gamma_p M_{\boldsymbol{p}} \chi_{\boldsymbol{p},\boldsymbol{p}} n(\varepsilon_p) \varrho_{\text{rev}}$$

$$- \frac{\lambda^2}{2\hbar^2} \sum_{\boldsymbol{p},\boldsymbol{k}} \frac{e^{\beta(\varepsilon_k - \varepsilon_p)} - 1}{\varepsilon_k - \varepsilon_p} \gamma_p M_{\boldsymbol{p}} \chi_{\boldsymbol{p},\boldsymbol{k}} A_{\boldsymbol{p}}^\dagger A_{\boldsymbol{k}} \varrho_{\text{rev}}$$

$$- \frac{\lambda^2}{2\hbar^2} \sum_{\boldsymbol{p},\boldsymbol{k}} \frac{e^{\beta(\varepsilon_p - \varepsilon_k)} - 1}{\varepsilon_p - \varepsilon_k} \gamma_p M_{\boldsymbol{p}} \chi_{\boldsymbol{k},\boldsymbol{p}} A_{\boldsymbol{k}}^\dagger A_{\boldsymbol{p}} \varrho_{\text{rev}}.$$

$$\text{(E28)}$$

Since the operators $A_{\boldsymbol{p}}^\dagger A_{\boldsymbol{p}'} \varrho_{\text{rev}}$ for all $\boldsymbol{p}, \boldsymbol{p}'$, and ϱ_{rev} form an operator basis in the self-consistency condition (E22), $\chi_{\boldsymbol{p},\boldsymbol{p}'}$ are determined by equating the coefficients of these operators between the left- and right-hand sides of Eq. (E22). At this point, note that the master equation (E3) is symmetric with respect to rotations of momenta $\boldsymbol{p}$ and $\boldsymbol{p}'$ where $p = p'$, and so is the time evolution $\varrho(t)$ (if the initial state has the same symmetry), and thus $\chi_{\boldsymbol{p},\boldsymbol{p}'} \equiv \chi_p$ are the same for all such $\boldsymbol{p}$ and $\boldsymbol{p}'$. Let us focus on the derivation of $\chi_{\boldsymbol{p},\boldsymbol{p}} = \chi_p$, which appears in the coefficient of the operator $A_{\boldsymbol{p}}^\dagger A_{\boldsymbol{p}} \varrho_{\text{rev}}$ in Eq. (E28). This coefficient must be equal to the similar coefficient in Eq. (E23), according to the self-consistency condition (E22). Notice also that the substance Hamiltonian and particle number operators can be rewritten as $H = \sum_{\boldsymbol{p}} \varepsilon_p A_{\boldsymbol{p}}^\dagger A_{\boldsymbol{p}}$ and $N = \sum_{\boldsymbol{p}} A_{\boldsymbol{p}}^\dagger A_{\boldsymbol{p}}$, respectively, since the rotated modes $A_{\boldsymbol{p}}$ are linear combinations of all the original modes $a_{\boldsymbol{p}}$ corresponding to the same energy.

The computation sketched above results in

$$\chi_p = \frac{2\hbar^2}{\lambda^2 \beta \bar{\theta} M_{\boldsymbol{p}}} (\xi \mu + \tilde{\xi} \varepsilon_p), \qquad \text{(E29)}$$

where

$$\xi = -\frac{\beta}{V} \frac{\partial V}{\partial t'} - \frac{\partial \beta}{\partial t'} - \frac{\beta}{\mu} \frac{\partial \mu}{\partial t'}, \qquad \text{(E30)}$$

$$\tilde{\xi} = \frac{\beta}{V} \frac{\partial V}{\partial t'} + \frac{\partial \beta}{\partial t'} \qquad \text{(E31)}$$

depend on the bath external parameters (volume, chemical potential, and temperature) and their time derivatives. Note that ξ and $\tilde{\xi}$ are intensive and remain finite also in BEC phases where $\mu \to 0$.

Recalling that $M_{\boldsymbol{p}} \sim \mathcal{M}_{\varepsilon_p}$, $M_{\boldsymbol{p}}$ are estimated by Eq. (E17), whose size scalings are used later in the computation of work and heat corrections in the noncondensed and in the dD-BEC phases. Moreover, only the terms with

$p = p'$ in the expression (E27) contribute to the first corrections to work and heat given by ρ_{irr}, as shown in the next subsection.

5. Work and heat corrections

The heat and work exchanges of irreversible transformations are the right-hand sides of Eqs. (D1), (D3), and (D4). Plugging there the expansion (E21), the approximations (24) and (25) are derived with the following first-order contributions in $\bar{\theta}/\tau$:

$$W_{\text{irr}}^{\text{M}} = -\int_0^1 dt' \, \text{Tr} \left(\varrho_{\text{irr}} \left(\frac{\partial H}{\partial t'} - \mu \frac{\partial N}{\partial t'} \right) \right), \qquad \text{(E32)}$$

$$W_{\text{irr}}^{\text{C}} = -\int_0^1 dt' \, \mu \, \text{Tr} \left(N \frac{\partial \varrho_{\text{irr}}}{\partial t'} + \varrho_{\text{irr}} \frac{\partial N}{\partial t'} \right)$$

$$= \mu(0) \, \text{Tr}\big(\varrho_{\text{irr}}(0) N(0)\big) - \mu(\tau) \, \text{Tr}\big(\varrho_{\text{irr}}(\tau) N(\tau)\big)$$

$$+ \int_0^1 dt' \, \frac{\partial \mu}{\partial t'} \, \text{Tr}(N \varrho_{\text{irr}}), \qquad \text{(E33)}$$

$$Q_{\text{irr}} = \int_0^1 dt' \, \text{Tr} \left((H - \mu N) \frac{\partial \varrho_{\text{irr}}}{\partial t'} \right)$$

$$= \text{Tr}\big((H(\tau) - \mu(\tau) N(\tau)) \varrho_{\text{irr}}(\tau)\big)$$

$$- \text{Tr}\big((H(0) - \mu(0) N(0)) \varrho_{\text{irr}}(0)\big)$$

$$- \int_0^1 dt' \, \text{Tr} \left(\varrho_{\text{irr}} \frac{\partial (H - \mu N)}{\partial t'} \right), \qquad \text{(E34)}$$

where integration by parts has been used. Note that the traces involving the time derivatives of N and H can be written, by virtue of Eqs. (E14) and (E15), as

$$\text{Tr} \left(\varrho_{\text{irr}} \frac{\partial N}{\partial t'} \right) = \text{Tr} \left(\varrho_{\text{irr}} \frac{\partial N}{\partial V} \right) \frac{\partial V}{\partial t'} \simeq \frac{\text{Tr}(N \varrho_{\text{irr}})}{V} \frac{\partial V}{\partial t'}, \qquad \text{(E35)}$$

$$\text{Tr} \left(\varrho_{\text{irr}} \frac{\partial H}{\partial t'} \right) = \text{Tr} \left(\varrho_{\text{irr}} \frac{\partial H}{\partial V} \right) \frac{\partial V}{\partial t'} \simeq \frac{\text{Tr}(H \varrho_{\text{irr}})}{V} \frac{\partial V}{\partial t'}. \qquad \text{(E36)}$$

Therefore, the traces $\text{Tr}(N \varrho_{\text{irr}})$ and $\text{Tr}(H \varrho_{\text{irr}})$ are the only relevant traces to be computed in Eqs. (E32), (E33), and (E34). Since the operators H and N are linear combinations of $A_{\boldsymbol{p}}^\dagger A_{\boldsymbol{p}}$, only the terms with $\boldsymbol{p} = \boldsymbol{p}'$ in the expression (E27) for ϱ_{irr} contribute to the computation of these traces. Using the expression (E27), $\text{Tr}((A_{\boldsymbol{p}}^\dagger A_{\boldsymbol{p}})^2 \varrho_{\text{rev}}) = 2n^2(\varepsilon_p) + n(\varepsilon_p)$, and the continuum approximation, one

obtains

$$\mathrm{Tr}(N\varrho_{\mathrm{irr}}) = \beta \sum_{\boldsymbol{p}} \chi_p \left(n^2(\varepsilon_p) + n(\varepsilon_p)\right)$$

$$\simeq \frac{\beta V}{(2\pi\hbar)^3} \int d\boldsymbol{p}\, \chi_p \left(n^2(\varepsilon_p) + n(\varepsilon_p)\right)$$

$$+ \frac{\beta V^{d\mathrm{D}}}{(2\pi\hbar)^d} \int d\boldsymbol{p}\, \delta(\boldsymbol{p} - \boldsymbol{p}^{d\mathrm{D}})\chi_p$$

$$\times \left(n^2(\varepsilon_p) + n(\varepsilon_p)\right), \tag{E37}$$

$$\mathrm{Tr}(H\varrho_{\mathrm{irr}}) = \beta \sum_{\boldsymbol{p}} \varepsilon_p\, \chi_p \left(n^2(\varepsilon_p) + n(\varepsilon_p)\right)$$

$$\simeq \frac{\beta V}{(2\pi\hbar)^3} \int d\boldsymbol{p}\, \varepsilon_p\, \chi_p \left(n^2(\varepsilon_p) + n(\varepsilon_p)\right)$$

$$+ \frac{\beta V^{d\mathrm{D}}}{(2\pi\hbar)^d} \int d\boldsymbol{p}\, \delta(\boldsymbol{p} - \boldsymbol{p}^{d\mathrm{D}})\varepsilon_p\, \chi_p$$

$$\times \left(n^2(\varepsilon_p) + n(\varepsilon_p)\right). \tag{E38}$$

The last terms in Eqs. (E37) and (E38) are the contributions of the dD-BEC, as described in Appendix B, formed of energy eigenstates with momenta $\boldsymbol{p}^{d\mathrm{D}}$, where $\boldsymbol{p}^{2\mathrm{D}} = (p_x, p_y, 0)$ are momenta in the x-y plane, $\boldsymbol{p}^{1\mathrm{D}} = (p_x, 0, 0)$ are momenta along the x axis, and $\boldsymbol{p}^{0\mathrm{D}} = (0, 0, 0)$, and $V^{2\mathrm{D}} = L_x L_y$, $V^{1\mathrm{D}} = L_x$, and $V^{0\mathrm{D}} = 1$. These contributions emerge only after the trace and not in the operators because of the singularity of bosonic occupancies when $e^{\beta\mu} \to 1$. On the other hand, if $e^{\beta\mu} \neq 1$, the BEC contributions are negligible.

After plugging the coefficient χ_p in Eq. (E29) into Eqs. (E37) and (E38), one has to assume the functional form of γ_p in order to compute the integrals. Therefore, consider the general power series $\gamma_p^{-1} = \sum_j \kappa_j \varepsilon_p^{\alpha_j}$. Furthermore, the change of variable $p \to \varepsilon_p =: \varepsilon$ in Eqs. (E37) and (E38) results in the following types of integrals:

$$\int d\boldsymbol{p}\, f(p) = (2m)^{3/2}\pi \int_0^\infty d\varepsilon\, \sqrt{\varepsilon} f\left(\sqrt{2m\varepsilon}\right), \tag{E39}$$

$$\int d\boldsymbol{p}\, \delta(\boldsymbol{p} - \boldsymbol{p}^{d\mathrm{D}})f(p) = \frac{(2\pi m)^{d/2}}{\Gamma\left(\frac{d}{2}\right)}$$

$$\times \int_0^\infty d\varepsilon\, \varepsilon^{d/2-1} f\left(\sqrt{2m\varepsilon}\right), \tag{E40}$$

$$\int d\boldsymbol{p}\, \delta(\boldsymbol{p} - \boldsymbol{p}^{0\mathrm{D}})f(p) = f(0), \tag{E41}$$

with $d = 1, 2$ in Eq. (E40). The traces (E37) and (E38) are then linear combinations of the following prototypical

integrals:

$$I_a^A = \int_A^\infty d\varepsilon\, \varepsilon^a \left(n^2(\varepsilon) + n(\varepsilon)\right)$$

$$= \int_A^\infty d\varepsilon\, \varepsilon^a \sum_{j=1}^\infty j e^{j\beta(\mu-\varepsilon)} = \sum_{j=1}^\infty \frac{e^{j\beta\mu}}{j^a \beta^{a+1}} \Gamma(a+1, j\beta A), \tag{E42}$$

where A is one of the energy bounds in Eq. (E16), and $\Gamma(s, z)$ is the incomplete Gamma function. The series representation

$$\Gamma(s, z) = \int_z^\infty dt\, t^{s-1} e^{-t}$$

$$= \Gamma(s) \left(1 - z^s e^{-z} \sum_{k=0}^\infty \frac{z^k}{\Gamma(s+k+1)}\right) \quad \text{if } -s \notin \mathbb{N} \tag{E43}$$

implies the following series:

$$I_a^A = \frac{\Gamma(a+1)}{\beta^{a+1}} \left(\mathrm{Li}_a(e^{\beta\mu})\right.$$

$$\left. - \sum_{k=0}^\infty \frac{(\beta A)^{a+k+1}}{\Gamma(a+k+2)} \mathrm{Li}_{-k-1}\left(e^{\beta(\mu-A)}\right)\right) \quad \text{if } -a \notin \mathbb{N}^+. \tag{E44}$$

For $a = -1$, the sum on the right-hand side of Eq. (E42) is approximated by an integral

$$I_{-1}^A = \int_1^\infty dj\, j e^{j\beta\mu} \Gamma(0, j\beta A) = \frac{1}{\beta^2 \mu^2(A-\mu)}$$

$$\times \left[\mu e^{\beta(\mu-A)} + (A-\mu)\left((1-\beta\mu)e^{\beta\mu}\Gamma(0, \beta A)\right.\right.$$

$$\left.\left. - \Gamma(0, \beta A - \beta\mu)\right)\right], \tag{E45}$$

where $A > 0$ and $\mu < 0$ for the ideal Bose gas have been used. We also define

$$I_a^{A,B} = \int_A^B d\varepsilon\, \varepsilon^a \left(n^2(\varepsilon) + n(\varepsilon)\right) = I_a^A - I_a^B. \tag{E46}$$

With all these manipulations, Eqs. (E37) and (E38) become

$$\mathrm{Tr}(N\varrho_{\mathrm{irr}}) \simeq \frac{2\hbar^2\sqrt{\pi\beta}L_z}{\lambda^2\lambda_T\bar{\theta}} \sum_j C\kappa_j \left(\xi\mu I^{\lambda_T^2/\beta L_z^2}_{\alpha_j-1/2} + \tilde{\xi}I^{\lambda_T^2/\beta L_z^2}_{\alpha_j+1/2}\right)$$

$$+ (\delta_{d,2} + \delta_{d,1})\left(\frac{2\pi\hbar^2\beta^{d/2-1}V^{d\mathrm{D}}}{\Gamma(d/2)\lambda^2\lambda_T^{d-2}\bar{\theta}L_xL_y} \sum_j C\kappa_j \left(\xi\mu I^{\lambda_T^2/\beta L_z^2}_{\alpha_j+d/2-2} + \tilde{\xi}I^{\lambda_T^2/\beta L_z^2}_{\alpha_j+d/2-1}\right)\right.$$

$$\left. + \frac{2\sqrt{\pi}\hbar^2\beta^{(d-1)/2}V^{d\mathrm{D}}}{\Gamma(d/2)\lambda^2\lambda_T^{d-1}\bar{\theta}L_x} \sum_j G\kappa_j \left(\xi\mu I^{\lambda_T^2/\beta L_y^2,\lambda_T^2/\beta L_z^2}_{\alpha_j+(d-3)/2} + \tilde{\xi}I^{\lambda_T^2/\beta L_y^2,\lambda_T^2/\beta L_z^2}_{\alpha_j+(d-1)/2}\right)\right)$$

$$+ \delta_{d,1}\frac{4\hbar^2\beta^{d/2}V^{d\mathrm{D}}}{\Gamma(d/2)\lambda^2\lambda_T^d\bar{\theta}} \sum_j \kappa_j \left(\xi\mu I^{\lambda_T^2/\beta L_x^2,\lambda_T^2/\beta L_y^2}_{\alpha_j+d/2-1} + \tilde{\xi}I^{\lambda_T^2/\beta L_x^2,\lambda_T^2/\beta L_y^2}_{\alpha_j+d/2}\right) + \delta_{d,0}\frac{2\hbar^2}{\lambda^2\gamma_{0,0}\bar{\theta}}\frac{\xi\mu e^{\beta\mu}}{(e^{\beta\mu}-1)^2}, \quad (E47)$$

$$\mathrm{Tr}(H\varrho_{\mathrm{irr}}) = \frac{2\hbar^2\sqrt{\pi\beta}L_z}{\lambda^2\lambda_T\bar{\theta}} \sum_j C\kappa_j \left(\xi\mu I^{\lambda_T^2/\beta L_z^2}_{\alpha_j+1/2} + \tilde{\xi}I^{\lambda_T^2/\beta L_z^2}_{\alpha_j+3/2}\right)$$

$$+ (\delta_{d,2} + \delta_{d,1})\left(\frac{2\pi\hbar^2\beta^{d/2-1}V^{d\mathrm{D}}}{\Gamma(d/2)\lambda^2\lambda_T^{d-2}\bar{\theta}L_xL_y} \sum_j C\kappa_j \left(\xi\mu I^{\lambda_T^2/\beta L_z^2}_{\alpha_j+d/2-1} + \tilde{\xi}I^{\lambda_T^2/\beta L_z^2}_{\alpha_j+d/2}\right)\right.$$

$$\left. + \frac{2\sqrt{\pi}\hbar^2\beta^{(d-1)/2}V^{d\mathrm{D}}}{\Gamma(d/2)\lambda^2\lambda_T^{d-1}\bar{\theta}L_x} \sum_j G\kappa_j \left(\xi\mu I^{\lambda_T^2/\beta L_y^2,\lambda_T^2/\beta L_z^2}_{\alpha_j+(d-1)/2} + \tilde{\xi}I^{\lambda_T^2/\beta L_y^2,\lambda_T^2/\beta L_z^2}_{\alpha_j+(d+1)/2}\right)\right)$$

$$+ \delta_{d,1}\frac{2\hbar^4\beta^{d/2}V^{d\mathrm{D}}}{\Gamma(d/2)\lambda^2\lambda_T^d\bar{\theta}} \sum_j \kappa_j \left(\xi\mu I^{\lambda_T^2/\beta L_x^2,\lambda_T^2/\beta L_y^2}_{\alpha_j+d/2} + \tilde{\xi}I^{\lambda_T^2/\beta L_x^2,\lambda_T^2/\beta L_y^2}_{\alpha_j+d/2+1}\right). \quad (E48)$$

In the absence of a BEC, only the first sum in Eqs. (E47) and (E48) contributes for large size, with $I^{\lambda_T^2/\beta L_z^2}_a$ replaced by I^0_a. In the classical limit ($z = e^{\beta\mu} \ll 1$ for ideal gases), one obtains $I^0_a = \mathcal{O}(z)$ from Eq. (B3), so that $\mathrm{Tr}(N\varrho_{\mathrm{irr}})$ and $\mathrm{Tr}(H\varrho_{\mathrm{irr}})$ scale as $\mathcal{O}(Vz\ln z)$, recalling the size scaling of the relaxation time (E20). These scalings in Eqs. (E33) and (E34) imply $W^{\mathrm{C}}_{k,\mathrm{irr}} = \mathcal{O}(Vz\ln^2 z)$ and $W^{\mathrm{C}}_{k,\mathrm{irr}} - Q_{k,\mathrm{irr}} = \mathcal{O}(Vz\ln z)$. In the quantum regime, the chemical potential is finite, the integrals I^0_a are finite, and $\mathrm{Tr}(N\varrho_{\mathrm{irr}})$ and $\mathrm{Tr}(H\varrho_{\mathrm{irr}})$ scale as $\mathcal{O}(V)$, and consequently $W^{\mathrm{C}}_{k,\mathrm{irr}} = \mathcal{O}(V)$ and $W^{\mathrm{C}}_{k,\mathrm{irr}} - Q_{k,\mathrm{irr}} = \mathcal{O}(V)$. If the system is in a BEC phase (see Appendix B), then $\mu \simeq 0$ and is much smaller than some of the $\lambda_T^2/L^2_{x,y,z}$, and the integrals I^A_a must be evaluated for both $A = \lambda_T^2/(\beta L^2_{x,y,z})$ and μ approaching zero at large size:

$$I^A_a \underset{\substack{\mu\simeq 0 \\ A\simeq 0}}{\simeq} \begin{cases} \dfrac{1}{\beta^{a+1}}\Gamma(a+1)\zeta(a) + \dfrac{\pi a}{\sin(\pi a)}\dfrac{(-\mu)^{a-1}}{\beta^2} - \dfrac{1}{a+1}\dfrac{A^{a+1}}{\beta^2(A-\mu)^2} & \text{if } 1 < a < 2, \\[3mm] -\dfrac{\ln(-\beta\mu)}{\beta^2} - \dfrac{1}{2\beta^2(1-\mu/A)^2} & \text{if } a = 1, \\[3mm] \dfrac{\pi a}{\sin(\pi a)}\dfrac{(-\mu)^{a-1}}{\beta^2} - \dfrac{1}{a+1}\dfrac{A^{a+1}}{\beta^2(A-\mu)^2} & \text{if } a < 1 \text{ and } -a \notin \mathbb{N}^+, \\[3mm] \dfrac{1}{\beta^2\mu^2}\ln\left(\dfrac{\mu}{A}\right) & \text{if } a = -1 \text{ and } -\mu \gg A, \\[3mm] \dfrac{1}{2\beta^2 A^2} & \text{if } a = -1 \text{ and } -\mu \ll A. \end{cases} \quad (E49)$$

Recall now that $\gamma_0 \neq 0$ (required for the uniqueness of the steady state as discussed at the end of Sec. E 1) and assume that γ_0 is finite. Under these conditions, one finds the series $\gamma_p^{-1} = \kappa + \sum_j \kappa_j \varepsilon_p^{\alpha_j}$ with $\kappa > 0$ and $\alpha_j > 0$ for all j: examples are the constant function $\gamma_p = \kappa$, the Lorentzian shapes $\gamma_p = 1/(\kappa + \kappa'\varepsilon_p)$ or $h(\varepsilon_p) = 1/(\sqrt{2\pi\kappa} + \kappa''\varepsilon_p)$, and the exponential functions $\gamma_p = e^{-\kappa'\varepsilon_p}/\kappa$ or $h(\varepsilon_p) = e^{-\kappa'\varepsilon_p}/\sqrt{2\pi\kappa}$. In order to identify the leading terms in Eqs. (E47)

and (E48), we exploit the scaling of the box sizes and the chemical potential in BEC phases: $L_y \gtrsim e^{\alpha L_z}\text{poly}(L_z)$ and $-\beta\mu \simeq e^{-f\,\rho L_z\lambda_T^2} \geqslant \mathcal{O}(\lambda_T^2/L_y^2)$ for 2D-BEC; $L_x \gtrsim \alpha' L_y L_z$ and $-\beta\mu \simeq \pi(f\,\rho L_y L_z \lambda_T)^{-2} \geqslant \mathcal{O}(\lambda_T^2/L_x^2)$ for 1D-BEC; and $L_x \sim L_y \sim L_z$ and $-\beta\mu = (f\,\rho V)^{-1}$ for 0D-BEC (see Appendix B). Equation (E47) becomes

$$
\mathrm{Tr}(N\varrho_{\mathrm{irr}}) \simeq
\begin{cases}
-\dfrac{2\hbar^2\kappa}{\lambda^2\beta^2\mu\bar\theta}\left(\pi C\tilde\xi + 2\sqrt\pi G\left(\xi + \dfrac{\lambda_T^2\tilde\xi}{3\beta\mu L_y^2}\right)\right) & \text{2D-BEC,} \\[14pt]
\dfrac{\hbar^2 C\kappa\lambda_T}{\lambda^2\bar\theta L_y}\sqrt{\dfrac{\pi^3}{-\beta^5\mu^3}}(\tilde\xi - 3\xi) + \dfrac{8\hbar^2\kappa\xi\mu L_x L_y^3}{\sqrt\pi\lambda^2\lambda_T^4} & \text{1D-BEC,} \\[14pt]
\dfrac{2\hbar^2\xi}{\lambda^2\gamma_0\beta^2\mu\bar\theta} & \text{0D-BEC,}
\end{cases}
$$

$$
\simeq
\begin{cases}
\dfrac{2\hbar^2\kappa}{\lambda^2\beta\bar\theta}\,e^{f\,\rho L_z\lambda_T^2}\left(\pi\,C\tilde\xi + 2\sqrt\pi G\left(\xi - \dfrac{\tilde\xi\lambda_T^2 e^{f\,\rho L_z\lambda_T^2}}{3L_y^2}\right)\right) & \text{2D-BEC,} \\[14pt]
\dfrac{\sqrt\pi\hbar^2\kappa}{\lambda^2\beta\bar\theta}\left(C(\tilde\xi - 3\xi)f^3\rho^3\lambda_T^4 L_y^2 L_z^3 - \dfrac{8\kappa\xi}{f^2\rho^2\lambda_T^6}\dfrac{L_x L_y}{L_z^2}\right) & \text{1D-BEC,} \\[14pt]
-\dfrac{2\hbar^2\xi f\,\rho V}{\lambda^2\gamma_0\beta\bar\theta} & \text{0D-BEC,}
\end{cases}
\tag{E50}
$$

where the first term of the 1D-BEC case dominates if $\alpha' L_y L_z \lesssim L_x < \mathcal{O}(L_y L_z^5)$ and the second term dominates when $L_x > \mathcal{O}(L_y L_z^5)$. The leading orders of Eq. (E48) are

$$
\mathrm{Tr}(H\varrho_{\mathrm{irr}}) \simeq
\begin{cases}
\dfrac{2\hbar^2\sqrt\pi\kappa}{\lambda^2\beta^2\bar\theta}\left(\dfrac{2G\tilde\xi L_y}{5L_z} + \left(\text{terms} \propto \tilde\xi\ln(-\beta\mu)\text{ and }\propto\tilde\xi V^0\right) - \sqrt\pi C\xi - \dfrac{G\xi\lambda_T^2}{3\beta\mu L_y^2}\right) & \text{2D-BEC,} \\[14pt]
\dfrac{3\pi\zeta\left(\frac32\right)\hbar^2 C\kappa\tilde\xi L_z}{2\lambda^2\beta^2\lambda_T\bar\theta} + \dfrac{\hbar^2\lambda_T C\kappa}{\lambda^2\bar\theta L_y}\sqrt{\dfrac{\pi^3}{-\beta^5\mu}}(\tilde\xi - \xi) + \dfrac{8\hbar^2\kappa\tilde\xi L_x}{5\sqrt\pi\lambda^2\beta^2\bar\theta L_y} + \dfrac{8\hbar^2\kappa\xi\mu L_x L_y}{3\sqrt\pi\lambda^2\beta\lambda_T^2\bar\theta} & \text{1D-BEC,} \\[14pt]
\dfrac{3\pi\zeta\left(\frac32\right)\hbar^2 C\kappa\tilde\xi L_z}{2\lambda^2\beta^2\lambda_T\bar\theta} + \dfrac{\hbar^2 C\kappa L_z}{\lambda^2\lambda_T\bar\theta}\sqrt{\dfrac{-\pi^3\mu}{\beta^3}}(3\tilde\xi - \xi) & \text{0D-BEC,}
\end{cases}
\tag{E51}
$$

$$
\simeq
\begin{cases}
\dfrac{2\hbar^2\sqrt\pi\kappa}{\lambda^2\beta^2\bar\theta}\left(\dfrac{2G\tilde\xi L_y}{5L_z} + \left(\text{terms} \propto \tilde\xi L_z\text{ and }\propto\tilde\xi V^0\right) - \sqrt\pi C\xi + G\xi e^{f\,\rho L_z\lambda_T^2}\dfrac{\lambda_T^2}{3L_y^2}\right) & \text{2D-BEC,} \\[14pt]
\dfrac{\hbar^2\kappa}{\lambda^2\beta^2\bar\theta}\left(\dfrac{3\pi\zeta\left(\frac32\right)C\tilde\xi L_z}{2\lambda_T} + \sqrt\pi C(\tilde\xi - \xi)f\rho\lambda_T^2 L_z + \dfrac{8\tilde\xi L_x}{5\sqrt\pi L_y} - \dfrac{8\xi L_x}{3\sqrt\pi f^2\rho^2\lambda_T^4 L_y L_z^2}\right) & \text{1D-BEC,} \\[14pt]
\dfrac{\pi\hbar^2\kappa}{\lambda^2\beta^2\bar\theta}\left(\dfrac{3\zeta\left(\frac32\right)C\tilde\xi L_z}{2\lambda_T} + C(3\tilde\xi - \xi)\sqrt{\dfrac{\pi^3 L_z}{f\,\rho\lambda_T^2 L_x L_y}}\right) & \text{0D-BEC,}
\end{cases}
\tag{E52}
$$

where the third term in the 1D-BEC phase dominates if $L_x > \mathcal{O}(L_y L_z)$ and the fourth term dominates the first two terms if $L_x > \mathcal{O}(L_y L_z^3)$. Higher-order terms relevant in isothermal-isochoric transformations, where $\tilde\xi = 0$, are explicitly written.

The above expressions for $\mathrm{Tr}(N\varrho_{\mathrm{irr}})$ and $\mathrm{Tr}(H\varrho_{\mathrm{irr}})$, together with Eqs. (E35) and (E36), provide the size scaling of work and heat corrections in Eqs. (E32), (E33), and (E34). Using these scalings, one estimates the maximum power of irreversible cycles in the perturbative regime discussed here, the optimal times of each stroke, and the efficiency at maximum power, as reported in Appendix F and in Sec. III.

APPENDIX F: IRREVERSIBLE THERMOCHEMICAL CYCLES

In this appendix, the size scaling of the first-order work and heat corrections in Eqs. (E32), (E33), and (E34) are used to derive the size scalings of the optimal times τ_j^*, of the maximum power π_*, and of the corresponding efficiency η_* for irreversible thermochemical cycles.

1. Irreversible cycles without BEC and in the classical limit

In the absence of BEC phases during the cycle, the computations in Sec. E 5 in Appendix E result in $W_{k,\mathrm{irr}}^{\mathrm{C}} = \mathcal{O}(V)$ and $W_{k,\mathrm{irr}}^{\mathrm{C}} - Q_{k,\mathrm{irr}} = \mathcal{O}(V)$ for all k. The load of the reversible cycles was proven to be extensive, $W_{\mathrm{rev}}^{\mathrm{M}} = \mathcal{O}(V)$, in Sec. II. These scalings imply that the optimal times in Eq. (28) for every stroke have the same size scaling of the relaxation time $\bar{\theta} = \mathcal{O}(L_z/V)$. The output power is therefore maximized, within the perturbative regime $\tau_j^* \gg \bar{\theta}$, for the scaling $\tau_j^* = \mathcal{O}(L_z/sV)$ with $s \ll 1$. Consequently, the maximum power scales as $\pi_* = \mathcal{O}(sV^2/L_z)$, the corresponding load as $W_*^{\mathrm{M}} = W_{\mathrm{rev}}^{\mathrm{M}} + \mathcal{O}(sV)$, and the efficiency as $\eta_* = \eta_{\mathrm{rev}} + \mathcal{O}(sV^0)$.

The size scalings in the classical limit are obtained from those without BECs imposing the condition (8). This condition for ideal gases reads $\mathcal{N} \simeq z_{\mathrm{cl}} V/\lambda_T^3$ with small fugacity $z_{\mathrm{cl}} = e^{\beta\mu} \ll 1$ (see Appendices A and B). The classical limit and the first law of thermodynamics for reversible isothermal cycles then imply $W_{\mathrm{rev}}^{(M)} = -W_{\mathrm{rev}}^{(C)} = \mathcal{O}(z_{\mathrm{cl}} V)$, while irreversible energy corrections are $W_{k,\mathrm{irr}}^{\mathrm{C}} = \mathcal{O}(Vz_{\mathrm{cl}} \ln^2 z_{\mathrm{cl}})$ and $W_{k,\mathrm{irr}}^{\mathrm{C}} - Q_{k,\mathrm{irr}} = \mathcal{O}(Vz_{\mathrm{cl}} \ln z_{\mathrm{cl}})$. The optimal time in Eq. (28) is $\tau_{\mathrm{class}} = \mathcal{O}(L_z/V|\ln z_{\mathrm{cl}}|)$, the maximum power is $\pi_{\mathrm{class}} = \mathcal{O}(z_{\mathrm{cl}} V^2/|\ln z_{\mathrm{cl}}|L_z)$, and the efficiency at maximum power scales as $\eta_{\mathrm{class}} = \mathcal{O}(z_{\mathrm{cl}})$.

In the cycles discussed in Sec. II, η_{rev} is finite and approaches 1 close to BEC transitions, and thus the quantum regime even without BECs exhibits much higher efficiency than the classical limit and larger power if $s > z_{\mathrm{cl}}/|\ln z_{\mathrm{cl}}|$.

2. Irreversible cycles with BECs

Different BEC phases of the working substance emerge at different confinement anisotropies. The three cases considered in Sec. III B for dD-BECs are:

$$d = 2: L_z = \mathcal{O}(\ln V) \text{ and } L_x \simeq L_y = \mathcal{O}\left(\sqrt{V/\ln V}\right);$$
$$d = 1: L_x = \mathcal{O}\left(V^{\frac{\chi}{\chi+1}}\right) \text{ and } L_y \sim L_z = \mathcal{O}\left(V^{\frac{1}{2\chi+2}}\right) \text{ with}$$
$$\chi \geqslant 1, \text{ i.e., } L_x = \mathcal{O}(L_y L_z)^\chi; \text{ and}$$
$$d = 0: L_x \sim L_y \sim L_z = \mathcal{O}(\sqrt[3]{V}).$$

The size scaling of the work and heat corrections in Eqs. (E32), (E33), and (E34) depend on the function $h(\varepsilon)$, and are explicitly computed in Sec. E 5 in Appendix E

assuming $h(\varepsilon_p) \neq 0$ (or $\gamma_p \neq 0$) and finite $h(0)$. The condition $h(\varepsilon_p) \neq 0$ guarantees that the grand canonical ensemble is the unique steady state at every time, otherwise also the instantaneous Hamiltonian eigenstates with energy ε_p such that $h(\varepsilon_p) = 0$ are steady states. This large class of functions contains the constant function, the exponential decay, and the Lorentzian.

The result for the corrections to the chemical work in Eq. (E33) is

$$W_{k,\mathrm{irr}}^{\mathrm{C}} = \begin{cases} \mathcal{O}\left(\dfrac{V}{L_z}\right) & \text{2D-BEC,} \\ \mathcal{O}(V) + \mathcal{O}\left(\dfrac{L_x^2}{L_z^4}\right) & \text{1D-BEC,} \\ \mathcal{O}\left(\dfrac{V}{L_z}\right) & \text{0D-BEC,} \end{cases} \quad \text{(F1)}$$

where the first (second) term for the 1D-BEC dominates if $L_x < \mathcal{O}(L_y L_z^5)$ (if $L_x > \mathcal{O}(L_y L_z^5)$). The other energy corrections used in the computation of (28), namely $W_{k,\mathrm{irr}}^{\mathrm{C}} - Q_{k,\mathrm{irr}}$, have different size scalings for isothermal-isochoric transformations compared to the other strokes. Indeed, the leading orders for all other strokes are

$$W_{k,\mathrm{irr}}^{\mathrm{C}} - Q_{k,\mathrm{irr}} = \begin{cases} \mathcal{O}\left(\dfrac{L_x L_y^2}{L_z}\right) & \text{2D-BEC,} \\ \mathcal{O}(L_x^2) & \text{1D-BEC,} \\ \mathcal{O}(V) & \text{0D-BEC.} \end{cases} \quad \text{(F2)}$$

Nevertheless, these size scalings originate from orders that multiply $\tilde{\xi}$, namely, the time derivative of the temperature or that of the volume, and these contributions vanish for isothermal-isochoric processes. The size scaling for isothermal-isochoric transformations, resulting from computations in Sec. E 5 in Appendix E with $\tilde{\xi} = 0$, is

$$W_{k,\mathrm{irr}}^{\mathrm{C}} - Q_{k,\mathrm{irr}} = \begin{cases} \mathcal{O}\left(\dfrac{V}{L_z}\right) & \text{2D-BEC,} \\ \mathcal{O}(V) + \mathcal{O}\left(\dfrac{L_x^2}{L_z^2}\right) & \text{1D-BEC,} \\ \mathcal{O}(\sqrt{V}) & \text{0D-BEC,} \end{cases} \quad \text{(F3)}$$

with the first (second) term of the 1D-BEC dominating when $L_x < \mathcal{O}(L_y L_z^3)$ (when $L_x > \mathcal{O}(L_y L_z^3)$).

The isothermal chemical Carnot and Otto cycles are treated separately in the following, because isothermal-isochoric transformations are part only of the latter.

a. Irreversible chemical Carnot cycle with a BEC during the third stroke

If the system is a BEC only when chemical work is released (during the third stroke), the reversible load (12)

is extensive, $W_{\text{rev}}^{\text{M}} = \mathcal{O}(V)$, such that the scaling (F2) and that without BECs imply

$$
\tau_{1,2,4}^* =
\begin{cases}
\mathcal{O}\left(\dfrac{1}{\sqrt[4]{V^3 \ln V}}\right) & \text{2D-BEC,} \\[2ex]
\mathcal{O}\left(\dfrac{1}{s V^{\frac{3}{4}}}\right) & \text{1D-BEC, } \chi = 1, \\[2ex]
\mathcal{O}\left(\dfrac{1}{V^{\frac{\chi+2}{2\chi+2}}}\right) & \text{1D-BEC, } \chi > 1, \\[2ex]
\mathcal{O}\left(\dfrac{1}{s V^{\frac{2}{3}}}\right) & \text{0D-BEC,}
\end{cases}
\tag{F4}
$$

and

$$
\tau_3^* =
\begin{cases}
\mathcal{O}\left(\dfrac{1}{\sqrt{V(\ln V)^3}}\right) & \text{2D-BEC,} \\[2ex]
\mathcal{O}\left(\dfrac{1}{s V^{\frac{3}{4}}}\right) & \text{1D-BEC, } \chi = 1, \\[2ex]
\mathcal{O}\left(\dfrac{1}{V^{\frac{3}{2\chi+2}}}\right) & \text{1D-BEC, } \chi > 1, \\[2ex]
\mathcal{O}\left(\dfrac{1}{s V^{\frac{2}{3}}}\right) & \text{0D-BEC.}
\end{cases}
\tag{F5}
$$

The factor $s \ll 1$ has been introduced in order to remain in the perturbative regime, when the optimal times in Eq. (28) scale as the relaxation time $\bar{\theta} = \mathcal{O}(L_z/V)$, as discussed in Sec. F 1.

Using the scalings of $W_{\text{rev}}^{\text{M}}$, τ_j^*, and (F1), one derives the efficiency at maximum power and the maximum power normalized to the classical limit of Sec. III B 1.

b. Irreversible chemical Carnot cycle with a BEC during all the strokes

If the system is in the same BEC phase during the entire chemical Carnot cycle, the load in the reversible limit is subextensive. Applying the above scalings of the chemical potential and of the box size $L_{x,y,z}$ to the work done during the entire chemical Carnot cycle (see Sec. II A) at finite density, one obtains

$$
W_{\text{rev}}^{\text{M}} = (\mu_3 - \mu_1)(\mathcal{N}_1 - \mathcal{N}_3)
$$

$$
=
\begin{cases}
\mathcal{O}(\ln V) & \text{2D-BEC,} \\[1ex]
\mathcal{O}\left(V^{\frac{\chi-1}{\chi+1}}\right) & \text{1D-BEC,} \\[1ex]
\mathcal{O}(V^0) & \text{0D-BEC,}
\end{cases}
\tag{F6}
$$

where it has been assumed in the 2D-BEC case that the chemical potential saturates its lower bound, $-\beta\mu \geqslant \mathcal{O}(\lambda_T^2/L_y^2)$, which provides a lower bound for the scaling of $W_{\text{rev}}^{\text{M}}$ and consequently an upper bound for the times τ_j^*.

[see Eq. (28)]. Therefore, the time needed for every stroke is

$$
\tau_j^* =
\begin{cases}
\mathcal{O}\left(\sqrt{\dfrac{V}{(\ln V)^5}}\right) & \text{2D-BEC,} \\[2ex]
\mathcal{O}\left(V^{\frac{1}{2\chi+2}}\right) & \text{1D-BEC,} \\[2ex]
\mathcal{O}\left(V^{\frac{1}{3}}\right) & \text{0D-BEC.}
\end{cases}
\tag{F7}
$$

The efficiency at maximum power is

$$
\eta_* = \frac{\eta_{\text{rev}}}{2} +
\begin{cases}
\mathcal{O}\left(\sqrt{\dfrac{(\ln V)^3}{V}}\right) & \text{2D-BEC,} \\[2ex]
\mathcal{O}\left(\dfrac{1}{V^{\frac{\chi-1}{\chi+1}}}\right) & \text{1D-BEC, } 1 \leqslant \chi \leqslant 3, \\[2ex]
\mathcal{O}\left(\dfrac{1}{V^{\frac{2}{\chi+1}}}\right) & \text{1D-BEC, } \chi \geqslant 3, \\[2ex]
\mathcal{O}\left(\dfrac{1}{V^{\frac{1}{3}}}\right) & \text{0D-BEC.}
\end{cases}
\tag{F8}
$$

As discussed in Sec. II A, the efficiency η_{rev} is finite when the substance is always in the same BEC phase and approaches 1 for 2D-BEC and large size. Therefore, the efficiency at maximum power in (F8) is again much larger than the classical limit $\eta_{\text{class}} = \mathcal{O}(z_{\text{cl}}) \ll 1$. Nevertheless, the subextensive load (F6) and the scaling of optimal times (F7) imply small output power.

c. Irreversible chemical Otto cycle with a BEC during the third stroke

In the chemical Otto cycle, the first and the third strokes are isothermal-isochoric processes, and one has to consider the corrections (F3) instead of (F2). If the system is a BEC only during the third stroke, as discussed in Sec. II B, the load is extensive, $W_{\text{rev}}^{\text{M}} = \mathcal{O}(V)$. Therefore, the optimal times for each stroke are

$$
\tau_{1,2,4}^* =
\begin{cases}
\mathcal{O}\left(\dfrac{\ln V}{s V}\right) & \text{2D-BEC,} \\[2ex]
\mathcal{O}\left(\dfrac{1}{s V^{\frac{2\chi+1}{2\chi+2}}}\right) & \text{1D-BEC, } \chi \leqslant 2, \\[2ex]
\mathcal{O}\left(\dfrac{1}{V^{\frac{\chi+3}{2\chi+2}}}\right) & \text{1D-BEC, } \chi \geqslant 2, \\[2ex]
\mathcal{O}\left(\dfrac{1}{s V^{\frac{2}{3}}}\right) & \text{0D-BEC,}
\end{cases}
\tag{F9}
$$

and

$$
\tau_3^* = \begin{cases} \mathcal{O}\left(\dfrac{\ln V}{sV}\right) & \text{2D-BEC,} \\[4mm] \mathcal{O}\left(\dfrac{1}{sV^{\frac{2\chi+1}{2\chi+2}}}\right) & \text{1D-BEC, } \chi \leqslant 2, \\[4mm] \mathcal{O}\left(\dfrac{1}{V^{\frac{5}{2\chi+2}}}\right) & \text{1D-BEC, } \chi \geqslant 2, \\[4mm] \mathcal{O}\left(\dfrac{1}{V^{\frac{11}{12}}}\right) & \text{0D-BEC.} \end{cases} \tag{F10}
$$

Recall that, when the times in Eq. (28) do not fulfill the condition $\tau_j^* \gg \bar{\theta}$, the optimal times within the perturbative regime are $\tau_j^* = \bar{\theta}/s = \mathcal{O}(L_z/sV)$ with $s \ll 1$.

Using the scalings derived so far, one obtains the efficiency at maximum power and the maximum power normalized to the classical limit of Sec. III B 2.

d. Irreversible chemical Otto cycle with a BEC during all the strokes

When the system is in the same BEC phase during the entire cycle, Eqs. (18), (19), (20), (21), (22), and (23) imply that the reversible load, $W_{\text{rev}}^{\text{M}} = -W_{1,\text{rev}}^{\text{C}} - W_{3,\text{rev}}^{\text{C}}$, scales as

$$
W_{\text{rev}}^{\text{M}} = \begin{cases} \mathcal{O}(V^0) & \text{2D-BEC,} \\ \mathcal{O}(V^{\frac{\chi-1}{\chi+1}}) & \text{1D-BEC,} \\ \mathcal{O}(V^0) & \text{0D-BEC.} \end{cases} \tag{F11}
$$

Therefore, the times needed for each stroke are

$$
\tau_{1,3}^* = \begin{cases} \mathcal{O}\left(\dfrac{V}{(\ln V)^3}\right)^{\frac{1}{4}} & \text{2D-BEC,} \\[4mm] \mathcal{O}\left(V^{\frac{2-\chi}{2\chi+2}}\right) & \text{1D-BEC, } \chi \leqslant 2, \\[2mm] \mathcal{O}(V^0) & \text{1D-BEC, } \chi \geqslant 2, \\[2mm] \mathcal{O}\left(V^{\frac{1}{12}}\right) & \text{0D-BEC,} \end{cases} \tag{F12}
$$

and

$$
\tau_{2,4}^* = \begin{cases} \mathcal{O}\left(\sqrt{\dfrac{V}{(\ln V)^3}}\right) & \text{2D-BEC,} \\[4mm] \mathcal{O}\left(V^{\frac{1}{2\chi+2}}\right) & \text{1D-BEC,} \\[2mm] \mathcal{O}\left(V^{\frac{1}{3}}\right) & \text{0D-BEC.} \end{cases} \tag{F13}
$$

The efficiency at maximum power is

$$
\eta_* = \frac{\eta_{\text{rev}}}{2} + \begin{cases} \mathcal{O}\left(\dfrac{(\ln V)^3}{V}\right)^{\frac{1}{4}} & \text{2D-BEC,} \\[4mm] \mathcal{O}\left(\dfrac{1}{V^{\frac{\chi-1}{2\chi+2}}}\right) & \text{1D-BEC, } 1 \leqslant \chi \leqslant 2, \\[4mm] \mathcal{O}\left(\dfrac{1}{V^{\frac{2\chi-3}{2\chi+2}}}\right) & \text{1D-BEC, } 2 \leqslant \chi \leqslant 3, \\[4mm] \mathcal{O}\left(\dfrac{1}{V^{\frac{3}{2\chi+2}}}\right) & \text{1D-BEC, } \chi \geqslant 3, \\[4mm] \mathcal{O}\left(\dfrac{1}{V^{\frac{1}{12}}}\right) & \text{0D-BEC.} \end{cases} \tag{F14}
$$

As for the chemical Carnot cycle, the efficiency at maximum power in (F14) is again much larger than the classical limit, $\eta_{\text{class}} = \mathcal{O}(z_{\text{cl}}) \ll 1$, but with small output power because of the subextensive load (F11) and of the scaling of optimal times (F12) and (F13).

---

[1] K. Y. Cheong, G. Impellizzeri, and M. A. Fraga, eds. *Emerging Materials for Energy Conversion and Storage* (Elsevier, Amsterdam, 2018).

[2] M. D. Hasanuzzaman and N. A. Rahim, eds. *Energy for Sustainable Development* (Elsevier, London, San Diego, Cambridge, Oxford, 2020).

[3] H. B. Callen, *Thermodynamics and an Introduction to Thermostatistics Second Edition* (John Wiley & Sons, New York, 1985).

[4] A. Bejan, *Advanced Engineering Thermodynamics Fourth Edition* (John Wiley & Sons, Hoboken, 2016).

[5] L. Chen, F. Sun, C. Wu, and J. Yu, Performance characteristic of isothermal chemical engines, Energy Convers. Manag. **38**, 1841 (1997).

[6] A. Parmeggiani, F. Jülicher, A. Ajdari, and J. Prost, Energy transduction of isothermal ratchets: Generic aspects and specific examples close to and far from equilibrium, Phys. Rev. E **60**, 2127 (1999).

[7] T. Schmiedl and U. Seifert, Efficiency of molecular motors at maximum power, EPL **83**, 30005 (2008).

[8] M. Esposito, K. Lindenberg, and C. Van den Broeck, Universality of Efficiency at Maximum Power, Phys. Rev. Lett. **102**, 130602 (2009).

[9] U. Seifert, Efficiency of Autonomous Soft Nanomachines at Maximum Power, Phys. Rev. Lett. **106**, 020601 (2011).

[10] U. Seifert, Stochastic thermodynamics, fluctuation theorems and molecular machines, Rep. Prog. Phys. **76**, 126001 (2012).

[11] H. Hooyberghs, B. Cleuren, A. Salazar, J. O. Indekeu, and C. Van den Broeck, Efficiency at maximum power of a chemical engine, J. Chem. Phys. **139**, 134111 (2013).

[12] F. Jülicher, A. Ajdari, and J. Prost, Modeling molecular motors, Rev. Mod. Phys. **69**, 1269 (1997).

[13] M. Schliwa, ed. *Molecular Motors* (Wiley-VCH, Weinheim, 2003).

[14] P. Hänggi and F. Marchesoni, Artificial Brownian motors: Controlling transport on the nanoscale, Rev. Mod. Phys. **81**, 387 (2009).

[15] N. Golubeva, A. Imparato, and L. Peliti, Efficiency of molecular machines with continuous phase space, EPL **97**, 60005 (2012).

[16] R. Krechetnikov, Thermodynamics of chemical Marangoni-driven engines, Soft Matter **13**, 4931 (2017).

[17] C. Agrafiotis, M. Roeb, and C. Sattler, A review on solar thermal syngas production via redox pair-based water/carbon dioxide splitting thermochemical cycles, Renew. Sust. Energ. Rev. **42**, 254 (2015).

[18] D. Moreno and M. C. Hatzell, Efficiency of Carnot and conventional capacitive deionization cycles, J. Phys. Chem. C **122**, 22480 (2018).

[19] D. Moreno and M. C. Hatzell, Constant chemical potential cycles for capacitive deionization, Phys. Chem. Chem. Phys. **21**, 24512 (2019).

[20] J. Liu, J. Baeyens, Y. Deng, T. Tan, and H. Zhang, The chemical CO_2 capture by carbonation-decarbonation cycles, J. Environ. Manage. **260**, 110054 (2020).

[21] Y. Shuai, H. Zhang, B. G. Lougou, B. Jiang, A. Mustafa, C.-H. Wang, F. Wang, and J. Zhao, Solar-driven thermochemical redox cycles of ZrO_2 supported $NiFe_2O_4$ for CO_2 reduction into chemical energy, Energy **223**, 120073 (2021).

[22] Y. Xiong, J. Zhao, Z. Zheng, and W. Li, Effect of copper dopant on the mixed cobalt-iron oxides for hydrogen generation via chemical looping redox cycles, Int. J. Hydrog. Energy **45**, 28372 (2020).

[23] M. Li, Y. Qiu, M. Li, D. Cui, S. Zhang, D. Zeng, and R. Xiao, Efficient hydrogen production through the chemical looping redox cycle of YSZ supported iron oxides, Green Energy Environ. **6**, 875 (2021).

[24] Y. Yan, K. Wang, P. T. Clough, and E. J. Anthony, Developments in calcium/chemical looping and metal oxide redox cycles for high-temperature thermochemical energy storage: A review, Fuel Process. Technol. **199**, 106280 (2020).

[25] R. Chein and W.-H. Chen, Thermodynamic analysis of integrated adiabatic chemical looping combustion and supercritical CO_2 cycle, Energy Convers. Manag.: X **10**, 100078 (2021).

[26] S. Dai, Y. Yin, W. Li, and F. Zhang, Thermodynamic analysis of a novel chemical heat pump cycle based on the physical-chemical thermal effects of reversible reaction, Energy Convers. Manag. **225**, 113419 (2020).

[27] M. U. de Vivanco, M. Zschornak, H. Stöcker, S. Jachalke, E. Mehner, T. Leisegang, and D. Meyer, Pyroelectrically-driven chemical reactions described by a novel thermodynamic cycle, Phys. Chem. Chem. Phys. **22**, 17781 (2020).

[28] R. Chen, R. Zhao, S. Deng, L. Zhao, and W. Xu, A cycle research methodology for thermo-chemical engines: From ideal cycle to case study, Energy **228**, 120599 (2021).

[29] C. Wang, C. Ha, X. Pan, J. Qin, and H. Huang, Thermodynamic analysis of chemical precooled turbine combined engine cycle, Energy Convers. Manag. **239**, 114184 (2021).

[30] H. Saygin and A. Sisman, Brayton refrigeration cycle working at quantum degeneracy conditions, Appl. Energy **69**, 77 (2001).

[31] H. Saygin and A. Sisman, Quantum degeneracy effect on the work output from a Stirling cycle, J. Appl. Phys. **90**, 3086 (2001).

[32] T. E. Humphrey, R. Newbury, R. P. Taylor, and H. Linke, Reversible Quantum Brownian Heat Engines for Electrons, Phys. Rev. Lett. **89**, 116801 (2002).

[33] J. He, J. Chen, and B. Hua, Influence of quantum degeneracy on the performance of a Stirling refrigerator working with an ideal Fermi gas, Appl. Energy **72**, 541 (2002).

[34] J. Chen and B. Lin, Low-temperature behaviour of an ideal Bose gas and some forbidden thermodynamic cycles, J. Phys. A **36**, 11385 (2003).

[35] S. W. Kim, T. Sagawa, S. De Liberato, and M. Ueda, Quantum Szilard Engine, Phys. Rev. Lett. **106**, 070401 (2011).

[36] A. M. Zagoskin, S. Savel'ev, F. Nori, and F. V. Kusmartsev, Squeezing as the source of inefficiency in the quantum Otto cycle, Phys. Rev. B **86**, 014501 (2012).

[37] J. Bengtsson, M. N. Tengstrand, A. Wacker, P. Samuelsson, M. Ueda, H. Linke, and S. M. Reimann, Quantum Szilard Engine with Attractively Interacting Bosons, Phys. Rev. Lett. **120**, 100601 (2018).

[38] X. L. Huang, D. Y. Guo, S. L. Wu, and X. X. Yi, Multilevel quantum Otto heat engines with identical particles, Quantum Inf. Process. **17**, 27 (2018).

[39] T. D. Kieu, The Second Law, Maxwell's Demon, and Work Derivable from Quantum Heat Engines, Phys. Rev. Lett. **93**, 140403 (2004).

[40] H. T. Quan, Y.-X. Liu, C. P. Sun, and F. Nori, Quantum thermodynamic cycles and quantum heat engines, Phys. Rev. E **76**, 031105 (2007).

[41] M. J. Henrich, G. Mahler, and M. Michel, Driven spin systems as quantum thermodynamic machines: Fundamental limits, Phys. Rev. E **75**, 051118 (2007).

[42] J. Anders and V. Giovannetti, Thermodynamics of discrete quantum processes, New J. Phys. **15**, 033022 (2013).

[43] J. Goold, M. Huber, A. Riera, L. Lídia del Rio, and P. Skrzypczyk, The role of quantum information in thermodynamics – A topical review, J. Phys. A **49**, 143001 (2016).

[44] S. Vinjanampathy and J. Anders, Quantum thermodynamics, Contemp. Phys. **57**, 545 (2016).

[45] G. Benenti, G. Casati, K. Saito, and R. S. Whitney, Fundamental aspects of steady-state conversion of heat to work at the nanoscale, Phys. Rep. **694**, 1 (2017).

[46] S. Bhattacharjee and A. Dutta, Quantum thermal machines and batteries, Eur. Phys. J. B **94**, 239 (2021).

[47] G. T. Landi and M. Paternostro, Irreversible entropy production: From classical to quantum, Rev. Mod. Phys. **93**, 035008 (2021).

[48] J. P. Pekola and B. Karimi, Colloquium: Quantum heat transport in condensed matter systems, Rev. Mod. Phys. **93**, 041001 (2021).

[49] F. Ciccarello, S. Lorenzo, V. Giovannetti, and G. M. Palma, Quantum collision models: Open system dynamics from repeated interactions, Phys. Rep. **954**, 1 (2022).

[50] W. Gräfe, *Quantum Mechanical Models of Metal Surfaces and Nanoparticles* (Springer, Cham, Heidelberg, New York, Dordrecht, London, 2015).

[51] D. G. Steel, *Introduction to Quantum Nanotechnology: A Problem Focused Approach* (Oxford University Press, New York, 2021).

[52] R. Esteban, A. G. Borisov, P. Nordlander, and J. Aizpurua, Bridging quantum and classical plasmonics with a quantum-corrected model, Nat. Commun. **3**, 825 (2012).

[53] W. Li, Physics models of plasmonics: Single nanoparticle, complex single nanoparticle, nanodimer, and single nanoparticle over metallic thin film, Plasmonics **13**, 997 (2018).

[54] T. Ding, Q. Gan, D. Li, L. Mao, X. Wang, H. Xu, C. Zhang, and G. Zhang, Switching plasmonic nanogaps between classical and quantum regimes with supramolecular interactions, Sci. Adv. **8**, 9752 (2020).

[55] F. Tebbenjohanns, M. Frimmer, V. Jain, D. Windey, and L. Novotny, Motional Sideband Asymmetry of a Nanoparticle Optically Levitated in Free Space, Phys. Rev. Lett. **124**, 013603 (2020).

[56] C. You, M. Hong, N. Bhusal, J. Chen, M. A. Quiroz-Juárez, J. Fabre, F. Mostafavi, J. Guo, I. De Leon, R. J. León-Montiel, and O. S. Magaña Loaiza, Observation of the modification of quantum statistics of plasmonic systems, Nat. Commun. **12**, 5161 (2021).

[57] M. Yamaki, S. Nakayama, K. Hoki, H. Konoa, and Y. Fujimura, Quantum dynamics of light-driven chiral molecular motors, Phys. Chem. Chem. Phys. **11**, 1662 (2009).

[58] I. Goychuk, Molecular machines operating on the nanoscale: From classical to quantum, Beilstein J. Nanotechnol. **7**, 328 (2016).

[59] B. Oruganti, J. Wang, and B. Durbeej, Quantum chemical design of rotary molecular motors, Int. J. Quantum Chem. **118**, e25405 (2018).

[60] A. Majumdar and T. L. C. Jansen, Quantum-classical simulation of molecular motors driven only by light, J. Phys. Chem. Lett. **12**, 5512 (2021).

[61] P. W. Brouwer, Scattering approach to parametric pumping, Phys. Rev. B **58**, R10135 (1998).

[62] M. Switkes, C. M. Marcus, K. Campman, and A. C. Gossard, An adiabatic quantum electron pump, Science **283**, 1905 (1999).

[63] R. Bustos-Marún, G. Refael, and F. von Oppen, Adiabatic Quantum Motors, Phys. Rev. Lett. **111**, 060802 (2013).

[64] A. Bruch, S. V. Kusminskiy, G. Refael, and F. von Oppen, Interacting adiabatic quantum motor, Phys. Rev. B **97**, 195411 (2018).

[65] M. F. Ludovico and M. Capone, Enhanced performance of a quantum-dot-based nanomotor due to Coulomb interactions, Phys. Rev. B **98**, 235409 (2018).

[66] L. Demetrius, Quantum statistics and allometric scaling of organisms, Physica A **322**, 477 (2003).

[67] L. Demetrius, The origin of allometric scaling laws in biology, J. Theor. Biolg. **243**, 455 (2006).

[68] L. Demetrius and J. A. Tuszynski, Quantum metabolism explains the allometric scaling of metabolic rates, J. R. Soc. Interface **7**, 507 (2010).

[69] A. Jinich, D. Rappoport, I. Dunn, B. Sanchez-Lengeling, R. Olivares-Amaya, E. Noor, A. Bar Even, and A. Aspuru-Guzik, Quantum chemical approach to estimating the thermodynamics of metabolic reactions, Sci. Rep. **4**, 7022 (2014).

[70] A. Lábas, B. K, and J. Oláh, Combined docking and quantum chemical study on CYP-mediated metabolism of estrogens in man, Chem. Res. Toxicol. **2**, 583 (2017).

[71] C. J. Brabec, V. Dyakonov, J. Parisi, and N. S. Sariciftci, eds. *Organic Photovoltaics Concepts and Realization* (Springer, Berlin, Heidelberg, 2003).

[72] T. Markvart, From steam engine to solar cells: Can thermodynamics guide the development of future generations of photovoltaics?, WIREs Energy Environ. **5**, 543 (2016).

[73] C. J. Pethick and H. Smith, *Bose-Einstein Condensation in Dilute Gases* (Cambridge University Press, New York, 2002).

[74] L. Pitaevskii and S. Stringari, *Bose-Einstein Condensation* (Oxford University Press, New York, 2003).

[75] M. H. Anderson, J. R. Ensher, M. R. Matthews, and C. E. Wieman, E. A. Cornell, Observation of Bose-Einstein condensation in a dilute atomic vapor, Science **269**, 198 (1995).

[76] C. C. Bradley, C. A. Sackett, J. J. Tollett, and R. G. Hulet, Evidence of Bose-Einstein Condensation in an Atomic Gas with Attractive Interactions, Phys. Rev. Lett. **75**, 1687 (1995).

[77] K. B. Davis, M.-O. Mewes, M. R. Andrews, N. J. van Druten, D. S. Durfee, D. M. Kurn, and W. Ketterle, Bose-Einstein Condensation in a Gas of Sodium Atoms, Phys. Rev. Lett. **75**, 3969 (1995).

[78] S. Jochim, M. Bartenstein, A. Altmeyer, G. Hendl, S. Riedl, C. Chin, J. H. Denschlag, and R. Grimm, Bose-Einstein condensation of molecules, Science **302**, 2101 (2003).

[79] K. Xu, T. Mukaiyama, J. R. Abo-Shaeer, J. K. Chin, D. E. Miller, and W. Ketterle, Formation of Quantum-Degenerate Sodium Molecules, Phys. Rev. Lett. **91**, 210402 (2003).

[80] I. Carusotto and C. Ciuti, Quantum fluids of light, Rev. Mod. Phys. **85**, 299 (2013).

[81] H. Deng, H. Haug, and Y. Yamamoto, Exciton-polariton Bose-Einstein condensation, Rev. Mod. Phys. **82**, 1489 (2010).

[82] J. Tang, J. Zhang, Y. Lv, H. Wang, F. F. Xu, C. Zhang, L. Sun, J. Yao, and Y. S. Zhao, Room temperature exciton–polariton Bose–Einstein condensation in organic single-crystal microribbon cavities, Nat. Commun. **12**, 3265 (2021).

[83] S. O. Demokritov, V. E. Demidov, O. Dzyapko, G. A. Melkov, A. A. Serga, B. Hillebrands, and A. N. Slavin, Bose–Einstein condensation of quasi-equilibrium magnons at room temperature under pumping, Nature **443**, 430 (2006).

[84] V. L. Safonov, *Nonequilibrium Magnons: Theory, Experiment and Applications* (Wiley-VCH, Weinheim, 2013).

[85] O. V. Misochko, M. Hase, K. Ishioka, and M. Kitajima, Transient Bose–Einstein condensation of phonons, Phys. Lett. A **321**, 381 (2004).

[86] I. Nardecchia, J. Torres, M. Lechelon, V. Giliberti, M. Ortolani, P. Nouvel, M. Gori, Y. Meriguet, I. Donato, J. Preto, L. Varani, J. Sturgis, and M. Pettini, Out-of-Equilibrium Collective Oscillation as Phonon

Condensation in a Model Protein, Phys. Rev. X **8,** 031061 (2018).

[87] D. A. Krueger, Impossibility of Bose Condensation or Superconductivity in Partially Finite Geometries, Phys. Rev. Lett. **19,** 563 (1967).

[88] D. A. Krueger, Finite geometries and ideal Bose gases, Phys. Rev. **172,** 211 (1968).

[89] J. J. Rehr and N. D. Mermin, Condensation of the rotating two-dimensional ideal Bose gas, Phys. Rev. B **1,** 3160 (1970).

[90] M. van den Berg and T. Lewis, On generalized condensation in the free boson gas, Physica A **110,** 550 (1982).

[91] M. van den Berg, On condensation in the free-boson gas and the spectrum of the Laplacian, J. Stat. Phys. **31,** 623 (1983).

[92] M. van den Berg, T. Lewis, and J. Pulé, A general theory of Bose-Einstein condensation, Helv. Phys. Acta **59,** 1271 (1986).

[93] M. van den Berg, T. Lewis, and M. Lunn, On the general theory of Bose-Einstein condensation and the state of the free boson gass, Helv. Phys. Acta **59,** 1289 (1986).

[94] W. Ketterle and N. J. van Druten, Bose-Einstein condensation of a finite number of particles trapped in one or three dimensions, Phys. Rev. A **54,** 656 (1996).

[95] N. J. van Druten and W. Ketterle, Two-Step Condensation of the Ideal Bose Gas in Highly Anisotropic Traps, Phys. Rev. Lett. **79,** 549 (1997).

[96] M. Beau and V. A. Zagrebnov, The second critical density and anisotropic generalised condensation, Condens. Matter Phys. **13,** 23003 (2010).

[97] W. J. Mullin and A. R. Sakhel, Generalized Bose-Einstein condensation, J. Low Temp.Phys. **166,** 2125 (2012).

[98] M. F. M. Osborne, The Bose-Einstein condensation for thin films, Phys. Rev. **76,** 396 (1949).

[99] D. L. Mills, Ground-state occupancy of an ideal Bose-Einstein gas confined to a finite volume, Phys. Rev. **134,** A306 (1964).

[100] B. M. Khorana and D. H. Douglass, Bose-Einstein condensation in narrow channels, Phys. Rev. **138,** A35 (1965).

[101] D. F. Goble and L. E. H. Trainor, Liquid helium and the properties of finite Bose-Einstein assemblies, Can. J. Phys. **44,** 27 (1966).

[102] D. F. Goble and L. E. H. Trainor, New correlation length in Bose-Gas models of liquid helium, Phys. Rev. **157,** 167 (1967).

[103] E. A. Sonin, Quantization of the magnetic flux of superconducting rings and Bose condensation, Sov. Phys. JETP **29,** 520 (1969).

[104] H. Wallis, Bose gas in a gravito-optical trap, Quantum Semiclass Opt. **8,** 727 (1996).

[105] O. Zobay and B. M. Garraway, Atom trapping and two-dimensional Bose-Einstein condensates in field-induced adiabatic potentials, Phys. Rev. A **69,** 023605 (2004).

[106] A. Görlitz, J. M. Vogels, A. E. Leanhardt, C. Raman, T. L. Gustavson, J. R. Abo-Shaeer, A. P. Chikkatur, S. Gupta, S. Inouye, T. Rosenband, and W. Ketterle, Realization of Bose-Einstein Condensates in Lower Dimensions, Phys. Rev. Lett. **87,** 130402 (2001).

[107] M. Greiner, I. Bloch, O. Mandel, T. W. Hänsch, and T. Esslinger, Exploring Phase Coherence in a 2D Lattice of Bose-Einstein Condensates, Phys. Rev. Lett. **87,** 160405 (2001).

[108] J. Esteve, J.-B. Trebbia, T. Schumm, A. Aspect, C. I. Westbrook, and I. Bouchoule, Observations of Density Fluctuations in an Elongated Bose Gas: Ideal Gas and Quasicondensate Regimes, Phys. Rev. Lett. **96,** 130403 (2006).

[109] A. H. van Amerongen, J. J. P. van Es, P. Wicke, K. V. Kheruntsyan, and N. J. van Druten, Yang-Yang Thermodynamics on an Atom Chip, Phys. Rev. Lett. **100,** 090402 (2008).

[110] I. M. Georgescu, S. Ashhab, and F. Nori, Quantum simulation, Rev. Mod. Phys. **86,** 153 (2014).

[111] C. Monroe, W. C. Campbell, L.-M. Duan, Z.-X. Gong, A. V. Gorshkov, P. W. Hess, R. Islam, K. Kim, N. M. Linke, G. Pagano, P. Richerme, C. Senko, and N. Y. Yao, Programmable quantum simulations of spin systems with trapped ions, Rev. Mod. Phys. **93,** 025001 (2021).

[112] T. K. Hakala, A. J. Moilanen, A. I. Väkeväinen, R. Guo, J.-P. Martikainen, K. S. Daskalakis, H. T. Rekola, A. Julku, and P. Törmä, Bose–Einstein condensation in a plasmonic lattice, Nat. Phys. **14,** 739 (2018).

[113] A. I. Väkeväinen, A. J. Moilanen, M. Nečada, T. K. Hakala, K. S. Daskalakis, and P. Törmä, Bose–Einstein condensation in a plasmonic lattice, Nat. Commun. **11,** 3139 (2020).

[114] P. R. Johnson, E. Della Torre, L. H. Bennett, and R. E. Watson, Nonequilibrium quantum dynamics in ferromagnetic nanoparticles: Conditions for Bose–Einstein condensation, J. Appl. Phys. **105,** 07E115 (2009).

[115] M. Chakravorty, A. K. Raychaudhuri, T. Sarkar, and M. S. Andersson, Proposed Bose–Einstein condensation of magnons in nanostructured films of Gd at low temperature and its manifestations in electrical resistivity and magnetoresistance, J. Phys.: Condens. Matter **29,** 255701 (2017).

[116] L. Amico *et al.*, Roadmap on atomtronics: State of the art and perspective, AVS Quantum Sci. **3,** 039201 (2021).

[117] T. L. Hill, *Thermodynamics of Small Systems* (Dove Publications, New York, 1994).

[118] A. Campa, L. Casetti, I. Latella, A. Pérez-Madrid, and S. Ruffo, Concavity, response functions and replica energy, Entropy **20,** 12 (2018).

[119] U. Marzolino, μPT statistical ensemble: Systems with fluctuating energy, particle number, and volume, Sci. Rep. **11,** 15096 (2021).

[120] R. V. Chamberlin, Mean-field cluster model for the critical behaviour of ferromagnets, Nature **408,** 6810 (2000).

[121] T. L. Hill, A different approach to nanothermodynamics, Nano Lett. **1,** 273 (2001).

[122] T. L. Hill, Fluctuations in energy in completely open small systems, Nano Lett. **2,** 609 (2002).

[123] H. Qian, Hill's small systems nanothermodynamics: A simple macromolecular partition problem with a statistical perspective, J. Biol. Phys. **38,** 201 (2012).

[124] R. V. Chamberlin, The big world of nanothermodynamics, Entropy **17,** 52 (2015).

[125] I. Latella, A. Pérez-Madrid, A. Campa, L. Casetti, and S. Ruffo, Thermodynamics of Nonadditive Systems, Phys. Rev. Lett. **114,** 230601 (2015).

[126] D. Bedeaux and S. Kjelstrup, Hill's nanothermodynamics is equivalent with Gibbs' thermodynamics for curved surfaces, Nano Lett. **707,** 40 (2018).

[127] Quasistatic thermodynamic transformations without exchange of particles require only one variable to be fixed because of the lack of the conjugated couple $(\mu, \mathcal{N})$.

[128] S. Giorgini, L. P. Pitaevskii, and S. Stringari, Theory of ultracold atomic Fermi gases, Rev. Mod. Phys. **80,** 1215 (2008).

[129] M. Fabrizio, *A Course in Quantum Many-Body Theory* (Springer, Cham, 2022).

[130] L. Olivares-Quiroz and V. Romero-Rochin, Isotherms, order parameter and density profiles for weakly interacting Bose gases within three mean-field theories, J. Low Temp. Phys. **164,** 23 (2011).

[131] V. A. Zagrebnov and J.-B. Bru, The Bogoliubov model of weakly imperfect Bose gas, Phys. Rep. **350,** 291 (2001).

[132] G. M. Bhuiyan, Bose condensation and the Casimir effects of an imperfect Bose gas in a *d*-dimensional configuration space, J. Phys.: Conf. Ser. **1718,** 012006 (2021).

[133] W.-S. Dai and M. Xie, Interacting quantum gases in confined space: Two- and three-dimensional equations of state, J. Math. Phys. **48,** 123302 (2007).

[134] J. J. R. M. van Heugten, Ph.D. thesis, Utrecht University, 2012.

[135] V. Vovchenko, D. V. Anchishkin, and M. I. Gorenstein, Van der Waals equation of state with Fermi statistics for nuclear matter, Phys. Rev. C **91,** 064314 (2015).

[136] K. Redlich and K. Zalewski, Thermodynamics of van der Waals fluids with quantum statistics, Acta Phys. Pol. B **47,** 1943 (2016).

[137] F. J. Sevilla and L. Olivares-Quiroz, Chemical potential for the interacting classical gas and the ideal quantum gas obeying a generalized exclusion principle, Eur. J. Phys. **33,** 709 (2012).

[138] S. R. de Groot, G. J. Hooymann, and C. A. ten Seldam, On the Bose-Einstein condensation, Proc. R. Soc. Lond. A **203,** 266 (1950).

[139] J. Oliva, Density profile of the weakly interacting Bose gas confined in a potential well: Nonzero temperature, Phys. Rev. B **39,** 4197 (1989).

[140] Z. Yan, M. Li, L. Chen, C. Chen, and J. Chen, Density of states and thermodynamic properties of an ideal system trapped in any dimension, J. Phys. A **32,** 4069 (1999).

[141] J. G. Martínez-Herrera, J. García-Nila, and M. A. Solís, Bose gas with generalized dispersion relation plus an energy gap, Physica Scripta **94,** 075002 (2019).

[142] D. Momeni, Bose–Einstein condensation for an exponential density of states function and Lerch zeta function, Physica A **541,** 123264 (2020).

[143] D. C. Wood, *The computation of polylogarithm*, Technical report 15-92 (University of Kent, Computing Laboratory, 1992).

[144] V. Cavina, A. Mari, and V. Giovannetti, Slow Dynamics and Thermodynamics of Open Quantum Systems, Phys. Rev. Lett. **119,** 050601 (2017).

[145] G. Schaller, Quantum equilibration under constraints and transport balance, Phys. Rev. E **83,** 031111 (2011).

[146] N. M. Myers and S. Deffner, Bosons outperform fermions: The thermodynamic advantage of symmetry, Phys. Rev. E **101,** 012110 (2020).

[147] N. Gupt, S. Bhattacharyya, and A. Ghosh, Statistical generalization of regenerative bosonic and fermionic Stirling cycles, Phys. Rev. E **104,** 054130 (2021).

[148] N. M. Myers, N. O. Peñas, F. J. and, P. Vargas, G. De Chiara, and S. Deffner, Boosting engine performance with Bose–Einstein condensation, New J. Phys. **24,** 025001 (2022).

[149] S. Sur and A. Ghosh, Quantum advantage of thermal machines with Bose and Fermi gases, Entropy **25,** 372 (2023).

[150] B. Yadin, B. Morris, and K. Brandner, Thermodynamics of permutation-invariant quantum many-body systems: A group-theoretical framework, Phys. Rev. Res. **5,** 033018 (2023).

[151] J. Koch, K. Menon, E. Cuestas, S. Barbosa, E. Lutz, T. Fogarty, T. Busch, and A. Widera, A quantum engine in the BEC–BCS crossover, Nature **621,** 723 (2023).

[152] M. Janovitch, M. Brunelli, and P. P. Potts, Wave-particle duality in a quantum heat engine, Phys. Rev. Res. **5,** L042007 (2023).

[153] T. K. Konar, L. G. C. Lakkaraju, S. Ghosh, and A. Sen(De), Quantum battery with ultracold atoms: Bosons vs. fermions, Phys. Rev. A **106,** 022618 (2022).

[154] F. Benatti, R. Floreanini, and U. Marzolino, Sub-shot-noise quantum metrology with entangled identical particles, Ann. Phys. **325,** 924 (2010).

[155] F. Benatti, R. Floreanini, and U. Marzolino, Entanglement and squeezing with identical particles: Ultracold atom quantum metrology, J. Phys. B **44,** 091001 (2011).

[156] F. Benatti, R. Floreanini, and U. Marzolino, Entanglement in fermion systems and quantum metrology, Phys. Rev. A **89,** 032326 (2014).

[157] U. Marzolino and D. Braun, Precision measurements of temperature and chemical potential of quantum gases, Phys. Rev. A **88,** 063609 (2013).

[158] D. Braun, G. Adesso, F. Benatti, R. Floreanini, U. Marzolino, M. W. Mitchell, and S. Pirandola, Quantum-enhanced measurements without entanglement, Rev. Mod. Phys. **90,** 035006 (2018).

[159] Patrick P. Potts, Jonatan Bohr Brask, and Nicolas Brunner, Fundamental limits on low-temperature quantum thermometry with finite resolution, Quantum **3,** 161 (2019).

[160] F. Benatti, R. Floreanini, U. Marzolino, and F. Franchini, Entanglement in indistinguishable particle systems, Phys. Rep. **878,** 1 (2020).

[161] T. J. F. Johann and U. Marzolino, Locality and entanglement of indistinguishable particles, Sci. Rep. **11,** 15478 (2021).

[162] F. Benatti, R. Floreanini, and U. Marzolino, Entanglement and non-locality in quantum protocols with identical particles, Entropy **23,** 479 (2021).

[163] H. Fehske, R. Schneider, and Weiße, eds. *Computational Many-Particle Physics* (Springer, Berlin, Heidelberg, 2008).

[164] V. E. Korepin, N. M. Bogoliubov, and A. G. Izergin, eds. *Quantum Inverse Scattering Method and Correlation*

Functions (Cambridge University Press, Cambridge, 1993).

[165] T. Takahashi, ed. *Thermodynamics of One-Dimensional Solvable Models* (Cambridge University Press, New York, 1999).

[166] G. G. N. Angilella and N. H. March, eds. *Exactly Solvable Models in Many-Body Theory* (World Scientific, Singapore, 2016).

[167] A. Maluckov, J. Petrovic, G. Gligorić, L. Hadzžievski, P. Lombardi, F. Schäfer, and F. S. Cataliotti, Control of a Bose–Einstein condensate on a chip by external optical and magnetic potentials, Ann. Phys. **327,** 2152 (2012).

[168] M. Tajik, B. Rauer, T. Schweigler, F. Cataldini, J. Sabino, F. S. Møller, S.-C. Ji, I. E. Mazets, and J. Schmiedmayer, Designing arbitrary one-dimensional potentials on an atom chip, Opt. Express **27,** 33474 (2019).

[169] D. Rey, S. Thomas, R. Sharma, T. Badr, L. Longchambon, R. Dubessy, and H. Perrin, Loading a quantum gas from a hybrid dimple trap to a shell trap, J. Appl. Phys. **132,** 214401 (2022).

[170] U. Hohenester, OCTBEC – A Matlab toolbox for optimal quantum control of Bose-Einstein condensates, Comput. Phys. Commun. **185,** 194 (2014).

[171] J.-F. Mennemann, D. Matthes, R.-M. Weishäupl, and T. Langen, Optimal control of Bose–Einstein condensates in three dimensions, New J. Phys. **17,** 113027 (2015).

[172] M. van Frank, S. Bonneau, J. Schmiedmayer, S. Hild, C. Gross, M. Cheneau, I. Bloch, T. Pichler, A. Negretti, T. C, and S. Montangero, Optimal control of complex atomic quantum systems, Sci. Rep. **6,** 34187 (2016).

[173] S. Amri, R. Corgier, D. Sugny, E. M. Rasel, N. Gaaloul, and E. Charron, Optimal control of the transport of Bose-Einstein condensates with atom chips, Sci. Rep. **9,** 5346 (2019).

[174] S. J. M. Kuppens, K. L. Corwin, K. W. Miller, T. E. Chupp, and C. E. Wieman, Loading an optical dipole trap, Phys. Rev. A **62,** 013406 (2000).

[175] M. Falkenau, V. V. Volchkov, J. Rührig, A. Griesmaier, and T. Pfau, Continuous Loading of a Conservative Potential Trap from an Atomic Beam, Phys. Rev. Lett. **106,** 163002 (2011).

[176] M. Schneider, T. Brächer, D. Breitbach, V. Lauer, P. Pirro, D. A. Bozhko, H. Y. Musiienko-Shmarova, B. Heinz, Q. Wang, T. Meyer, F. Heussner, S. Keller, E. T. Papaioannou, B. Lägel, T. Löber, C. Dubs, A. N. Slavin, V. S. Tiberkevich, A. A. Serga, A. A. Serga, B. Hillebrands, and A. V. C, Bose–Einstein condensation of quasiparticles by rapid cooling, Nat. Nanotechnol. **15,** 457 (2020).

[177] S. Autti, P. J. Heikkinen, J. T. Mäkinen, G. E. Volovik, V. V. Zavjalov, and V. B. Eltsov, AC Josephson effect between two superfluid time crystals, Nat. Mater. **20,** 171 (2021).

[178] C. Safranski, I. Barsukov, H. K. Lee, T. Schneider, A. A. Jara, A. Smith, H. Chang, K. Lenz, J. Lindner, Y. Tserkovnyak, M. Wu, and I. N. Krivorotov, Spin caloritronic nano-oscillator, Nat. Commun. **8,** 117 (2017).

[179] V. E. Demidov, S. Urazhdin, B. Divinskiy, V. D. Bessonov, A. B. Rinkevich, S. O. Ustinov, and V. V. Demokritov, Chemical potential of quasi-equilibrium magnon gas driven by pure spin current, Nat. Commun. **8,** 1579 (2017).

[180] M. Schneider, D. Breitbach, R. O. Serha, Q. Wang, A. A. Serga, A. N. Slavin, V. S. Tiberkevich, B. Heinz, B. Lägel, T. Brächer, C. Dubs, S. Knauer, O. V. Dobrovolskiy, P. Pirro, B. Hillebrands, and A. V. Chumak, Control of the Bose-Einstein Condensation of Magnons by the Spin Hall Effect, Phys. Rev. Lett. **127,** 237203 (2021).

[181] S. Kohler and F. Sols, Chemical potential standard for atomic Bose–Einstein condensates, New J. Phys. **5,** 94 (2003).

[182] G. Gallavotti, *Statistical Mechanics: A Short Treatise* (Springer, Berlin, Heidelberg, 1999).

[183] W. J. Mullin, Bose-Einstein condensation in a harmonic potential, J. Low Temp. Phys. **106,** 615 (1997).

[184] P. Bialas, J. Spiechowicz, and J. Łuczka, Quantum counterpart of classical equipartition of energy, J. Phys. A **52,** 15LT01 (2019).

[185] J. Łuczka, Quantum counterpart of classical equipartition of energy, J. Stat. Phys. **179,** 839 (2020).

[186] L. E. Reichl, *A Modern Course in Statistical Physics Fourth, Revised Edition* (Wiley-VCH, Weinheim, 2016).

[187] H. B. Callen, *Advances in Thermodynamics of the van der Waals Fluid* (Morgan & Claypool Publishers, Singapore, 2014).

[188] V. Vovchenko, D. V. Anchishkin, and M. I. Gorenstein, Particle number fluctuations for the van der Waals equation of state, J. Phys. A **48,** 305001 (2015).

[189] R. Alicki, The quantum open system as a model of the heat engine, J. Phys. A **12,** L103 (1979).

[190] G. B. Cuetara, M. Esposito, and G. Schaller, Quantum thermodynamics with degenerate eigenstate coherences, Entropy **18,** 447 (2016).

[191] E. Amorim, On a center-of-mass system of coordinates for symmetric classical and quantum many body problems, J. Math. Phys. **60,** 111901 (2019).

[192] H.-P. Breuer and F. Petruccione, *The Theory of Open Quantum Systems* (Oxford University Press, New York, 2002).

[193] F. Benatti and R. Floreanini, Open quantum dynamics: Complete positivity and entanglement, Int. J. Mod. Phys. B **19,** 3063 (2005).

[194] T. Albash, S. Boixo, D. A. Lidar, and P. Zanardi, Quantum adiabatic Markovian master equations, New J. Phys. **14,** 123016 (2012).

[195] T. Albash, S. Boixo, D. A. Lidar, and P. Zanardi, Corrigendum: Quantum adiabatic Markovian master equations (2012 New J. Phys. 14, 123016), New J. Phys. **17,** 129501 (2015).

[196] M. Yamaguchi, T. Yuge, and T. Ogawa, Markovian quantum master equation beyond adiabatic regime, Phys. Rev. E **95,** 012136 (2017).

[197] R. Dann, A. Levy, and R. Kosloff, Time-dependent Markovian quantum master equation, Phys. Rev. A **98,** 052129 (2018).

[198] G. Amato, H.-P. Breuer, and B. Vacchini, Microscopic modeling of general time-dependent quantum Markov processes, Phys. Rev. A **99**, 030102(R) (2019).

[199] A. Sandulescu and H. Scutaru, Open quantum systems and the damping of collective modes in deep inelastic collisions, Ann. Phys. **173**, 311 (1987).

[200] A. Isar, A. Sandulescu, H. Scutaru, E. Stefanescu, and W. Scheid, Open quantum systems, Int. J. Mod. Phys. E **3**, 635 (1994).

[201] R. M. Wilcox, Exponential operators and parameter differentiation in quantum physics, J. Math. Phys. **8**, 962 (1967).